The role of active surface sites in CO2 gasification of polymer char and coal chars

Wang, Jisheng

Award date:
1989

Awarding institution:
University of Bath

THE ROLE OF ACTIVE SURFACE SITES IN CO_2 GASIFICATION OF POLYMER CHAR AND COAL CHARS

submitted by

Jisheng Wang

for the degree of PhD

of the University of Bath

1989

ProQuest LLC
789 East Eisenhower Parkway
P.O. Box 1346
Ann Arbor, MI 48106-1346

ACKNOWLEDGEMENTS

My greatest debt of thanks is to my supervisor, Dr. B. McEnaney, for ideas, personal encouragement and above all patience and humour throughout the project. I also whish to express my sincere gratitude to Mr. M. Lock, a brilliant glass worker in the Science School Workshop, and Mr. P. Wakeford and Mr. P. Taylor, Senior Technicians in the School of Materials Science, and their staff, especially Mr. S. H. Bowman and Mr. I. Trussler for their technical help during the course of this work.

Acknowledgement is also made to British Coal Utilisation Research Association Ltd. for a grant in aid of this work.

To my mother, Mrs. Shufang Wang, and my motherland, China.

ABSTRACT

The role of active surface sites in CO_2 gasification of coal chars and a polymer char were investigated using a temperature-programmed desorption-mass spectrometric technique (TPD-MS) A new method was devised for quantitative calibration of the TPD-MS technique based upon the thermal decomposition of calcium carbonate and calcium oxalate. The secondary reaction between CO_2 produced in the second stage of decomposition of calcium oxalate and the carbon produced in the first stage was observed. TPD spectra measured on the chars saturated with oxygen consist of a broad CO_2 peak and three peaks and a shoulder for CO, at 953, 1083, 1223 and 1473 K, which were designated as the desorption peaks of α-, β-, γ- and δ-states of C-O surface complexes respectively. The peak temperatures are similar to those reported previously for polycrystallite graphite. Total active surface areas (TASA) were obtained by measuring the oxygen chemisorption capacity of the chars. Reactive active surface areas (RASA) were measured after rapidly quenching the chars after CO_2 gasification. TASA values are much greater than RASA values and the latter give a better linear correlation with reactivity. By applying flash desorption theory to the TPD spectra, it is shown that the broad CO_2 peak consists of three overlapping peaks, and CO_2

and CO desorption are both second-order kinetic processes. The desorption activation energies of the three CO_2 peaks are 17, 36 and 41 kcal/mol and those of α-, β-, γ- and δ-states of C-O surface complexes are 17, 45, 55 and 82 kcal/mol respectively. The structures of γ- and δ-states of C-O surface complexes were assigned as semiquinones and ether groups respectively and a mechanism for CO_2 gasification was proposed. This mechanism assumes gasification starts at those active surface sites occupied by oxygen atoms and explains the regeneration of active surface sites during gasification.

NOMENCATURE

A_o: cross-section area of oxygen on carbon surface

A^+: parent ion produced by ionisation of gas A

A_i^+: any ion produced by ionisation of gas A

A_a: pre-exponential factor for adsorption

A_d: pre-exponential factor for desorption

C_f: free active surface site

C(O): active surface site filling with oxygen atom

C_t: total concentration of surface C-O complexes

C_XO_Y: C-O surface complexes

E_a: adsorption activation energy

E_b: chemical bond energy

E_d: desorption activation energy

f_i: abundance of ith ion relative to the parent ion

$H(A^+)$: current of A^+ ion

$H(A_i^+)$: current of A_i^+ ion

$H(CO^+)$: current of CO^+ ion

$H_{CO}(CO^+)$: current of CO^+ produced from CO

$H_{CO_2}(CO^+)$: current of CO^+ produced by CO_2^+ fragmentation

$H(CO_2^+)$: current of CO_2^+ ion

$I(A^+)$: area under TPD curve of A^+ ion

$I(CO^+)$: area under TPD curve of CO^+ ion

$I_{CO}(CO^+)$: area under TPD curve of CO^+ produced by CO

$I_{CO2}(CO^+)$: area under TPD curve of CO^+ produced by CO_2

$I(CO_2^+)$: area under TPD curve of CO_2^+ ion

k: rate constant

k_a: adsorption rate constant

k_d: desorption rate constant

m/e: ratio of mass and electronic amount

n_A: molar amount of gas A

N_{Avo}: Avogadro's number

N_0: total molar amount

N_O: molar amount of oxygen atom

N_P: molar amount desorbed until peak temperature

P_A: true pressure of gas A

P_A': pressure of gas A read on mass spectrometer

Q_A: effective pumping speed of the vacuum system

R: gas constant

S_A: sensitivity of gas A relative to nitrogen

T: temperature

T_P: temperature of maximum desorption

w: weight of the sample

α, β, γ, δ: adsorbed states of C-O surface complexes

θ: surface coverage by C-O complexes

θ_0: initial surface coverage

θ_P: surface coverage at peak temperature

χ: correlation coefficient

CONTENT

INTRODUCTION

Coal has long been the dominant resource of energy for mankind. The techniques of its utilization have played an important role in the development of modern civilization. As it has become appreciated that coal resources are limited and competition for the use of coal is increased, the necessity to improve efficiency has become more and more urgent. In recent times, the need for the conservation of coal sources and the need to protect the environment have increased the pressure for improvement. The improvement, however, does not happen automatically. It requires considerable effort by scientists and engineers collaborating together to improve existing industrial process and to introduce new technology. Successful innovation is the product of fruitful interaction between fundamental research, applied research and strategic research on a national or international scale. The work reported in this thesis is a contribution to this subject designed to elucidate the role of active surface sites in the gasification of coal chars by carbon dioxide.

It has long been known that coal gasification by H_2O and CO_2 proceeds by the formation of carbon-oxygen complexes on

active sites. The active surface sites only cover a fraction of the total surface area, called the active surface area (ASA). The extent of ASA is thought to be a function of properties such as: crystallite size and orientation; defects in carbon layer planes and extent of edge carbon atoms, concentration of oxygen containing functional groups, mineral matter, *etc* [1]. The desorption of CO and CO_2 from active surface sites is an important step in most reaction kinetic schemes for the gasification of carbon and, in many schemes, it is the rate-controlling step. Consequently, the nature of the active sites on carbon surface and the chemistry of the surface complexes which form and decompose on them are crucial to understanding the kinetics of gasification process. Despite the vast amount of work which has been carried out on gasification of carbon, there is an increasing recognition that the role of active surface sites is one which requires further study.

Several methods have been used for measuring ASA on a wide range of carbons, from relatively pure and highly crystalline materials, such as graphitised carbon black, to highly heterogeneous carbon such as coal chars. The most widely used technique for estimating ASA on carbons is oxygen chemisorption, by both volumetric [2] and dynamic methods [3]. However, these methods have limitations; the principal one is that oxygen is chemisorbed under conditions

which are far removed from those pertaining during gasification conditions. Typically, a carbon is saturated with oxygen at 523 K and 1 atm and a wide variety of oxygen-containing functional groups may exist under these conditions. By contrast, under gasification conditions in H_2O and CO_2, temperatures are in the range of 1073-1273 K and the oxygen partial pressure is very low, being controlled by H_2O/H_2 and CO_2/CO ratios respectively. This leads to the first thesis of this work that only a fraction of the ASA measured by the conventional method participates in the gasification reaction. It is expected that under gasification conditions only simple thermal stable C-O surface complexes are present on the carbon surface.

The objective of this work was therefore to design and construct an apparatus for measuring ASA of coal chars using a temperature-programmed desorption combined with mass spectrometry (TPD-MS) system. The experimental system also enables gasification of the chars to be carried out *in situ* and ASA to be measured during gasification by quenching the sample. The work explores the relationships between the conventional ASA and the ASA after gasification and quenching. Since the TPD-MS technique measures desorbed gases it was also used to study the kinetics of desorption of CO and CO_2. This study leads to new insight into gasification mechanism for coal chars.

This thesis includes eight chapters in addition to Introduction. Chapter 1 is a literature survey on the theory of active surface sites. From this survey some unanswered questions were revealed which enabled the objectives of this research to be identified more clearly. Chapter 2 describes the experimental arrangements, including the materials used, the design and construction of the TPD-MS system and systems for data-collecting and analyses. Chapter 3 describes the calibration of TPD-MS system. The results of this research are presented in Chapter 4-7 and summarised in Chapter 8. Some suggestions for future work in this field are provided also in Cgapter 8.

References:

[1] N. M. Laurendau, *Prog. Energy Combust. Sci.*, **4**, 221(1978).

[2] N. R. Laine, F. J. Vastola and P. L. Walker, Jr., "*Proc. Fifth Carbon Conf., Vol. 2*", Pergamon Press, New York, p.221(1963).

[3] P. Causton and B. McEnaney, *Fuel*, **64**, 1447(1985).

Chapter 1

ACTIVE SURFACE SITES

Gasification of carbonaceous solid has been and remains an area of significant scientific and technological interest. It has long been recognized that a gross indicator of carbon reactivity is its total surface area (TSA). However, it is also well known that this property does not always correlate well with reactivity. This is not only due to the fact that it is not always possible to determine accurately the surface areas of carbons (especially those with significant microporosity), but also because only a fraction of the TSA is "active", at least under the particular experimental conditions used. In this chapter the theory of active surface sites are briefly introduced and the areas of potential difficulty and prospects for development are indicated.

1.1 Active Surface Sites

1.1.1 Historical

Smith [1.1], in 1863, was probably the first worker to suggest that when oxygen is adsorbed on a carbon surface it

undergoes a chemical change. He found that adsorption of oxygen on charcoal did not cease even after a month; and that while nitrogen and other gases adsorbed on charcoal could be easily removed as such, oxygen could be removed only on strong heating, and then as carbon dioxide. Baker [1.2], a few years later, showed that an outgassed charcoal could "fix" oxygen even at 260 K. Rhead and Wheeler [1.3, 1.4] concluded that oxygen combines with a mass of carbon directly to form physicochemical complexes, C_xO_y, of variable composition, which decompose over a wide range of temperature, giving a mixture of carbon monoxide and carbon dioxide. These observations were confirmed by Lowry and Hullett [1.5], who, while attempting to determine the content of the moisture and gas in charcoal, noticed that the gases evolved up to 1173 K consisted almost entirely of carbon dioxide and carbon monoxide, the former predominating at lower temperatures and the latter at higher temperatures.

Further evidence for chemisorption of fixation of oxygen on carbons was furnished by the work of Langmuir [1.6], Lamber [1.7], Lepin [1.8] and others [1.9, 1.10]. Ward and Rideal [1.11] found that the heat of adsorption of oxygen on charcoal, even at 273 K, was of the order of 40 kcal/mol, suggesting the chemical nature of the interaction involved. Other workers [1.12-1.15] reported even higher values, varying from 250 to 85 kcal/mol.

It is now known that oxygen is chemisorbed on carbon more readily than many other elements and almost all types of carbons are covered with oxygen complexes unless special care is taken to eliminate them and that C-O surface complexes are by far the most important in influencing gasification of carbons and chars. Thus, only these complexes are discussed in this thesis.

1.1.2 The Concept of Active Surface Sites

The combustion of coal chars and their gasification by H_2O and CO_2 proceed on the char-gas interface. The theory of active surface sites proposes [1.16-1.19] that, these reactions only occur at those favoured sites on the surface, named as active surface sites. They are provided by surface irregularities on which C-O surface complexes are formed. The resulting valence forces induce electron transfer and cause gas-solid bonding or chemisorption. For chars, the active surface sites can be attributed to crystalline size and orientation; defects in carbon layer planes and the extent of edge carbon atoms; concentration of oxygen and hydroxyl functional groups and mineral matter, *etc.* At each active site reactant chemisorption (adsorption), migration of intermediates and product desorption may sequentially take place. This theory usually presumes the following:

i. localized adsorption *via* collisions with vacant active sites;

ii. one adsorbed molecule or atom per site due to strong valence bonds, *i.e.*, x = y = 1 in the formula of C-O complexes, C_xO_y;

iii. a constant surface (chemisorption/migration desorption) mechanism;

iv. surface coverage less than a complete monomolecular layer.

This kind of single site chemisorption requires one free carbon site and may or may not lead to the simultaneous production of gaseous species, *e.g.*,

$$O_2 + 2C_f \longrightarrow 2C(O)$$

$$H_2O + C_f \longrightarrow C(O) + H_2$$

$$CO_2 + C_f \longrightarrow C(O) + CO$$

$$C(O) \longrightarrow CO + C_f$$

where C(O) denotes an active site filled with atomic oxygen, *i.e.*, C-O surface complexes, and C_f a free active surface site. The desorption of C-O surface complexes is probably the most important step in carbon gasification and combustion.

1.2 Methods of Study

The surface oxides of a variety of carbon compounds such as carbon black, carbon fibers, carbon films, coal chars and graphite have been extensively studied over the past two decades by an array of different methods including gravimetric balances [1.20-1.24], pH measurements [1.25], reactor studies [1.26], chemisorption kinetics [1.22, 1.23], optical microscopy [1.27], thermal desorption at sub-atmospheric pressures [1.28-1.34]. More recently new techniques such as infrared absorption [1.35-1.37], electron spin resonance [1.38-1.40], ultraviolet photoelectron spectroscopy (UPS) [1.41], Raman spectroscopy [1.42], and nuclear magnetic resonance (NMR) [1.43] and surface science tools such as X-ray photoelectron spectroscopy (XPS) [1.44-1.46], Auger electron spectroscopy (AES) [1.47, 1.48] and TPD measurement [1.49-1.52] have provided some useful information on the nature of these surface species.

1.3 Measurement of Active Surface Area

Although the concept of active surface sites had been proposed for almost a century, it was in 1961 that this concept was first quantified by Walker and co-workers [1.21, 1.53] by measuring the oxygen chemisorption capacity of Graphon by a volumetric method. The oxygen chemisorption

capacity can be also measured by a gravimetric method [1.24, 1.54] or a dynamic method [1.50] which measures the amount of CO and CO_2 desorbed upon a subsequent temperature-programmed desorption. The basic premise underlying these methods is that the measurement of oxygen uptake can yield an "active surface area" (ASA) if it is assumed that the resultant surface complexes consist of a single oxygen atom per carbon atom, and that the surface area occupied by the oxygen atom is the same as that of an edge atom in the (001) plane of graphite (0.083 nm^2). It has been shown or at least implied, by the results of various workers [1.20-1.54] that active surface area is a better predictor of char reactivity than is total surface area.

1.3.1 Oxygen Chemisorption Technique, Volumetric Method

The most widely used technique [1.21, 1.53, 1.55-1.57] for studying the concentrations of active surface site is a volumetric method, which involves continuous monitoring of reactant and product partial pressures with a mass spectrometer in a closed, constant volume system. Figure 1.1 shows the block diagram of volumetric system. The changes of reactant and product partial pressures lead to an estimate of the amount of oxygen chemisorbed on the surface of the sample at a given pressure and temperature and thence to the ASA. For low temperature chemisorption studies it is

crucially important to create an ultra-high vacuum system, up to 10^{-8} Pa, to obtain a very clean carbon surface on which CO, CO_2 and C-O surface complexes are formed. As pointed out by Walker and co-workers, much of the work before them on the chemisorption of oxygen was carried out on poorly defined carbon and/or on carbon surfaces contaminated with significant amount of previously adsorbed gases (such as hydrogen and oxygen). The ASA of the Graphon they calculated is as low as 0.02% of the BET surface area.

During the past 26 years, however, the application of volumetric methods has been extended to correlate the reactivities of a much wider variety of carbons and chars with respect to other oxidizing gases, and under a much wider range of conditions [1.21, 1.50-1.59]. Some workers reported very high reproducibility of this method [1.56].

1.3.2 Temperature-Programmed Desorption Technique, Dynamic Method

A dynamic technique for measuring ASA by temperature-programmed desorption of C-O surface complexes formed by oxygen saturation chemisorption was devised by Causton and McEnaney [1.50]. Figure 1.2 shows the block diagram of their dynamic system. In such a system, the sample was first outgassed to 10^{-5} Pa at 1223 K for 15 h to prepare a clean

surface of the char. Then the temperature was reduced to and held at 523 K; oxygen at atmospheric pressure was admitted into the reactor for another 12 h to saturate the surface. Subsequently, the pressure was reduced to 10^{-5} Pa again to remove all gaseous oxygen from the system. Finally, the char was subjected to TPD at a linear heating rate of 5 K/min up to some temperature under a total dynamic pressure range of 10^{-3}-10^{-5} Pa. C-O surface complexes on the char surface were desorbed as CO and CO_2 and their partial pressures were measured using a mass spectrometer.

Compared with the outgassing procedure in the volumetric method, it is noticeable that one assumption of the dynamic method is that the surface of the carbon sample can be cleaned sufficiently for ASA measurement at 10^{-5} Pa at 1223 K and another is that the amount of C-O surface complexes remaining on the sample surface after TPD is negligible under the experimental conditions.

1.4 ASA and Gasification Reactivity of Coal Chars

Since the time of Walker and co-workers, a vast amount of work has been done applying the standard method of oxygen chemisorption or other methods to heterogeneous surfaces of coal chars, in order to elucidate the mechanisms of gasification and combustion [1.60-1.67]. Variations in

reactivity of chars have been ascribed to different samples having, initially, different amount of ASA which change with burn-off. It is therefore reasonable to suggest that the large spread in reported values of reactivity per unit TSA is mainly due to different extents of ASA in coal chars.

The simplest mathematical model for single site mechanism [1.38] applicable to high temperature (>523 K) gas-solid reactions was developed by Langmuir. Hinshelwood later extended the model to a dual sites mechanism [1.68]. They made the following assumptions:

i. The surface is homogeneous, *i.e.* a uniform average activity can be defined for the entire surface. This assumption clearly requires a uniform distribution of active sites.

ii. No interaction occurs among adsorbed species, *i.e.*, the amount adsorbed has no effect on the adsorption rate per site.

iii. Surface migration is either nonexistent or so rapid that only adsorption and desorption can be rate-controlling.

It is noteworthy that the homogeneous, non-interacting surface implies that both the activation energy for adsorption E_a and desorption E_d remain constant in time, as well as from site to site.

Chemisorption arises from gas molecules striking the surface at locations not covered by previously adsorbed species. If θ is the active surface coverage, *i.e.*, the fraction of active surface sites covered by adsorbed species, the intrinsic rate of adsorption must be

$$R_a = k_a C(1-\theta)^n \qquad n = 1,2 \tag{1.1}$$

where C is the local gas concentration, n = 1,2 denotes single and dual site adsorption, respectively, and

$$k_a = A_a \exp(-E_a/RT) \tag{1.2}$$

where A_a is the pre-exponential factor of adsorption and E_a the adsorption activation energy. The adsorption rate R_a can be independently measured by exposing a clean surface (heat treatment in vacuum) to the gas.

The desorption rate is presumed proportional to the active surface coverage, i.e.,

$$R_d = k_d \theta^n \qquad n = 1,2 \tag{1.3}$$

where n = 1,2 refers to single or dual site desorption, respectively, and

$$k_d = A_d \exp(-E_d/RT) \tag{1.4}$$

where A_d is the pre-exponential factor of desorption and E_d the desorption activation energy. The desorption rate R_d can be independently measured by rapidly imposing a vacuum on the sample.

Langmuir-Hinshelwood theory has been applied to interpret the mechanism of combustion and gasification of chars [1.17-1.19, 1.21, 1.24, 1.50, 1.53-1.59]. The principal objective of this study is to improve the understanding of the nature of active sites on coal chars using this theory so as to refine the mechanism of CO_2 gasification.

1.5 Nature of The Surface Complexes

Although the active surface site theory has been developed quickly in recent years, there is still an increasing recognition that the nature of active surface sites is one which requires further study despite the vast amount of work has been carried out on it. Radovic [1.60] has recently pointed out that studies of the development of ASA with progressive gasification of coal chars have been few and that such studies may help to elucidate gasification mechanism.

1.5.1 Types of Active Surface Sites

Many of the studies about the nature of C-O surface complexes have been provided by Walker and his school. Initially the chemisorption of oxygen over the temperature range from 198 to 433 K at an oxygen pressure of 100 mTorr for times up to 24 h on the surface of ultra-clean Graphon

was studied. Graphon is a low porosity, graphitized carbon black, in which most of the active surface area is limited to edge carbons occurring at discontinuities in the graphite basal planes. The Graphon samples were first activated by preoxidation to 16.6 per cent weight loss at 878 K to increase the amount of active surface area. Walker *et al* [1.23, 1.69] reported that plots of amount of oxygen adsorbed *versus* log of time showed linear regions; in all, five linear regions were identified as shown in Figure 1.3. The slops change little within a linear region, however, it changes abruptly on going from one region to the next. The activation energy for chemisorption increases overall from 3 kcal/mol for the first linear region to 12 kcal/mol for the last. It was concluded that each linear region represented adsorption on different discrete types of active sites on the carbon surface. Similarly, Lussow *et al* [1.70] concluded that their O_2 chemisorption data indicated the presence of at least two types of active sites and Hart *et al* [1.22] found two distinct plateau in the amount of O_2 chemisorbed on Graphon; one between 298 and 473 K, and the other between 573 and 773 K. These data were interpreted as being due to different types of active sites on carbon surfaces.

Unfortunately, the work on the desorption of CO and CO_2 from active sites of carbon is not as detailed as that on chemisorption until now, although it is believed to be the

most important step in most kinetic schemes for the combustion or gasification of carbon, and in many schemes, it is the rate-controlling step [1.71]. Walker and co-workers also studied the desorption of C-O surface complexes from Graphon surface by the volumetric method. The result from Bansal *et al* [1.72] is shown in Figure 1.4, on which only four linear regions were shown on the plot of cumulative recovery of $CO+CO_2$ from C-O complexes at temperatures 700, 800, 900 and 1000 K, respectively. It is interesting to note the existence of different types and amounts of active sites obtained from chemisorption and desorption, however, this was not discussed by Bansal *et al* [1.72]. Similarly, Phillips *et al* [1.73] reported from their thermal decomposition data of surface C-O complexes formed on Graphon that each graph of accumulated CO against temperature consisted of a series of intersecting linear portions, suggesting that desorption was taking place from a number of discrete types of active sites on carbon surfaces.

Causton and McEnaney [1.50] reported the presence of two desorption curves of CO_2 and CO in the dynamic TPD spectra of C-O surface complexes from PVDC and coal chars.

From the dynamic TPD spectra of C-O surface complexes on PVC char gasified in water vapour atmosphere and quenched to 673 K, Hermann and Huttinger [1.74] observed that only CO

was desorbed and most CO was desorbed from some "extremely stable C-O surface complexes" on the surface of PVC char gasified and quenched, which gave a peak about 1173 K and could not be fully desorbed even above 1273 K.

Different types of active surface sites should have different adsorption and desorption energies. Oxygen atoms should be adsorbed first on active sites which possess the highest desorption energy and the C-O surface complexes formed on them should be the most stable ones. Therefore, it is reasonable to envisage that the differences between the types and amounts of active surface sites obtained from oxygen chemisorption and from desorption by Walker and co-workers are probably due to uncompleted desorption of C-O surface complexes in the latter process and some "extremely stable C-O complexes" which still remain on some type or types of active sites at the maximum desorption temperature used.

In a recent paper [1.51, 1.52] Marchon *et al* reported TPD spectra after O_2, CO_2, CO and H_2O adsorption on a clean polycrystalline graphite, on which the TPD curves of CO_2 show five peaks around 463, 573, 693, 793 and 903 K, and the curves of CO show three peaks around 973 (shoulder), 1073 and 1253 K.

1.5.2 Forms of Surface Functional Groups of C-O Complexes

A further important problem is the identification of the surface functional groups of C-O complexes formed on the four or five or even more active surface sites. In an infrared study of carbon films, Smith *et al* [1.75] concluded that the principal surface groups formed upon exposure to oxygen were carbonyls and lactones. In a more recent FTIR study, Starsinic *et al* [1.76] found that a large fraction of the surface complexes on a Saran char consisted of carboxylic acid groups, in addition to "more ill-defined oxygen complexes". In a recent TPD and acidic group neutralization study on phenol-formaldehyde char, Otake [1.77] demonstrated the CO_2 resulted from the thermal desorption of carboxylic and acidic anhydride groups.

1.5.3. Stoichiometry of C-O Surface Complexes

The assumption of carbon-oxygen complex stoichiometry of one-to-one is, obviously, an oversimplification, since it is well known that many different types of oxygen complexes form on carbon surface as discussed in Sections 1.5.1. and 1.5.2. For the same Saran char studied by Starsinic *et al* [1.76], Taylor [1.78] reported that the active surface area determined from the desorption of surface oxides after atmospheric burn-off, ***exceeded*** the TSA; but V3G carbon (a graphitized carbon black) behaved very similarly to the

Graphon studied by Laine *et al* [1.53]. One possible explanation for this unexpected discrepancy is that the number of O atoms per site may have been greater than unity, and that the 0.083 nm^2 value assumed for the cross sectional area of the C-O surface complexes may be inappropriate for the C_XO_Y complexes formed on the Saran char; for example, an O atom bridging across two carbon atoms on the basal plane, would occupy only 0.053 nm^2 [1.79].

For the identification of the stoichiometry of C-O surface complexes, the measurement of adsorption or desorption order may provide some evidence. Hermann and Huttinger [1.74] assumed "the extremely stable C-O surface complexes" were ether groups, however, they also assumed a first-order kinetic model for the desorption of this type of surface complex, but alter reaction orders (*e.g.*, second-order) are also possible. Marchon *et al* [1.51] assigned semiquinone structures to the surface complexes which desorbed as CO and calculated the activation energies of desorption of the surface complexes. Unfortunately, they did not report the reaction order of the desorptions. This aspect of the desorption of surface complexes from coal chars will be considered in detail in this work (Chapter 7).

1.6 Objectives of the Present Work

The broad aims of this work were stated in the Introduction. In this section more detailed aims of the work are set out in the light of the literature survey presented above.

1.6.1 The Types of Active Surface Sites and ASA Involved in Gasification

Although oxygen chemisorption and desorption is the standard method for estimating the concentration of active sites, it has limitations. For example, Suuberg *et al* [1.80] questioned the significance of oxygen chemisorption as a means to monitor ASA; they argued that the concept of active sites was too broad, as the reactive sites may be quite different in low-temperature chars from those in high-temperature graphitic carbons. It is also reasonable to propose that the principal limitation of the oxygen chemisorption technique is that oxygen is chemisorbed under conditions which are far removed from those pertaining during combustion and gasification conditions. Typically, oxygen is chemisorbed at 523 K and 1 atm of O_2 for the dynamic method [1.50]; under these conditions the carbon surface is saturated with oxygen and a wide variety of oxygen-containing functional groups may exist. By contrast,

during gasification in H_2O and CO_2, temperatures are in the range 1073-1473 K and the oxygen partial pressures are very low, being controlled by H_2O/H_2 and CO_2/CO ratios respectively. Consequently, it is expected that only a small fraction of active sites are covered with simple, thermally-stable, oxygen-containing functional groups. The extent of active site coverage and the range of chemical functionality is expected to be wider in combustion than in gasification, since the oxygen partial pressures are higher and the temperatures are lower. However, they may well be less than those found by oxygen chemisorption at 523 K. As stated in the Introduction of this thesis a principal objective proposed for this work is to attempt to verify these expectations.

For this purpose, ASA was measured in this work by desorption of CO and CO_2 using a modification of TPD technique devised previously by Causton and McEnaney [1.24]. Coal char specimens were gasified in CO_2 atmosphere at different temperatures in order to establish a concentration of surface complexes on active sites which are in dynamic equilibrium with gasifying medium. The "equilibrium" concentration of surface complexes was frozen by quenching the system by rapid cooling of the specimens. A specially-designed reactor was constructed to achieve rapid quenching. The surface complexes were decomposed during TPD and the

desorbed gas was analysed using a quadrupole mass spectrometer. The potential of this type of approach has been demonstrated in a paper on water vapour gasification of carbon [1.73].

1.6.2 Homogeneity and Heterogenity of Coal Char Surfaces

It is well-known that the surface of coal chars are highly heterogeneous. However, it is also well-known that coal chars are composed of highly defective carbon layer planes, some of which are stacked together in small packets of two or three layers. These have been described as "pseudo graphitic building blocks" [1.81], but this term is misleading since there is no evidence for 3-dimensional graphite ordering in coal chars. The defective carbon layer planes are held together by a tangled network of cross links. Edge carbon atoms in the defective carbon layer planes are thought of as examples of "active surface sites" during gasification of coal chars and 'dangling' carbon atoms have also been proposed [1.66]. Obviously, in such a defective structure, many other surface sites may also be active surface sites. ASA measurement is based on an assumption of a homogeneous surface of carbons and some workers [1.80] have drawn attention to the influence of surface heterogenity on the TPD spectra from coal chars. However, the similarity of TPD curves reported by different

authors using different methods and under different conditions provides some evidence for the presence of some common structural features on the surface of carbon and coal chars and this is one aspect of the desorption of carbon oxides on coal char surfaces which is investigated in this work.

1.6.3 Summary

It is clear from above discussion that the study on the active surface sites is a very promising field and there are still many questions to be answered, such as the following:

* How many types of active surface sites exist on the surface of carbons?
* On what type or types of active surface sites does gasification take place?
* What is the stoichiometry of C-O surface complexes, *i.e.*, what is the ratio of X/Y in the formula of C-O surface complexes C_XO_Y?
* How do these different active surface sites develop during gasification?
* Is it correct to apply the results obtained from pure carbon to highly heterogeneous coal chars?
* Can the catalyst effect of some minerals, such as potassium carbonate be explained using active surface sites theory?

The questions are addressed in the following chapters.

References

[1.1] R. A. Smith, *Proc. Roy. Soc. (London)*, **12**, 425(1863).

[1.2] C. G. Baker, *J. Chem. Soc.*, **76**, 249(1887).

[1.3] T. F. E. Rhead and R. V. Wheeler, *J. Chem. Soc.*, **101**, 846(1912).

[1.4] T. E. F. Rhead and R. V. Wheeler, *J. Chem. Soc.*, **103**, 461(1913).

[1.5] H. H. Lowry and C. A. Hullet, *J. Am. Chem. Soc.*, **42**, 1409(1920).

[1.6] J. D. Lambert, *Trans. Faraday Soc.*, **32**, 249(1931).

[1.7] L. Lepin, *Physik. Z. Sowjetunion*, **4**, 849(1957).

[1.8] F. E. Bartell and E. J. Miller, *J. Phys. Chem.*, **28**, 992(1924).

[1.9] W. E. Garner and D. McKie, *J. Chem. Soc.*, **117**, 2451(1927).

[1.10] A. F. C. H. Ward and E. K. Rideal, *J. Chem. Soc.*, **117**, 1317(1927).

[1.11] F. G. Keyes and M. J. Marshall, *J. Am. Chem. Soc.*, **51**, 2019(1929).

[1.12] M. J. Marshall and G. Bramston-Cook, *J. Am. Chem. Soc.*, **51**, 2019(1929).

[1.13] M. J. Marshall and G. Bramston-Cook, *Can. J. Research*, **B15**, 75(1937).

[1.14] D. McKie, *J. Chem. Soc.*, **118**, 2870(1928).

[1.15] B. R. Puri, D. D. Singh, J. Nath, and L. R. Sharma, *Ind. Eng. Chem.*, **50**, 1071(1958).

[1.16] B. R. Puri, *Chem. and Phys.of Carbon*, **5**, 191(1967).

[1.17] N. M. Laurendau, *Prog. Energy Combust. Sci.*, **4**, 21(1978).

[1.18] B. G. Tucker and M. F. R. Mulcahy, *Trans. Faraday Soc.*, **65**, 274(1969).

[1.19] R. H. Essenhigh in "*Chemistry of Coal Utilization, Second Supplement Volume*" (Ed. M. A. Elliot), Wiley, NY, PP.1172-1175(1981).

[1.20] G. Blyholder and H. Eyring, *J. Chem. Phys.* **63**, 1004(1959).

[1.21] N. R. Laine, F. J. Vastola and P. L. Walker, Jr., *J. Phys. Chem.*, **67**, 2030(1963).

[1.22] P. J. Hart, F. J. Vastola and P. L. Walker, Jr., *Carbon*, **5**, 363(1967).

[1.23] R. C. Bansal, F. J. Vastola and P. L. Walker, Jr., *J. Colloids and Interf. Sci.*, **32**, 187(1969).

[1.24] A. Cheng and P. Harriot, *Carbon*, **24**, 143(1986).

[1.25] T. J. Fabish and D. E. Schleifer, *Carbon*, **22**, 19(1984).

[1.26] P. D. Koenig, R. G. Squires and N. M. Laurendeau, *Carbon*, **23**, 531(1985).

[1.27] H. Marsh and T. E. O'Hair, *Carbon*, **7**, 703(1969).

[1.28] F. J. Vastola, P. J. Hart and P. L. Walker, Jr., *Carbon*, **2**, 65(1964).

[1.29] J. Dollimore, C. M. Freedman, B. H. Harrison and D. F. Quinn, *Carbon*, **8**, 587(1970).

[1.30] B. J. Tucker and M. F. R. Mulcahy, *Trans. Faraday Soc.*, **65**, 274(1969).

[1.31] F. S. Feates and C. W. Keep, *Trans. Faraday Soc.*, **66**, 3156(1970).

[1.32] S. S. Barton, G. L. Boulton and B. H. Harrison, *Carbon*, **10**, 395(1972).

[1.33] A. Sen and J. E. Bercaw, *J. Phys. Chem.*, **84**, 465(1980).

[1.34] J. A. Britten, J. L. Falconer and L. F. Brown, *Carbon*, **23**, 627(1987).

[1.35] C. Ishizaki and I. Marti, *Carbon*, **19**, 409(1981).

[1.36] M. S. Akhter, J. R. Keifer, A. R. Chughtai and D. M. Smith, *Carbon*, **23**, 589(1982).

[1.37] J. Zawadzki, *Chem. and Phys. of Carbon*, **23**, 187(1989).

[1.38] K. Antonowicz, *Proc. 5th Conf. Carbon*, Pergamon Press, New York, p.46(1962).

[1.39] B. Milsch, W. Windsch and H. Heinzelman, *Carbon*, **6**, 807(1968).

[1.40] W.F. DeGroot and F. Shafizadeh, *Carbon*, **21**, 61(1983).

[1.41] S. R. Keleman, H. Freund and C. A. Mims, *J. Vac. Sci.*

Technol., **A2**, 987(1984).

[1.42] G. Katagiri, H. Ishida and A. Ishitani, *Carbon*, **26**, 565(1988).

[1.43] C. A. Mins, K. D. Rose, M. T. Melchior and J. K. Pabst, *J. Am. Chem. Soc.*, **104**, 6886(1982).

[1.44] D. L. Perry and A. Grint, *Fuel*, **62**, 1024(1983).

[1.45] D. T. Clark and R. Wilson, *Fuel*, **62**, 1034(1983).

[1.46] T. Tagahagi and I. Ishitani, *Carbon*, **22**, 43(1984).

[1.47] S. R. Kelemen and H. Freund, *Carbon*, **23**, 619(1985).

[1.48] S. R. Kelemen and H. Freund, *Carbon*, **23**, 723(1985)

[1.49] S. S. Barton, B. H. Harrison and J. Dollimore, *J. Phys. Chem.*, **82**, 290(1978).

[1.50] P. Causton and B. McEnaney, *Fuel*, **64**, 1447(1985).

[1.51] B. Marchon, W. T. Tysoe, J. Carrazza, H. Heinemann and G. A. Somorjai, *Carbon*, **26**, 507(1988).

[1.52] B. Marchon, W. T. Tysoe, J. Carrazza, H. Heinemann and G. A. Somorjai, *J. Phys. Chem.*, **96**, 5744(1988).

[1.53] N. R. Laine, F. J. Vastola and P. L. Walker, Jr., " *Proceedings of the Fifth Carbon Conference, Vol. 2*", Pergamon, Oxford, p.211(1963).

[1.54] A. A. Lizzio, A. Piotrowski and L. R. Radovic, *Fuel*, **67**, 1691(1988)

[1.55] L. R. Radovic, P. L. Walker, Jr., and R. G. Jenkins, *Fuel*, **62**, 849(1983).

[1.56] I. M. K. Ismail, *Carbon*, **25**, 653(1987).

[1.57] R. L. Taylor and P. L. Walker, Jr., "*Extended*

Abstracts, 15th Bienial Conference on Carbon", Philadelphia, PA, p.437(1981).

[1.58] S. B. Tong, P. Pareja and M. H. Back, *Carbon*, **20**, 191(1982).

[1.59] R. Cypres, D. Planchon and C. Braekman-Danheux, *Fuel*, **64**, 1375(1985).

[1.60] L. Radovic, "*Carbon '86'*", Deutsche Keramische Gesselschaft, Baden-Baden FRG, pp.571-573(1986).

[1.61] E. Chornet, J. H. Baldasano and C. Braekman-Danheux, *Fuel*, **64**, 1375(1985).

[1.62] E. Chornet, J. H. Baldasano and H. T. Tarki, *Fuel*, **58**, 1375(1985).

[1.63] S. K. Bhatia and D. D. Perlmutter, *AIChE J.* **26**, 577(1980).

[1.64] G. A. Simons, *Carbon*, **20**, 117(1982).

[1.65] S.Reyes and K. F. Jensen, *Chem. Eng. Sci.* **41**, 333(1986).

[1.66] M. R. Khan, *Fuel*, **66**, 1626(1987).

[1.67] D. O. Hayward, and B. M. W. Trapnel, *Chemisorption*, Butterworths, London (1964).

[1.68] D. A. Frank-Kamenetskii, "*Diffusion and Heat Transfer in Chemical Kinetics*", Plenum, NY, p173(1969).

[1.69] P. L. Walker, Jr., R. C. Bansal, and F. J. Vastola, "*The Structure and Chemistry of Solid Surfaces* ", Wiley, NY, p.81(1980).

[1.70] R. O. Lussow, F. J. Vastola and P. L. Walker, Jr.,

Carbon, **5**, 591(1967).

[1.71] J. L. Johnson in "*Chemistry of Coal Utilization, Second Supplement Volume*", (Ed.M. A. Elliot), Wiley, NY, pp.1566-1598(1981).

[1.72] R. C. Bansal, F. J. Vastola and P. L. Walker, Jr., *Carbon*, **8**, 443(1970).

[1.73] R. Phillips, F. J. Vastola and P. L. Walker, Jr., *Carbon*, **8**, 197(1970).

[1.74] G. Hermann and K. J. Huttinger, *Carbon*, **24**, 705(1986).

[1.75] R. N. Smith, D. A. Young and R. A. Smith, *Trans. Faraday Soc.*, **62**, 2280(1966).

[1.76] M. Starsinic, R. L. Taylor and P. L. Walker, Jr., *Carbon*, **21**, 69(1980).

[1.77] Y. Otake, PhD Dissertation, The Pennsylvania State University(1986).

[1.78] R. L. Taylor, PhD Dissertation, The Pennsylvania State University(1986).

[1.79] J. M. Calo, E. M. Suuberg and M. Wojtowicz in "*Carbon '88'*", (Ed. B. McEnaney and T. J. Mays), IOP Publishing, Bristol, UK, pp.319-321(1988).

[1.80] E. M. Suuberg, J. M. Calo and M. Wojtowicz, *ACS Div. Fuel Chem. Prepr.*, **31**, 186(1986).

[1.81] P. L. Walker, Jr., and O. P. Mahajan, "*Analytical Methods for Coal and Coal Products, Vol. I*" (Ed. C. Karr), Academic, NY, pp.125-163(1978).

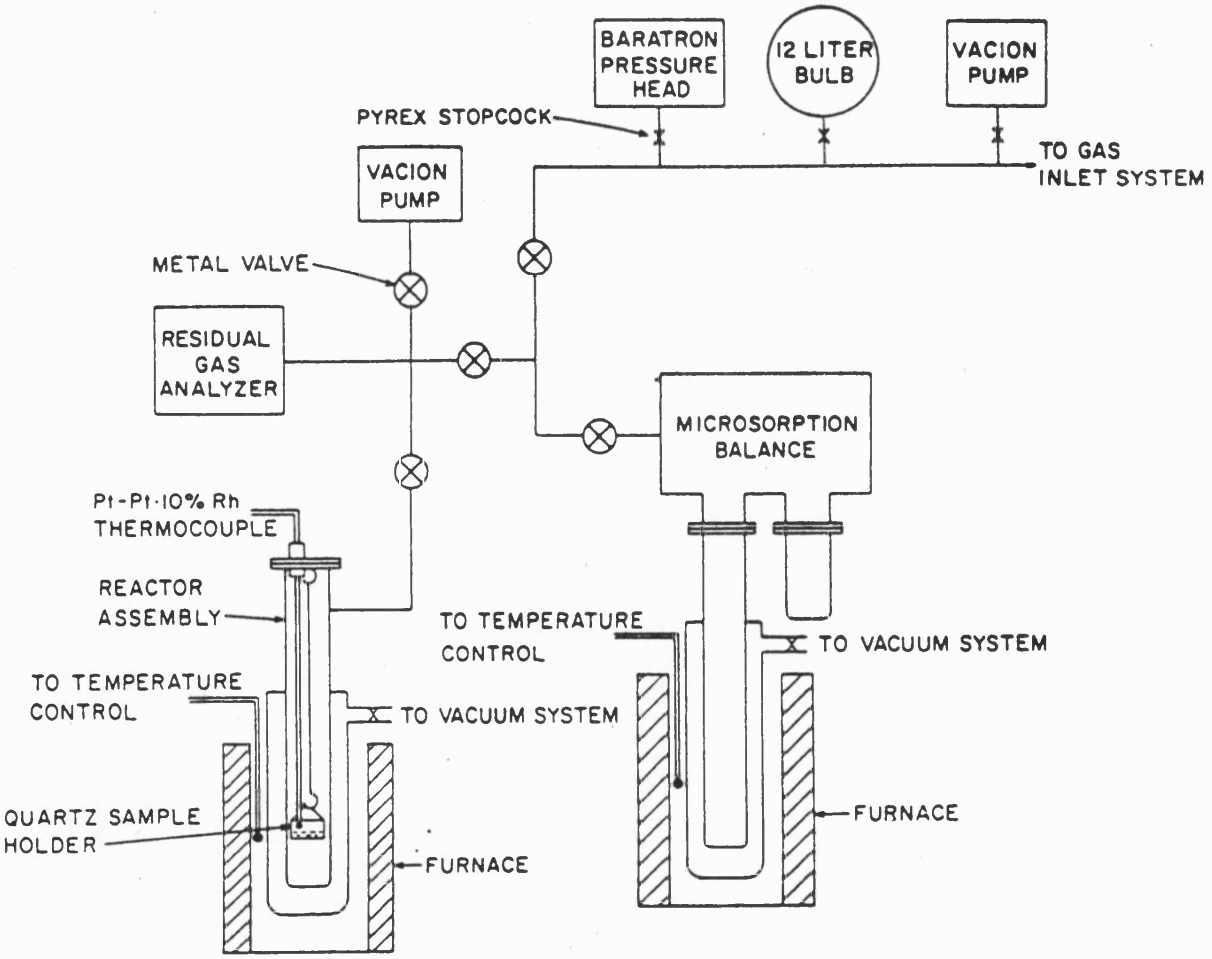

Figure 1.1 Schematic drawing of apparatus used by Walker *et al.* (Ref. [1.69])

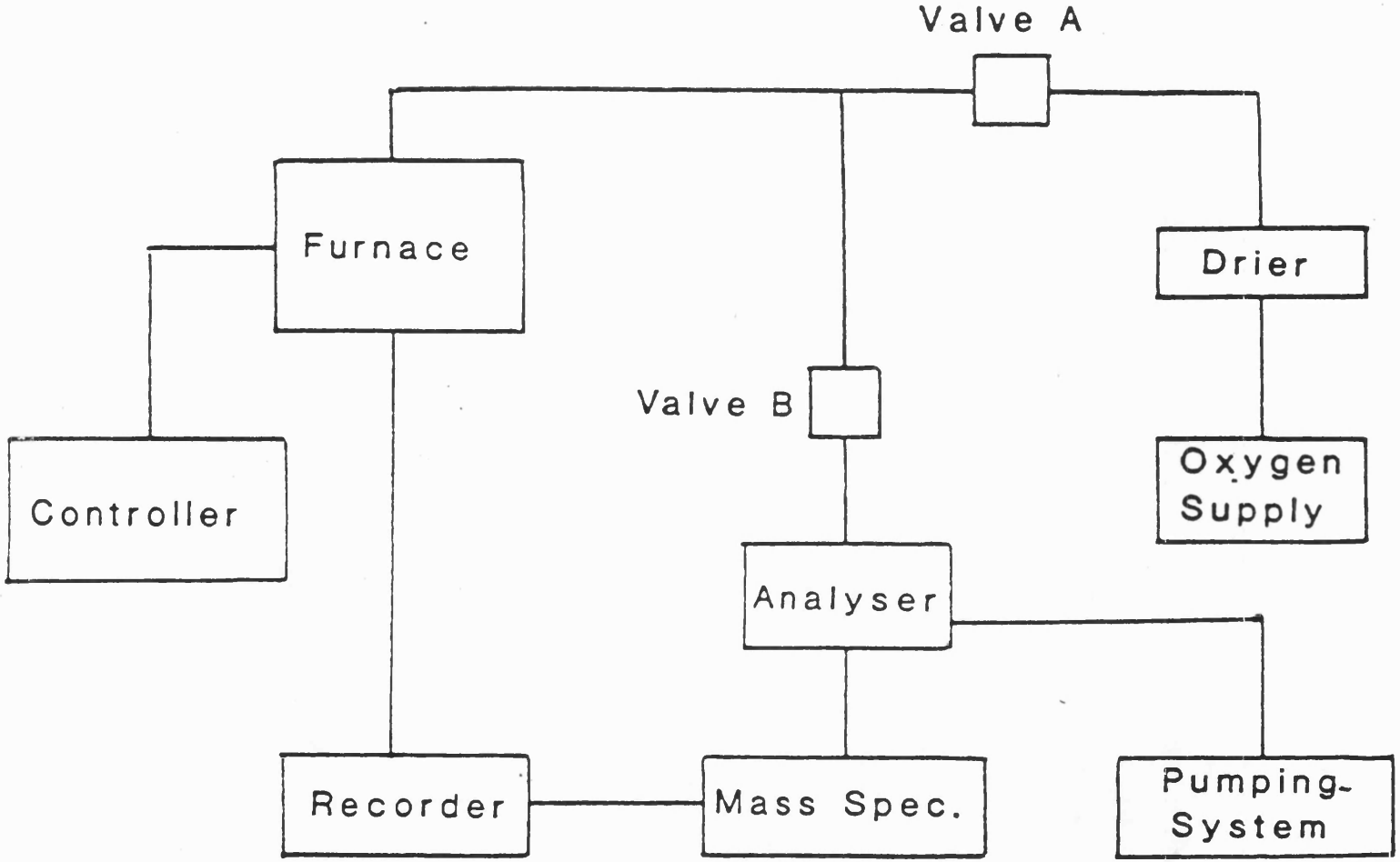

Figure 1.2 Schematic drawing of apparatus used by Causton and McEnaney. (Ref. [2.3])

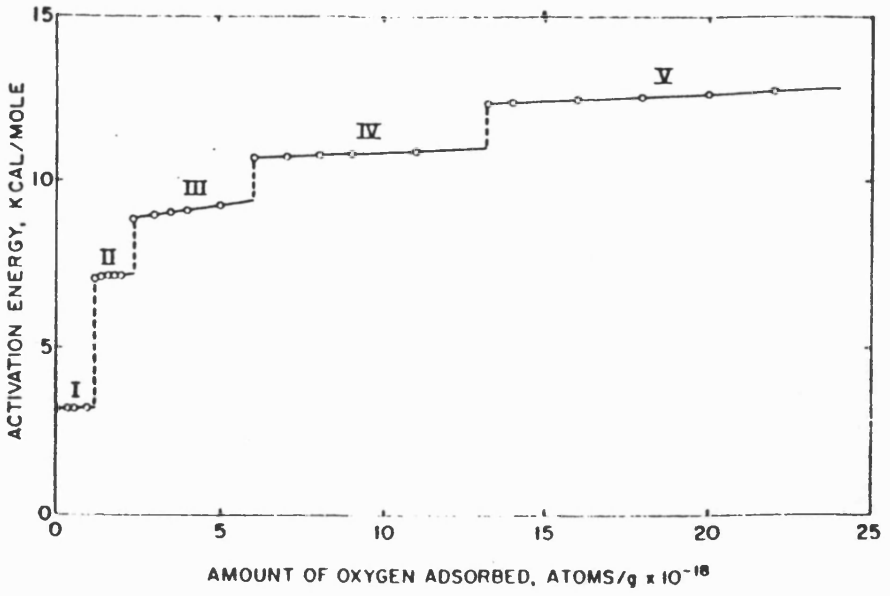

Figure 1.3 Slopes of Elovich plots as a function of oxygen adsorbed at 398 K obtained by Bansal *et al.* (Ref. [1.26])

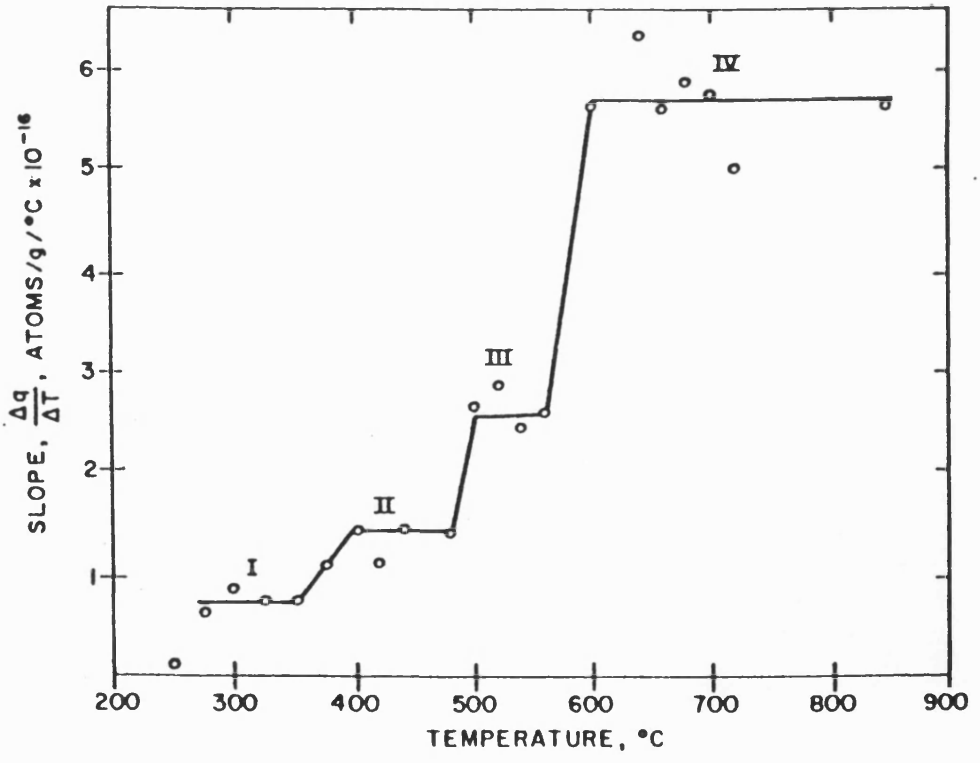

Figure 1.4 Slopes of the desorption plot as a function of temperature obtained by Bansal *et al.* (Ref. [1.72])

Chapter 2

EXPERIMENTAL

In this chapter, the materials used in this project, the experimental system and data-collection and treatment methods are described. The experimental procedures for calibration and various TPD measurements are described in Chapter 3 and Chapter 4 respectively.

2.1 Materials

2.1.1 Coal Chars

For this project the Coal Research Establishment (CRE), British Coal, Stoke orchard, provided five coals and a coal char. They are as follows:

Longannet coal

Bagworth coal

Tilmanstone coal

Cynheidre pumpquart coal

Baddesley coal

Baddesley coal char

Details of their proximate and ultimate analyses provided by CRE are given in Table 2.1-2.5. They were first size-graded

by collecting the fraction in the mesh screen range of 0.100 - 0.350 mm. The five coal particle samples were then carbonized in a horizontal tube furnace by heating at 3 K/min to 1273 K in a stream of deoxygenated argon (flow rate, 100 ml/min) and dwelling at 1273 K for 5 h. After carbonization they were size-graded again by collecting the fraction in the mesh screen range of 0.125 - 0.250 mm.

Since some of the mineral matter in the chars may be catalytic to CO_2 gasification, the five chars from as-received coals were washed with HCl and HF to remove essentially all the inorganic constituents [2.1] according to following procedures:

i. 40 ml of 5 N HCl were added to 6 g of coal in a plastic beaker, the mixture was stirred for 1 h at 330 - 335 K;

ii. the coal was then filtered off and mixed with 40 ml of full strength (29N) HF, the mixture was also stirred at 330 - 335 K for 1 h;

iii. subsequently, the coal was filtered off again and mixed with 40 ml of full-strength HCl for a third treatment at the same temperature for 1 h;

iv. finally, the coal was filtered off, washed with warm distilled water until no chloride ion was detected in the filtrate (with 0.1 N $AgNO_3$), and dried at 523 K.

The ash contents of these five demineralised coal chars are tabulated in Table 2.6 where they are compared with the ash content of an undemineralised Baddesley coal char.

2.1.2 PVDC Chars

A carbon obtained from a polyvinylidene chloride-polyacrylonitrile copolymer, supplied by Aldrich Chemical Company Inc, was used as model char in this study and was obtained using the same heating program as that for coal chars. The carbon yield of PVDC is 30.0 wt% of the polymer and its ash content is low in comparison with those of the coal chars in Table 2.6.

2.1.3 Other Chars and Carbons

Active surface area measurements were also made on an anode electrode carbon as used in aluminium smelting. The carbon was produced from a petroleum coke filler and a coal tar pitch binder by a conventional carbon manufacturing route. It also incorporates recycled anode carbon butts as additional filler materials. The electrode carbon was provided by Comalco Research Centre, Melboune, Australia, and is designated as Electrode 706.

2.1.4 Gases

All the gases used in this study were supplied by British Oxygen Corporation and were high purity grade (99.99%). Ar was further deoxygenated by passing through an oxygen trap to remove residue oxygen. Ar, CO and CO_2 were checked with mass spectrometer and no detectable oxygen was found before use. All the gases used in this work were dried by passing through 5 A molecular sieve before use.

2.2 Experimental System

Figure 2.1 shows the block diagram of the dynamic TPD-MS system used in this work. It consists of four parts: (i) reactor and gas inlet and outlet system, (ii) a furnace and temperature-controller, (iii) a high vacuum pumping assembly and (iv) a gas analyser, *i.e.*, a quadrupole mass spectrometer.

2.2.1 Reactor and Gas Inlet and Outlet System

The reactor used in the previous work [2.3] is shown in Figure 2.2, from which the chars after gasification had to be transferred to another reactor to measure ASA. This transfer means that the sample were exposed to atmosphere and the surface conditions could be changed and its burn-off

could not be assessed accurately. Hermann and Huttinger [2.4] used another type of reactor in the TPD study of chars quenched during H_2O gasification. However, it possesses the same problem. Therefore, a new quartz reactor and gas inlet and outlet system was designed.

This newly designed assembly shown schematically in Figure 2.3 enables gasification and TPD after quenching a sample during gasification to be performed in the same reactor. Gas is introduced into the double-wall reactor of A and preheated in the reactor jacket B before reaching the sample C. The bottom part of the reactor D was designed with only a single wall in order to achieve a high quenching rate. The moveable sample bucket at C could be taken out of the reactor to measure the burn-off of the sample after gasification. Gas exits the reactor at E and the whole reaction system was isolated from the atmosphere with an oil-sealing device F.

The operation procedure of the reactor was also carefully designed to prevent the sample being blown out of the reactor when gas was introduced directly from bottom. Note that after outgassing, the reactor chamber was under high vacuum so that there was a big difference of the pressures between the reactor chamber and the gas at 1 atm to be admitted.

In outgassing process, the valves 1, 2 and 4 were closed and the gas evolved was pumped out through valves 3 and 5. During oxygen chemisorption or CO_2 gasification process, valves 2 and 5 were first closed and the oxidant at atmospheric pressure was initially admitted through valves 1, 4 and 3 into the upper part of the reactor and down to the sample bucket. The amount of gas introduced was carefully controlled by adjusting valve 1. The inside pressure of the reactor was observed from the oil level of the oil-sealing device F. When the inside pressure was equal to the atmospheric pressure, valves 1 and 4 were closed and valves 2 and 5 were subsequently opened. Only at this time was the gas introduced into the bottom of the reactor and up to the outlet through the sample. By careful operation of above procedure, disturbance of the sample by the introduced gas to the sample was avoided.

2.2.2 Furnace and Temperature-Controller

The furnace used was a nickchrome-wound electrical resistance furnace with a maximum temperature of 1473 K. It was placed on a vertically movable stool for the quenching operation and controlled by an Eurotherm controller (Type 812) combined with a Ni/Cr-Ni/Al thermocouple. The furnace temperature was monitored by a potentiometric recorder. A

correction was made for the difference between the temperature of the sample position and the furnace control thermocouple, Figure 2.4. The equation of correction was included in computer program.

2.2.3 Vacuum Assembly

In a volumetric system for oxygen chemisorption study, a limited amount of oxygen is admitted to a constant volume chamber. Therefore, it is crucially important, as pointed by Walker *et al* [2.5], to first create an ultra-high vacuum system of up to 10^{-8} Pa to obtain a very clean surface for the subsequent oxygen chemisorption study. In the present experimental assembly for dynamic oxygen chemisorption study, oxygen flows through the sample continuously for as long as 12 h. Because of its strong affinity with carbon, the flowing oxygen displaces residue contaminates on sample surface like the carrier gas in a gas chromatographic column. For such experiments a conventional high vacuum system (minimum pressure 10^{-5} Pa, consisting of a diffusion pump backed with a rotary pump) is sufficient.

All of the joints in the gas inlet and outlet routine were sealed with rubber O-rings. In order to protect the connecting O-rings in the upper part of the reactor, a

water-cooled copper cooling pipe was wrapped on the outside of the reactor neck.

The total minimum pressure of the system read from the mass spectrometer was about 1.5×10^{-5} Pa at temperatures up to 523 K and 2.5×10^{-5} Pa at temperatures up to 1473 K. Figure 5.5 shows a typical result of blank assay. It confirms this vacuum system worked very well.

2.2.4 Mass Spectrometer

In the TPD-MS system the evolved gas was analysed by a quadrupole mass spectrometer, a Spectromass Visa produced by Spectrum Scientific Ltd. Its specifications are as follows:

Mass range: 1-100 amu

Minimum detectable partial pressure: 10^{-9} Pa

Maximum operating pressure: 10^{-2} Pa

Energy level of electrons from filament: 70 eV

Scanning period: fixed.

The mass spectrometer in "Preset peaks" mode could monitor partial pressures of the six factory-set masses. They are:

2 hydrogen

18 water

28 nitrogen/carbon monoxide

32 oxygen

43 hydro-carbon

44 carbon dioxide.

Each of the six masses was taken in turn and measured automatically. At the start of every scan the total pressure was also measured. All of the above measurements were auto gain, *i.e.*, when the peak height moved outside the auto range limits of 6% and 99%, the gain range was adjusted automatically to bring the measurement back within the above limits. However, only two digits of the pressure values were outputted leading to unsmooth TPD curves in some cases.

2.3 Data Collection and Treatment

The mass spectrometer was interfaced with a dedicated microcomputer (Type Amstrad PC1512DD) and software was written for control of experiments, data collection and analysis. The background contribution of nitrogen and other gases were determined from spectra taken immediately before TPD experiment and subtracted in every scanning period.

References

[2.1] L. R. Radovic, P. L. Walker, Jr. and R. G. Jenkins, *Fuel*, **62**, 849(1983).

[2.2] P. Causton and B. McEnaney, *Fuel*, **64**, 1447(1985).

[2.3] P. Causton, PhD Thesis, University of Bath (1985).

[2.4] G. Hermann and K. J. Huttinger, *Carbon*, **24**, 705(1986).

[2.5] P. L. Walker, Jr., R. C. Bansal and F. J. Vastola, "*The Structure and Chemistry of Solid Surfaces*", John Wiley, New York, p.81(1969).

Table 2.6 Ash contents of PVDC char and coal chars

Char		Ash content (%)
PVDC		0.27
Baddesley	(Undem)	13.95
Baddesley	(Dem)	1.18
Cynheidre	(Dem)	0.32
Bagworth	(Dem)	0.52
Longannet	(Dem)	1.18
Tilmanstone	(Dem)	0.70

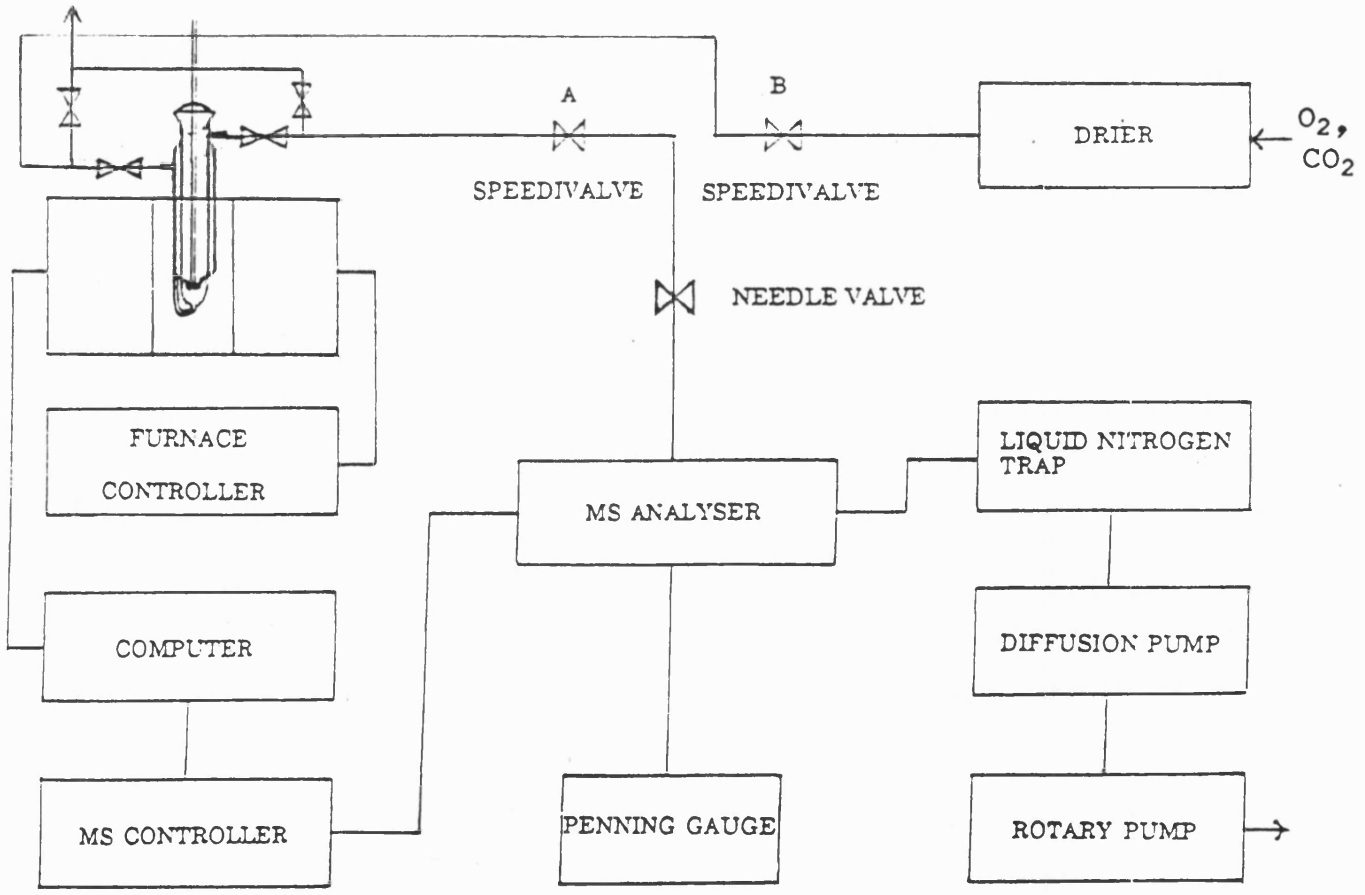

Figure 2.1 Block diagram of the TPD-MS system used in this work.

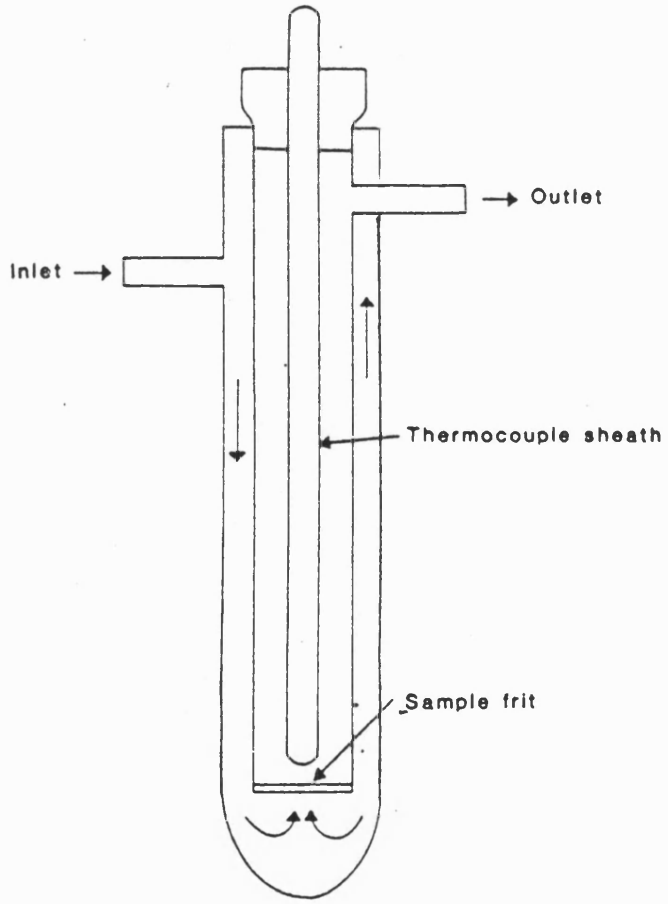

Figure 2.2 Gasification reactor (Ref [2.3])

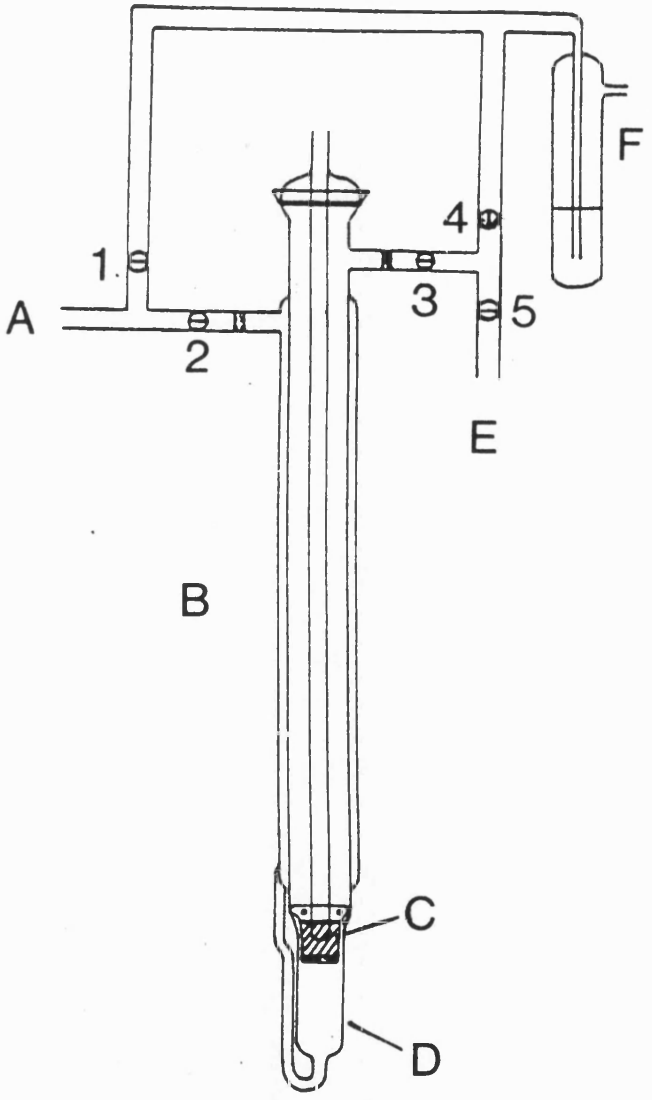

Figure 2.3 Reactor and gas inlet and outlet System

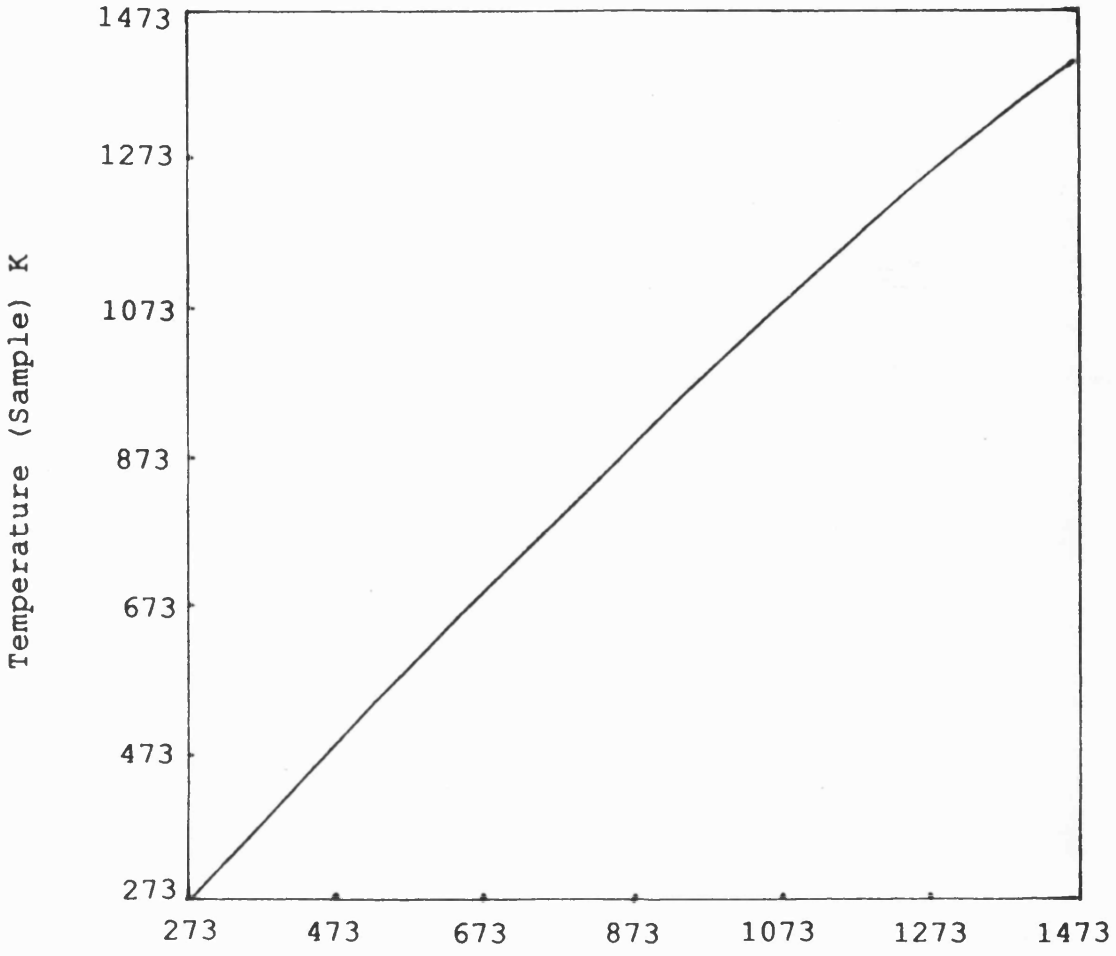

Figure 2.4 Plot of temperature correction.

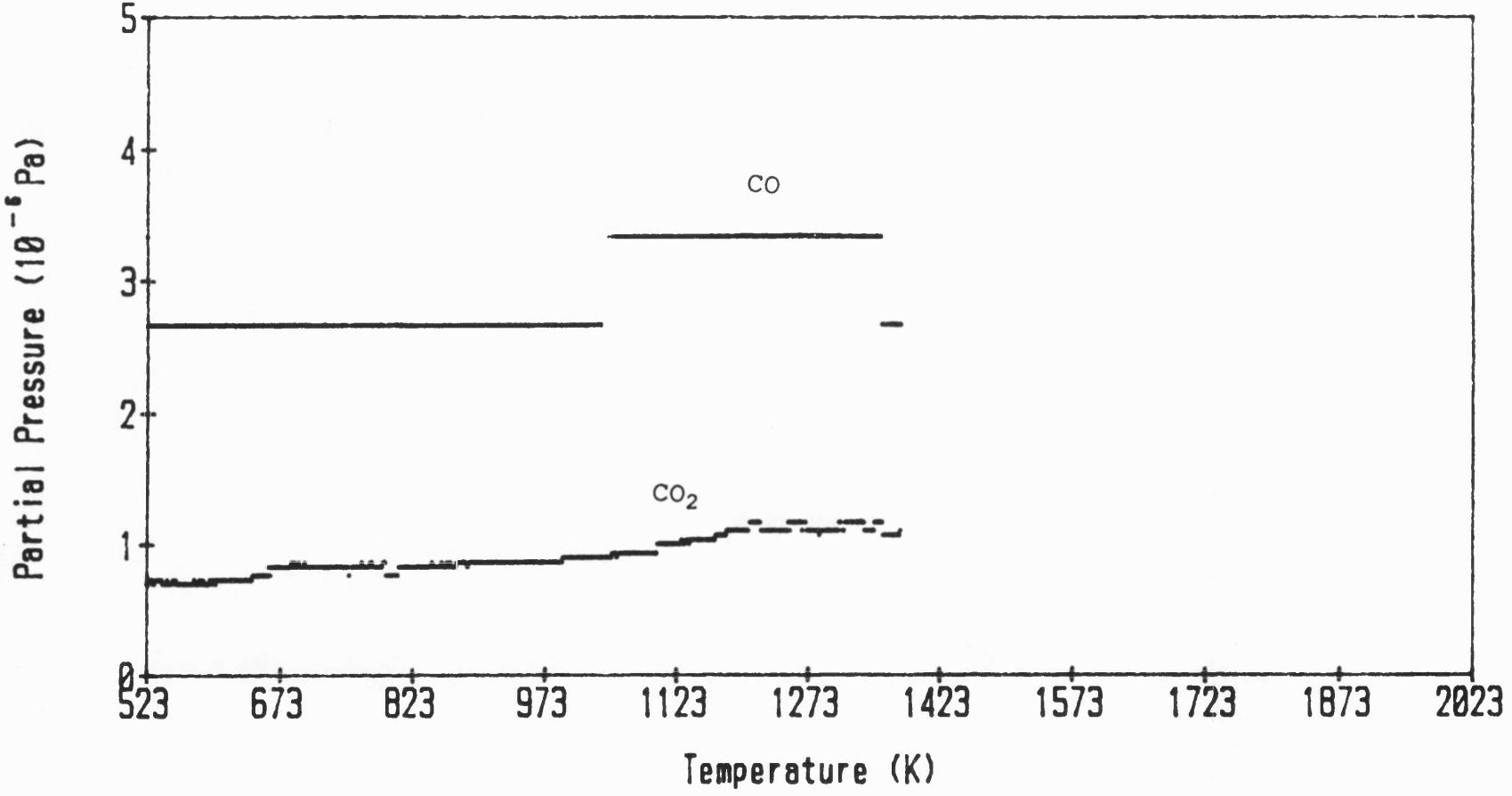

Figure 2.5 Blank assay.

Table 2.1 Proximate and Ultimate analyses of Longannet (Hirst) Coal

COAL: LONGANNET (HIRST)

NCB COAL RANK COAL: N/A

PROXIMATE ANALYSIS %

Moisture	]		9.2
Ash	]	ad	10.8
Volatile Matter	]		28.0
Fixed Carbon	]		52.0
Volatile Matter	[daf]		35.0

CAKING PROPERTIES

Swelling Index	2½
Gray-King Cake Type	C

CALORIFIC VALUE

kJ/kg	[daf]	32940

ASH FUSION RANGE*

Deformation Temperature	>1500
Hemisphere Temperature	>1500
Flow Temperature	>1500

ULTIMATE ANALYSIS %

Carbon	]		82.90
Hydrogen	]	dmmf	5.00
Oxygen	]		10.00
Nitrogen	]		1.63
Sulphur Organic	]		0.33
Sulphate as S	]		0.02
Pyritic Sulphur as S	]	db	0.02
Chlorine	]		0.12
Carbon Dioxide	]		0.13
Mineral Matter	]		12.98

MACERAL ANALYSIS

% Volume[2]	Vitrinite	81
	Exinite	4
	Inertinite	15

MEAN MAXIMUM REFLECTANCE[3] % - 0.688

SD % - 0.080

N/A Not applicable - ash content >10%

* Test atmosphere - Reducing (50% CO_2/50% H_2)

[2] Mineral matter/coal shale free basis

[3] Total no. of points - 100

ad - as analysed basis

db - dry basis

daf - dry, ash free basis

dmmf - dry, mineral matter free basis

Table 2.2 Proximate and Ultimate analyses of Bagworth Coal

COAL: BAGWORTH

NCB COAL RANK COAL: 902

PROXIMATE ANALYSIS %

Moisture	]		13.7
Ash	]	ad	7.6
Volatile Matter	]		34.1
Fixed Carbon	]		44.6
Volatile Matter	[daf]		43.3

CAKING PROPERTIES

Swelling Index	½
Gray-King Cake Type	B

CALORIFIC VALUE

kJ/kg	[daf]	32640

ASH FUSION RANGE*

Deformation Temperature	1180°C
Hemisphere Temperature	1210°C
Flow Temperature	1330°C

ULTIMATE ANALYSIS %

Carbon	]		80.60
Hydrogen	]	dmmf	5.4
Oxygen	]		11.30
Nitrogen	]		1.37
Sulphur Organic	]		0.69
Sulphate as S	]		0.03
Pyritic Sulphur as S	]	db	0.51
Chlorine	]		0.10
Carbon Dioxide	]		0.88
Mineral Matter	]		10.57

MACERAL ANALYSIS

% Volume[2]	Vitrinite	72
	Exinite	5
	Inertinite	23

MEAN MAXIMUM REFLECTANCE[3] % - 0.731

SD % - 0.062

* Test atmosphere - Reducing (50% CO_2/50% H_2)

[2] Mineral matter/coal shale free basis

[3] Total no. of points - 100

ad - as analysed basis

db - dry basis

daf - dry, ash free basis

dmmf - dry, mineral matter free basis

Table 2.3 Proximate and Ultimate analyses of Tilmanstone Coal

COAL: TILMANSTONE

NCB COAL RANK COAL: 203

PROXIMATE ANALYSIS %

Moisture	]		0.7
Ash	]	ad	5.4
Volatile Matter	]		16.0
Fixed Carbon	]		77.9
Volatile Matter	[daf]		17.0

CAKING PROPERTIES

Swelling Index	8
Gray-King Coke Type	G3

CALORIFIC VALUE

kJ/kg	[daf]	36500

ASH FUSION RANGE*

Deformation Temperature	1090°C
Hemisphere Temperature	1120°C
Flow Temperature	1160°C

ULTIMATE ANALYSIS %

Carbon	]		92.40
Hydrogen	]	dmmf	4.50
Oxygen	]		2.00
Nitrogen	]		1.45
Sulphur Organic	]		0.67
Sulphate as S	]		0.02
Pyritic Sulphur as S	]	db	0.54
Chlorine	]		0.08
Carbon Dioxide	]		0.34
Mineral Matter	]		6.53

MACERAL ANALYSIS

% Volume[2]	Vitrinite	65
	Exinite	0
	Inertinite	35

MEAN MAXIMUM REFLECTANCE[3] % - 1.680
SD % - 0.052

* Test atmosphere - Reducing (50% CO_2/50% H_2)
[2] Mineral matter/coal shale free basis
[3] Total no. of points - 100
ad - as analysed basis
db - dry basis
daf - dry, ash free basis
dmmf - dry, mineral matter free basis

Table 2.4 Proximate and Ultimate analyses of Cynheidre pumpquart Coal

COAL: CYNHEIDRE PUMPQUART

NCB COAL RANK COAL: 101

PROXIMATE ANALYSIS %

Moisture	ad	1.6
Ash	ad	1.8
Volatile Matter	ad	4.6
Fixed Carbon	ad	92.0
Volatile Matter	[daf]	4.8

CAKING PROPERTIES

Swelling Index	0
Gray-King Cake Type	A

CALORIFIC VALUE

kJ/kg	[daf]	35640

ASH FUSION RANGE*

Deformation Temperature	1210°C
Hemisphere Temperature	1230°C
Flow Temperature	1330°C

ULTIMATE ANALYSIS %

Carbon	dmmf	95.20
Hydrogen	dmmf	2.90
Oxygen	dmmf	0.90
Nitrogen	dmmf	1.00
Sulphur Organic	db	0.59
Sulphate as S	db	0.02
Pyritic Sulphur as S	db	0.02
Chlorine	db	0.03
Carbon Dioxide	db	0.22
Mineral Matter	db	2.11

MACERAL ANALYSIS

% Volume[2]	Vitrinite	74
	Exinite	0
	Inertinite	26

* Test atmosphere - Reducing (50% CO_2/50% H_2)
[2] Mineral matter/coal shale free basis
[3] Total no. of points - 100
ad - as analysed basis
db - dry basis
daf - dry, ash free basis
dmmf - dry, mineral matter free basis

Table 2.5 Proximate and Ultimate analyses of Baddesley Coal

Analysis wt (%)		Coal	Char
Moisture	ad	7.7	3.4
Ash	ad	3.6	33.6
Carbon	db	79.0	68.3
Hydrogen	db	5.2	ND
Oxygen	db	9.0	ND
Nitrogen	db	1.35	ND
Total sulphur	db	1.53	1.23
Sulphate	ad	0.02	ND
Pyritic	ad	0.26	ND
Vol Mat	daf	42.30	9.8
Cl^-	db	0.20	0.02
Na^+	db	0.054	0.18
K^+	db	0.027	0.115
Swelling Index		2	ND

Table 2.6 Ash contents of PVDC char and coal chars

Char		Ash content (%)
PVDC		0.27
Baddesley	(Undem)	13.95
Baddesley	(Dem)	1.18
Cynheidre	(Dem)	0.32
Bagworth	(Dem)	0.52
Longannet	(Dem)	1.18
Tilmanstone	(Dem)	0.70

Chapter 3

CALIBRATION OF TPD-MS SYSTEM

In this work the main experimental technique is TPD-MS, *i.e.*, temperature-programmed decomposition of solid or temperature-programmed desorption of gas from a solid (TPD) combined with mass spectrometry (MS). Generally, the most widely used techniques for evolved gas analysis are mass spectrometry and gas chromatography (GC). They both allow qualitative and quantitative measurements to be made. But because TPD-GC technique employs batch sampling, it is significantly slower in operation. Due to its high sensitivity and specificity, the TPD-MS technique has been applied more frequently in recent years to study the individual characteristics of gases evolved from a solid, and it has been proved to be more conducive to the understanding of thermal decomposition or desorption than techniques involving overall accumulative pressure measurement [3.1-3.5]. However, flow should be characterised in any TPD-MS system which involves less than instantaneous flow of gases from the sample to MS analyser. In addition the interactions between evolved gases must be understood and the system should be calibrated for those gases [3.6]. TPD-MS technique can be further simplified if the flow

characterisation and the calibration of the system for those gases can be carried out using the same mass spectrometer. However, the existing literature in this field is very limited [3.7-3.9].

3.1 Principles of Mass Spectrometry

Since mass spectrometry is the main analysis technique of this study, it is very important to understand its basic principles.

3.1.1 Quadrupole Mass Spectrometer

The mass spectrometer used in this study was a Spectramass Visa, produced by Spectrum Scientific Ltd. It is of quadrupole type and consists of three major components [3.10]: (i) an electron bombardment ion source, (ii) an electric quadrupole analyser, and (iii) a Faraday plate detector.

In the ion source, electrons are emitted from a heated filament and accelerated toward the source cage and pass through it at an energy of 70 eV. Some of the gas molecules entering the ionization chamber are bombarded by electrons and form positive ions, which are drawn or repelled out of

the ionization chamber by means of the focus electrode, which collimates the ion beam into the mass analyser.

The quadrupole analyser consists of four long, parallel electrodes, which are mounted symmetrically about the axis of the filter. The opposite pairs of electrodes are connected together electrically and antiphase DC and RF voltages are applied to the quadrupole array. By selecting appropriate voltages, all desired ions are resonant and so strike the quadrupole rods and are neutralised, only ions with the desired m/e ratio finally reach the collector. The ion current reaching the collector is measured by the Faraday plate detector.

3.1.2 Secondary Fragmentation of CO_2^+

The energy of the electrons in the ion source of the quadrupole mass spectrometer (70eV) is more than sufficient not only to cause significant ionization and formation of parent ions (*e.g.*, the first and the second ionisation potentials of CO and CO_2 are 14.01 and 27.7, 13.79 and 22.6 eV [3.11], respectively), but also to cause further dissociation of parent ions and formation of fragment ions. For carbon monoxide, the following reactions occur:

$$CO + e \longrightarrow CO^+ + 2e$$

$$CO^+ + e \longrightarrow CO^{++} + 2e$$

$$CO^+ + e \longrightarrow C^+ + O^+ + 2e$$

For carbon dioxide, the cracking pattern is more complicated:

$$CO_2 + e \longrightarrow CO_2^+ + 2e$$

$$CO_2^+ + e \longrightarrow CO_2^{++} + 2e$$

$$CO_2^+ + e \longrightarrow CO^+ + O^+ + 2e$$

$$CO^+ + e \longrightarrow C^+ + O^+ + 2e$$

The abundance of A_i^+ ion, f_i, relative to the parent ion A^+ produced from a pure gas A, is defined as the ratio of the ion current of A_i^+, $H(A_i^+)$, and the ion current of the parent ion A^+, $H(A^+)$ [3.12]:

$$f_i = \frac{H(A_i^+)}{H(A^+)} \qquad (3.1)$$

For a given mass spectrometer and a given filament condition, f_i can be regarded as constant in the mass spectrum. It can be seen, from the mass spectra of CO and CO_2 in Tables 3.1 and 3.2 [3.13-3.15], that the qualitative nature of the mass spectra of CO and CO_2 are similar and their quantitative nature depends only slightly upon the electron energies of different mass spectrometers.

3.1.3 Relationship between Gas Pressure and Ion Current

The ion current of the parent ion A^+, $H(A^+)$, of a pure gas A in the ionisation chamber is directly proportional to

the pressure of gas A. The relationship can be conveniently expressed as [3.16]:

$$P_A = H(A^+) \tag{3.2}$$

Also, P_A can be found from the current of an individual ion A_i formed from A by:

$$P_A = H(A_i^+)/f_i \tag{3.3}$$

For a binary mixture of CO and CO_2, the ion current of CO^+ at m/e = 28, $H(CO^+)$, has a contribution due to primary ionisation of CO, $H_{CO}(CO^+)$, and a contribution due to the fragmentation of CO_2^+, $H_{CO_2}(CO^+)$ [3.17]:

$$H(CO^+) = H_{CO}(CO^+) + H_{CO_2}(CO^+) \tag{3.4}$$

Applying Dalton's law of partial pressure, the partial pressure of CO and CO_2, P_{CO} and P_{CO_2}, respectively, can be related to the ion currents as follows:

$$P_{CO} = H(CO^+) - H_{CO_2}(CO^+)$$
$$= H(CO^+) - fH_{CO_2}(CO_2^+) \tag{3.5}$$

$$P_{CO_2} = H(CO_2^+) \tag{3.6}$$

where $H(CO_2^+)$ is the ion current of CO_2 at m/e=44 and f is the abundance of fragmented CO^+ to its parent ion CO_2^+.

3.1.4 Relative Sensitivity

The sensitivity of a mass spectrometer is quoted for dry nitrogen, other gases ionize either more or less readily. Thus the same pressure of different gases will give rise to different ion currents. It is therefore necessary to correct

the apparent partial pressure P_A' indicated on the mass spectrometer to its true pressure P_A by using the sensitivity of the gas relative to nitrogen S_A [3.18]:

$$S_A = \frac{P_A'}{P_A} \tag{3.7}$$

3.2 Principle of TPD-MS Analysis

Generally speaking, the principle of TPD-MS analysis is adapted to the principle of gas chromatographic analysis of TPD curves. The flow of carrier gas is constant in GC analysis. The pumping rate has also to be constant in a TPD-MS system. Indeed, this constant pumping rate is a characteristic of diffusion pumps in a wide range of working pressure.

3.2.1 For Pure Gas

A general analysis of TPD-MS may be developed [3.16] by considering a schematic evolution curve of pressure of a pure gas A, in which $P_A(t)$ is a function of time t (figure 3.1a) at the mass spectrometer sampling port at temperature T (K) (Figure 3.1b). Assuming ideal gas behaviour:

$$P_A(t)Q_A = n_A(t)RT \tag{3.8}$$

where Q_A is the pumping speed (m^3/s) for gas A from the sampling port,

$n_A(t)$ is the molar flux (mol/s) of gas A out of the sampling vessel at time t,

R is the universal gas constant.

Substituting Equation (3.7) into Equation (3.8) gives

$$\frac{P_A'(t)Q_A}{S_ART} = n_ART \qquad (3.9)$$

The assumption that Q_A is constant over the time interval t_1 to t_2 is valid if the pumping rate is controlled by Knudsen diffusion [3.19], as is the case in this study. The total pressure range of the TPD-MS system used in this work is within the range of 1.0 - 10^{-6} Pa where the pumping speed of the vacuum system is independent of total pressure [3.20].

Since the pressure of gas A is defined as the ion current of its parent ion $H(A^+)$, integration of the TPD curve in Figure 3.1a leads to:

$$\frac{Q_A}{S_A}\int_{t_1}^{t_2} H_A(t)\,dt = RT\int_{t_1}^{t_2} n_A(t)\,dt \qquad (3.10)$$

where t_1 and t_2 are the starting and finishing times, respectively. If the integral of the left-hand side of Equation (3.10) is $I(A^+)$, the area under the curve of ion current *versus* time t and the integral on the right-hand side is N_A, the total number of moles of gas A evolved in the time interval $t_2 - t_1$, then Equation (3.10) can further be written as:

$$N_A = \frac{Q_A I(A^+)}{RTS_A} = K_A(T)\, I(A^+) \qquad (3.11)$$

where $K_A(T) = Q_A/RTS_A$.

Subsequently, the amount of A can be determined directly from the integration of the curve. On the above basis, TPD-MS technique may be calibrated by determination of N_A and $I(A^+)$ using a reaction which gives rise to a known amount of gas A. The calibrated N_A - I_A curve should be a straight line passing through the origin.

3.2.2 For the Mixture of CO and CO_2

For the measurement of CO in a mixture of CO and CO_2, the contribution of the fragment of CO^+ from CO_2 must be considered as discussed in Section 3.1.2 and 3.1.3. Combining Equation (3.5) and (3.11) gives

$$N_{CO} = K_{CO}(T)\,[I(CO^+) - fI(CO_2^+)] \qquad (3.12)$$

The measurement of CO_2 is simple:

$$N_{CO2} = K_{CO_2}(T)\, I(CO_2^+) \qquad (3.13)$$

3.3 Calibration Experimental

Calcium carbonate and oxalate samples in the range of 10-50 μmole were firstly outgassed in a quartz reactor to 10^{-5} Pa at 523 K. They then subject to TPD at 150 K/h under

vacuum. Experiments were designed to ensure that the maximum total pressure and the partial pressures during TPD were within the pressure limitations for linear response of the mass spectrometer.

3.4 Calibration with $CaCO_3$

3.4.1 Principle of the Calibration with $CaCO_3$

Calcium carbonate decomposes completely at high temperature and evolves CO_2 according to the following equation [3.21]:

$$CaCO_3 = CaO + CO_2 \qquad (3.I)$$

The TPD-MS system was initially calibrated for CO_2 with different molar amounts of calcium carbonate using Equation (3.11). A typical TPD spectrum is shown in Figure 3.2. The main peak at m/e = 44 is due to the parent ion CO_2^+ and the minor peak at m/e = 28 is due to CO^+ ion formed from the secondary fragmentation of CO_2^+. The CO^+ curve follows the CO_2^+ curve faithfully because CO^+ ions were produced by CO_2^+ ions in the ionisation chamber of the mass spectrometer. From Equations (3.3) and (3.10) it can be deduced that the ratio of the area under CO^+ curve and the area under CO_2^+ should be the relative abundance of CO^+ in the spectrum of CO_2, *i.e.*,

$$f = \frac{\int_{t_1}^{t_2} H(CO^+)\,dt}{\int_{t_1}^{t_2} H(CO_2^+)\,dt} = \frac{I(CO^+)}{I(CO_2^+)} \qquad (3.14)$$

The molar amount N_{CO_2} of CO_2 produced should be linearly related to $I(CO_2^+)$, the areas under TPD curve of $CaCO_3$. According to Equation (3.11), this leads to the following equation:

$$N_{CO_2} = K_{CO_2} I(CO_2^+) \qquad (3.15)$$

3.4.2 Result of Calibration with $CaCO_3$

The calibration results are tabulated in Table 3.3 and plotted in Figure 3.3, which shows a linear relationship with a slope K_{CO_2} = 12.1 μmol/Pa.s. The relative abundance of CO^+ in the spectra of CO_2 was taken as the mean value of the ratios of $I(CO^+)/I(CO_2^+)$, *i.e.*, f = 0.114.

During TPD of $CaCO_3$ it was found that with increasing sample amount the maximum detecting pressure of 10^{-2} Pa was expected if the sample size was over 100 μmol with the result the upper part of TPD curve was cut off giving a flat peak and smaller I_{CO_2}/N_{CO_2} values. Although this phenomenon could be avoided both by carrying out calibrations using a

smaller heating rate and adjusting the needle valve to reduce the effective pumping speed, it was preferable to keep the needle valve fully open and to use a smaller heating rate, 150 K/h. This is because the throttling down the needle valve increases the pressure in the reactor chamber and may cause secondary reactions, such as the readsorption of the species desorbed.

3.5 Calibration with CaC_2O_4

3.5.1 Principle of Calibration with CaC_2O_4

For the calibration of TPD-MS system for both CO and CO_2 desorbed from carbons, the decomposition of anhydrous calcium oxalate seems to be appropriate, because it has been thoroughly investigated by means of TG, DTA and IR techniques [3.22-3.25]. Normally the following two stages have been identified in the decomposition:

Stage I: $CaC_2O_4 = CaCO_3 + CO$ (3.II)

Stage II: $CaCO_3 = CaO + CO_2$ (3.I)

However, most published research was carried out under static air atmosphere where reaction (3.II) being immediately followed by the heterogeneous exothermic reaction:

$$2CO + O_2 = 2CO_2 \quad (3.III)$$

which often occurs at the temperature of stage I due to the catalytic effect of such crucible materials as, for example, platinum.

A characteristic feature of stage I of the decomposition of calcium oxalate under high vacuum is the formation of carbon dioxide by the disproportionation of CO and the production of fine carbon particles in the reaction residue:

$$2CO = CO_2 + C \qquad (3.IV)$$

This feature was clearly demonstrated in the work by Price *et al* [3.26]. They studied this reaction with a time-of-flight mass spectrometer under various conditions and reported that the extent of reaction (3.IV) varies widely with the environmental conditions. Their typical finding is shown in Figure 3.4.

The typical TPD curve of calcium oxalate obtained in this work is shown in Figure 3.5, which consists of four peaks. In addition to the three peaks found by Price *et al* [3.26], a CO^+ peak was found at about 923 K associated with stage II decomposition. This is due to at least in part to the formation of the fragment ion of CO^+ from CO_2 and may also be due to the reverse of reaction (3.IV) (the Boudouard reaction) [3.27], *i.e.*,

$$CO_2 + C = 2CO \qquad (3.V)$$

In the present investigation very fine carbon particles were found with CaO remaining after the decomposition of calcium oxalate. This is in agreement with Price *et al* 3.26]. The high formation temperature of CO_2 and the existence of calcium oxide are favourable to this reaction.

In stage I, the total molar amount N_{CO} of CO produced should equal to the sum of the amount N^{I}_{CO} of CO formed directly and twice of the amount N^{II}_{CO2} of CO_2 produced by disproportionation:

$$N_{CO} = N^{I}_{CO} + 2N^{II}_{CO2} \qquad (3.16)$$

For the gas mixture produced in stage I, Equations (3.12) and (3.13) can be applied:

$$N^{I}_{CO} = K_{CO}(T)\,[I^{I}(CO^{+}) - fI^{I}(CO_2^{+})] \qquad (3.17)$$

$$N^{I}_{CO2} = K_{CO2}(T)\,I^{I}(CO_2^{+}) \qquad (3.18)$$

where $I^{I}(CO^{+})$ and $I^{I}(CO_2^{+})$ are the areas under the curves of the ion currents of CO^{+} and CO_2^{+} *versus* time t in stage I, respectively.

It can be seen from Equations (3.16), (3.17) and (3.18) that K_{CO} cannot be obtained by integration of the TPD peak for CO^{+} during stage I using different amount of calcium oxalate, if K_{CO2} and f are not obtained in advance.

In stage II, the total molar amount N_{CO2} of CO_2 produced should be the sum of the amount N^{II}_{CO2} of CO_2 formed directly

and a half of the amount N^{II}_{CO} of CO produced from reaction (3.V):

$$N_{CO2} = N^{II}_{CO2} + 0.5N^{II}_{CO} \quad (3.19)$$

Applying Equations (3.12) and (3.13) again leads to the following:

$$N^{II}_{CO2} = K_{CO_2}(T)\, I^{II}(CO_2^+) \quad (3.20)$$

$$N^{II}_{CO} = K_{CO}(T)\,[I^{II}(CO^+) - fI^{II}(CO_2^+)] \quad (3.21)$$

where $I^{II}(CO^+)$ and $I^{II}(CO_2^+)$ are the areas under the curves of the ion currents *versus* time of CO^+ and CO_2^+ in stage II, respectively.

To obtain K_{CO2} from stage II, it is necessary to obtain K_{CO} and f in advance, if reaction (3.V) cannot be neglected, as is the case in this work. Therefore, it is impossible to calibrate accurately the TPD-MS system only with different amount of calcium oxalate. It is necessary to calibrate the system first with calcium carbonate to obtain f, the relative abundance of CO^+ in the spectrum of CO_2 and K_{CO2}, the proportionality constant in Equation (3.15). For the decomposition of calcium oxalate, only stage I is useful for the calibration of the system for CO, although stage II can be used to double-check the calibration results with calcium carbonate.

3.5.2 Calibration Results with CaC_2O_4

Using $K_{CO_2}(T)$ = 12.1 μmol/Pa.s and f = 0.114, which were taken from the calibration result with calcium carbonate, to analyse the calibration results in stage I of the decomposition of calcium oxalate tabulated in Table 3.4 with Equations (3.16), (3.17) and (3.18), a good linear relationship between N_{CO} and $[I^I(CO^+) - fI^I(CO_2^+)]$ with $K_{CO}(T)$ = 10.4 μmol/Pa.s is shown in Figure 3.6. It can also be seen in Table 3.4 that the extent of reaction (3.IV) in stage I of the decomposition of calcium oxalate decreases following the increase of the sample size and varies from 52-54%, which indicates almost one half of the CO produced disproportionates.

Using $K_{CO}(T)$ = 10.4 μmol/Pa.s, which was taken from the calibration result of the stage I of the decomposition of calcium oxalate, and f = 0.114, which was taken from the calibration result with calcium carbonate, to analyse the calibration results in stage II of the decomposition of calcium oxalate tabulated in Table 6.5 with Equations (3.19), (3.20) and (3.21), a good linear relationship between $N^{II}_{CO_2}$ and $I^{II}(CO_2^+)$ with $K_{CO_2}(T)$ = 12.0 μmol/Pa.s is shown in Figure 3.7. This value of $K_{CO_2}(T)$ is in very good agreement with the value obtained from the calibration with calcium carbonate. It can also be seen that the ratio

$N^{II}(CO_2)/N(CO_2)$ decreases progressively from 0.977 to 0.935 with the increasing sample size. Thus, although it is small, the extent of the secondary reaction between CO_2 and residual carbon is significant and must be considered if an accurate calibration is to be achieved.

3.5 Calibration for Other Gases

The above method can be used to calibrate the TPD-MS system for CO and CO_2, although it is very complicated. For other gases because it is not always possible to find a suitable decomposition for calibration, it is important to find a universal method for the calibration.

From Equation (3.11), it can be deduce that the ratio between the proportional constants $K_A(T)$ of a gas A and $K_{CO2}(T)$ of CO_2 can be expressed as:

$$\frac{K_A(T)}{K_{CO2}(T)} = \frac{Q_A S_{CO2}}{Q_{CO2} S_A} \tag{3.23}$$

Assuming molecular flow, it is expected that [3.28]:

$$\frac{Q_A}{Q_{CO2}} = \left(\frac{M_{CO2}}{M_A} \right)^{0.5} \tag{3.24}$$

$$K_A(T) = K_{CO2}(T) \frac{S_{CO2}}{S_A} \left(\frac{M_{CO2}}{M_A} \right)^{0.5} \tag{3.25}$$

where $K_{CO2}(T)$ can be obtained from the calibration of the system with calcium carbonate. If the sensitivity of gas A

relative to CO_2 can be measured, the constant $K_A(T)$ may be calculated from Equation (3.25). Therefore, the TPD-MS system may be calibrated for any gas, no matter whether the gas can be produced by a quantitative decompasition of a chemical compound.

References

[3.1] H. L. Friedman, *Thermochim. Acta*, **1**, 199(1970).

[3.2] D.Price, "*Dynamic Mass Spectrometry, Vol. 4*", (ed. D. Price and J. F. J. Todd), Heyden and Sons., London, pp.1-9(1979).

[3.3] J. F. Smith, *Int. J. Mass Spectrom. Ion Phys.*, **26**, 149(1978).

[3.4] M. R. Holdiness, *Thermochim. Acta*, **75**, 361(1984).

[3.5] D. Price and G. A. Milnes, *Int. J. Mass Spectrom. Ion Phys*. **60**, 61(1984).

[3.6] D. Dollimore, G. A. Gamlen, and T. J. Taylor, *Thermochim. Acta*, **75**, 59(1984).

[3.7] D. E. Gilmartin, AD-A119 494, F04701-81-C-0082(1982).

[3.8] S. Bernal, R. Garcia and J. M. Rodriguez-Izquierdo, *Thermochim. Acta*, 70, 249(1983).

[3.9] P. Causton and B. McEnaney, *Fuel*, **64**, 447(1985).

[3.10] R. W. Kiser, "*Introduction to Mass Spectrometry and Its Application*", Prentice-Hall, New York, pp.86-

89(1965).

[3.11] R. W. Kiser, "*Introduction to Mass Spectrometry and Its Application*", Prentice-Hall, New York, pp.309-310(1965).

[3.12] R. W. Kiser, "*Introduction to Mass Spectrometry and Its Application*", Prentice-Hall, New York, pp.118-140(1965)

[3.13] "*Spectromass Product Instruction Manual*", Edwards High Vacuum, West Sussex, UK, p.6.16(1983).

[3.14] Mass Spectrometry Data Centre (Compil. edition), "*Eight Peak Index of Mass Spectra*", 2nd Edit., (1974).

[3.15] A. Cormi, R. Massot, "*Compilation of Mass Spectrum Data, Vol. 2*", 2nd Edit., Heyden and Sons., London, (1975).

[3.16] R. W. Kiser, "*Introduction to Mass Spectrometry and Its Application*", Prentice-Hall, New York, pp.118-120(1965).

[3.17] R. W. Kiser, "*Introduction to Mass Spectrometry and Its Application*", Prentice-Hall, New York, pp.216-226(1965).

[3.18] R. W. Kiser, "*Introduction to Mass Spectrometry and Its Application*", Prentice-Hall, New York, pp.226-229(1965).

[3.19] "*Vacuum Technology - Its Foundation, Formulae and Tables, 1*", HV152, Leybold-Heraeus GmbH, Section H-B,

p.62(1971).

[3.20] "*Edwards Vacuum Products Specification*", Edwards High Vacuum, West Sussex, UK, p.62(1982).

[3.21] K. M. Caldwell, P. K. Gallagher and D. W. Johnson, Jr., *Thermochim. Acta*, **15** 18(1977).

[3.22] W. W. Wendlandt, "*Thermal Methods of Analysis, Vol. 19*", Wiley, New York, p.319(1974).

[3.23] H. L. Frieman, *Thermochim. Acta*, **1**, 199(1970)

[3.24] J. F. Smith, *Int. J. Mass Spectrom. Ion Phys.*, **26**,149(1972).

[3.25] R. R. A. Abou-shaaban and R. Cali, *J. Thermochim. Acta*, **26**, 111(1978).

[3.26] D. Price, D. Dollimore, N. S. Fetemi and A. D. Whitehead, *Thermochim. Acta*, 42, 323(1980).

[3.27] N. M. Laurendau, *Prog. Energy Combust. Sci.*, **4**, 221(1978).

[3.28] G. Lewin, "*Fundamentals of Vacuum Science and Technology*", McGraw Hill, New York, p.13(1965).

Table 3.1 Relative Abundance of Ions in Mass Spectra of CO

m/e	28	16	14	13	12	29	ref.
f	100	2	1	-	5	-	[3.15]
	100	-	-	-	-	1	[3.14]
	100	-	1	-	5	-	[3.14]
	100	2	1	1	5	-	[3.14]
	100	1	1	1	5	-	[3.13]

Table 3.2 Relative Abundance of Ions in Mass Spectra of CO_2

m/e	44	28	16	12	22	45	ref.
f	100	10	10	4	2	1	[3.14]
	100	7	6	2	2	1	[3.14]
	100	13	9	1	1	-	[3.14]
	100	7	6	1	1	-	[3.14]
	100	8	9	7	-	-	[3.15]
	100	7	6	3	2	1	[3.15]
	100	7	6	1	1	1	[3.15]
	100	11	9	6	1	-	[3.13]
	100	11	-	-	-	-	this work

Table 3.3 Calibration Results with $CaCO_3$

N (μmol)	I_{CO_2} (Pa.s)	I_{CO} (Pa.s)	I_{CO}/I_{CO_2}
10.4	0.81	0.092	0.113
13.4	1.11	0.120	0.108
13.6	1.21	0.130	0.107
20.0	1.64	0.187	0.114
22.4	1.88	0.225	0.120
24.1	1.85	0.219	0.118
25.5	2.07	0.225	0.109
31.1	2.59	0.296	0.114
33.9	2.80	0.330	0.118
39.5	3.35	0.391	0.117
50.5	4.29	0.498	0.116
52.6	4.24	0.501	0.118

Table 3.4 Calibration Results with CaC_2O_4 (Stage I)

N_{CO} (μmole)	I^I_{CO} (Pa.s)	$I^I_{CO_2}$ (Pa.s)	N^I_{CO}/N_{CO_2} (%)
10.6	0.49	0.21	52.1
17.0	0.85	0.32	54.4
29.9	1.61	0.57	53.9
35.1	1.90	0.68	53.1
46.9	2.41	0.90	53.6
56.8	3.21	1.10	53.1

* $K_{CO_2}(T) = 12.1$ μmol/Pa.s
$f = 0.114$

Table 3.5 Calibration Results with CaC_2O_4 (Stage II)

N_{CO2} (μmole)	I^{II}_{CO} (Pa.s)	I^{II}_{CO2} (Pa.s)	N^{II}_{CO2}/N_{CO2} (%)
10.6	0.91	0.165	97.7
17.0	1.30	0.215	96.0
29.9	2.41	0.207	96.1
35.1	2.89	0.221	95.4
46.9	3.45	0.252	94.7
56.8	4.31	0.278	93.5

* $K_{CO}(T)$ = 10.4 μmol/Pa.s
f = 0.114

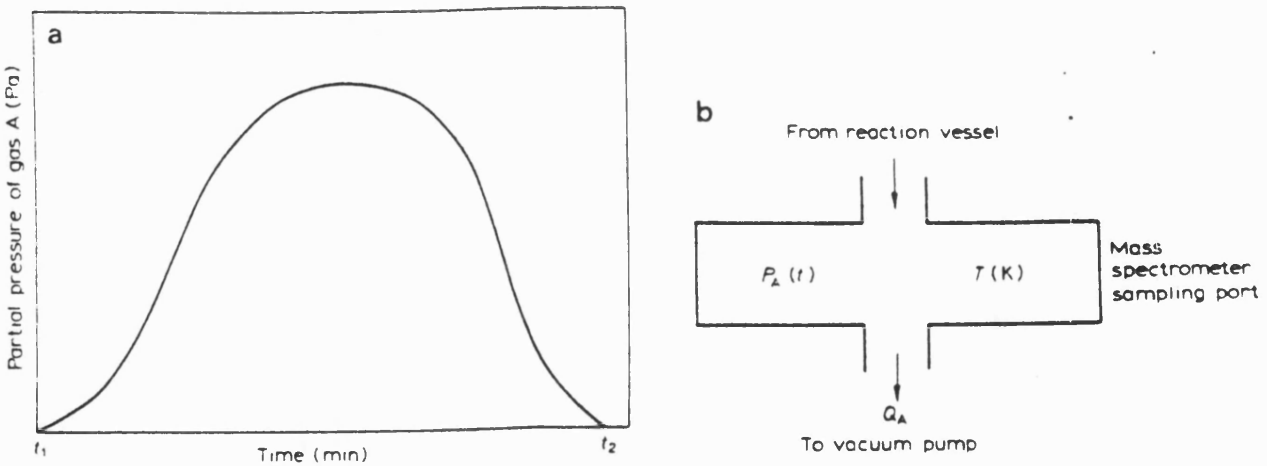

Figure 3.1 (a) Schematic TPD curve of partial pressure of gas A, $P_A(t)$, as a function of time t. (b) Conditions at the mass spectrometer sampling port.

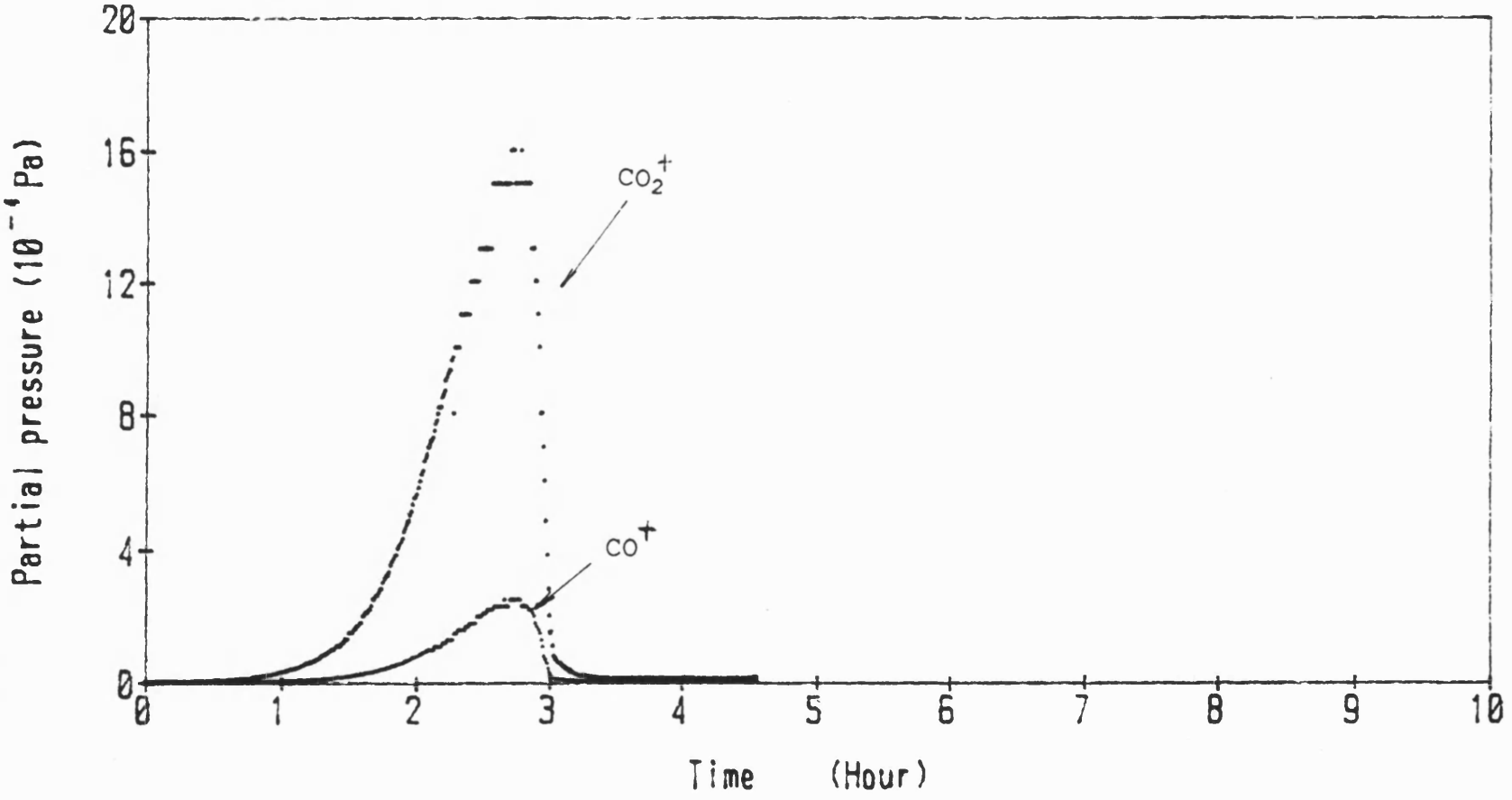

Figure 3.2 Typical TPD curve of $CaCO_3$ decomposition.
heating rate: 150 K/h, minimum temperature: 523 K

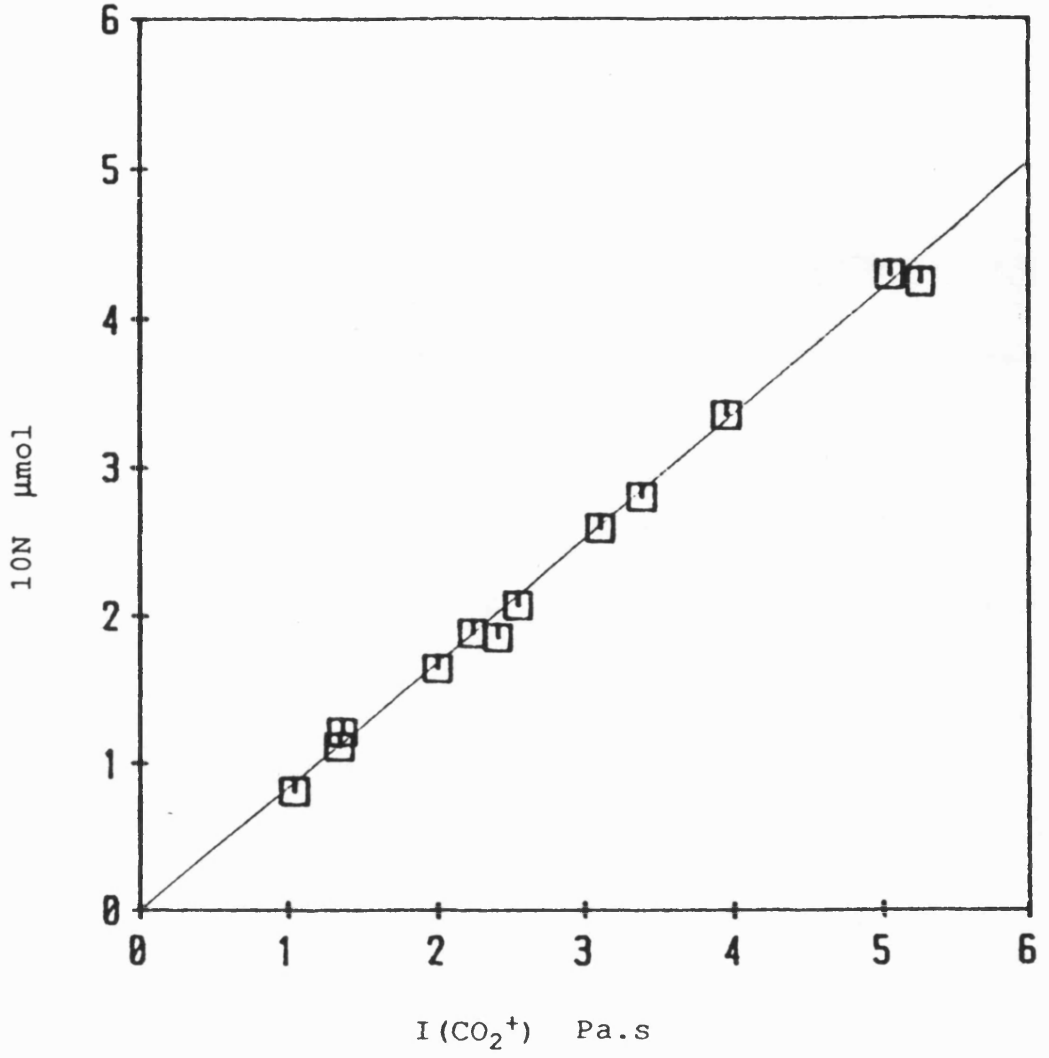

Figure 3.3 Calibration results with $CaCO_3$. heating rate: 150K/h

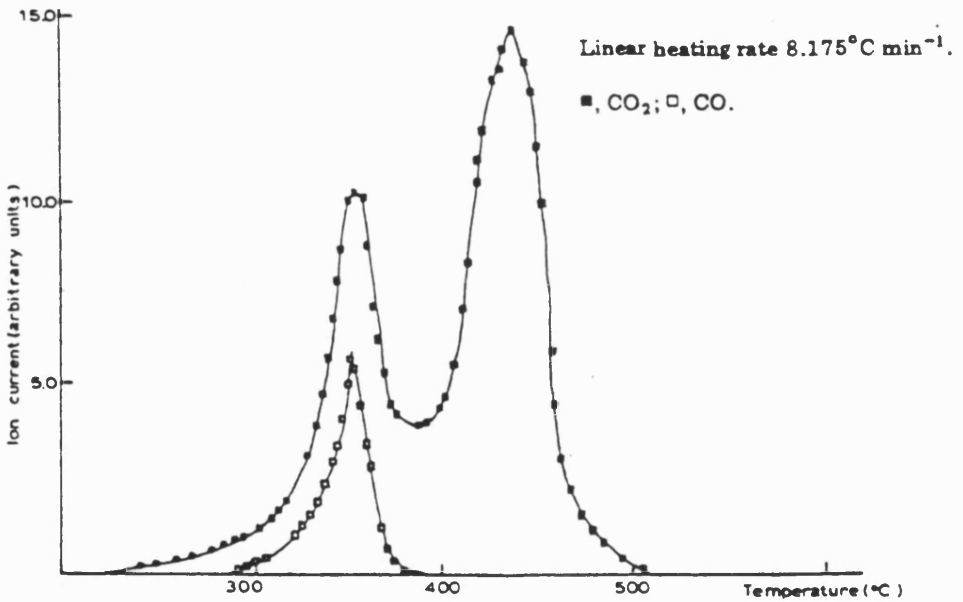

Figure 3.4 Typical TPD curve of CaC_2O_4 decomposition (Ref. [3.26])

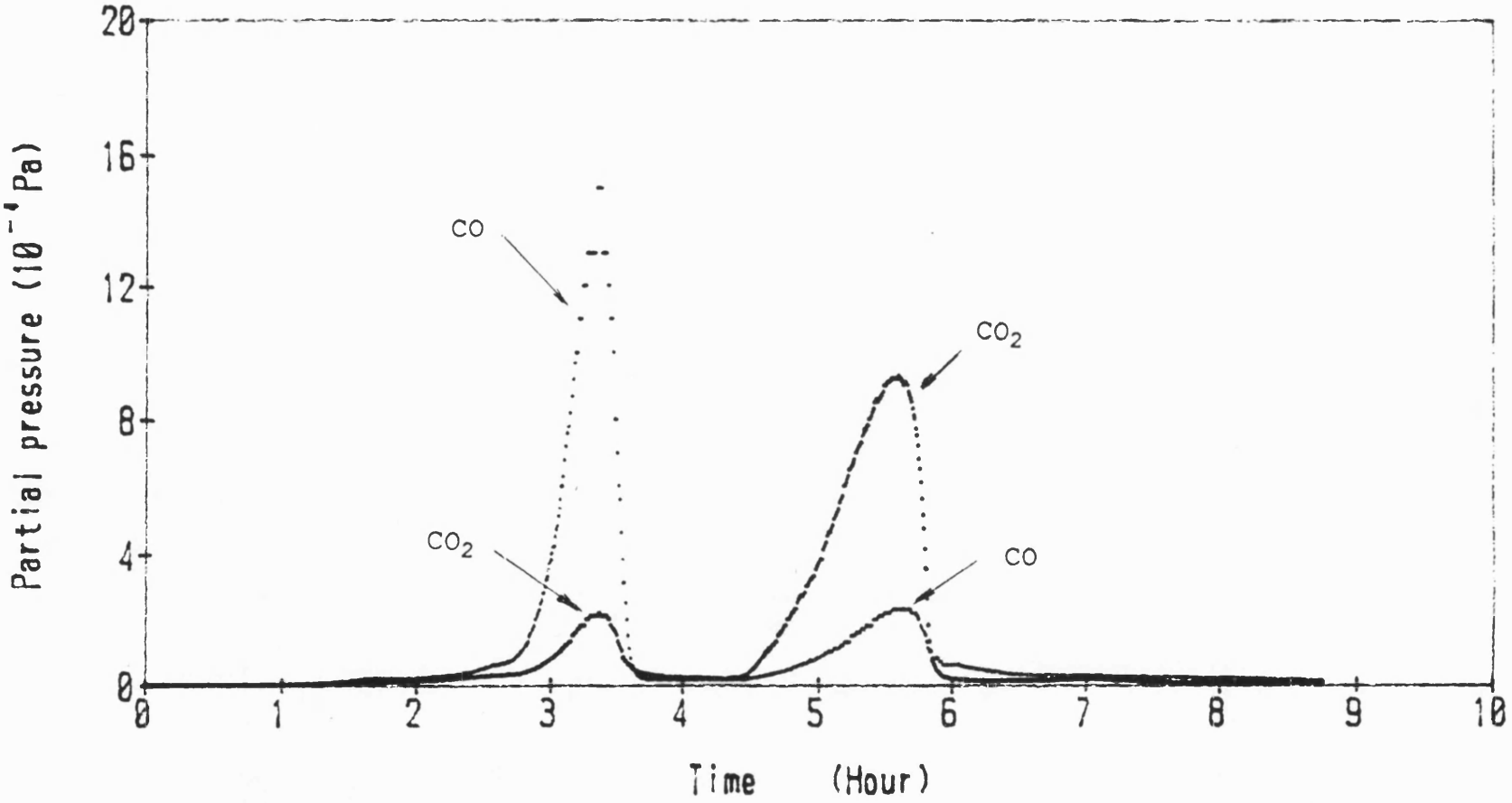

Figure 3.5 Typical TPD curve of CaC_2O_4 decomposition. heating rate: 150 K/h, minimum temperature: 523 K

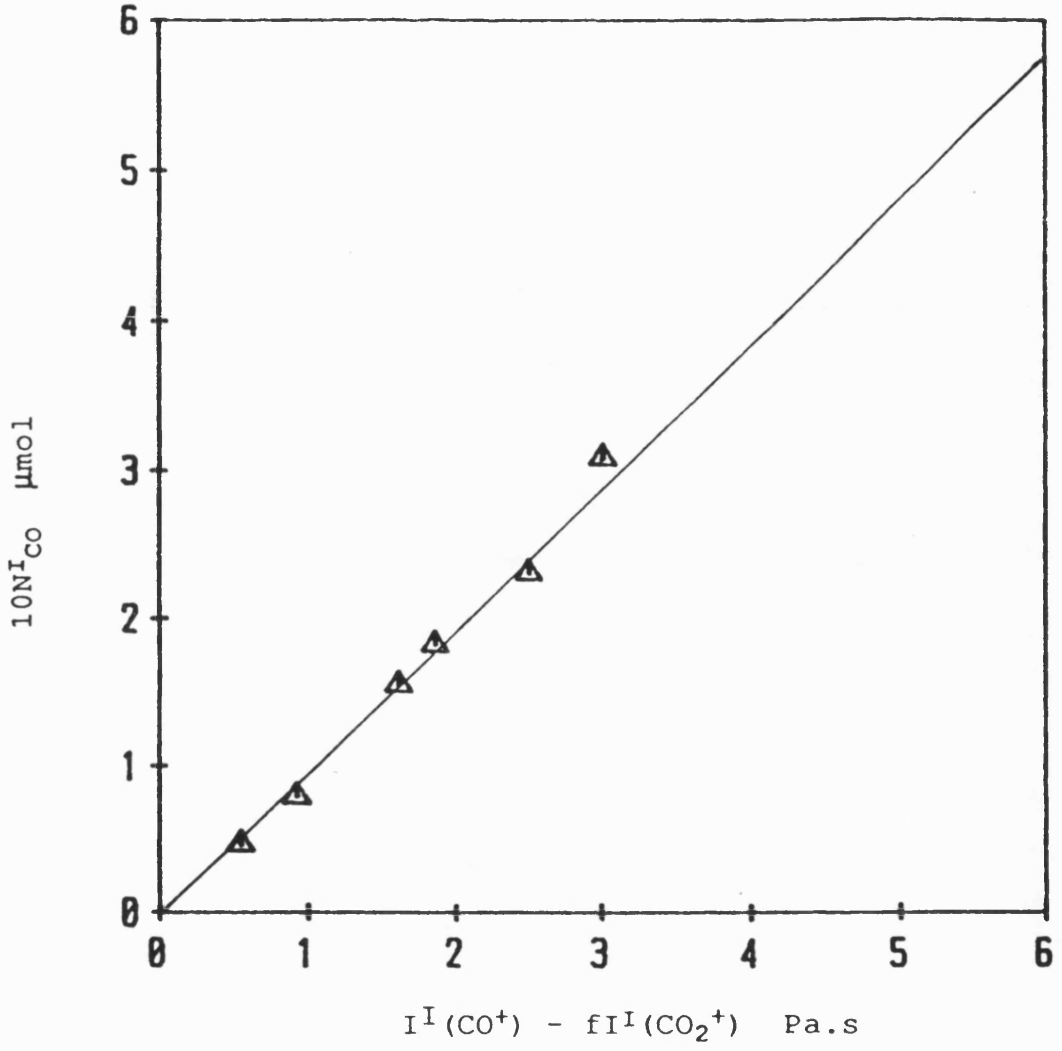

Figure 3.6 Calibration results with CaC_2O_4 (Stage I). heating rate: 150K/h

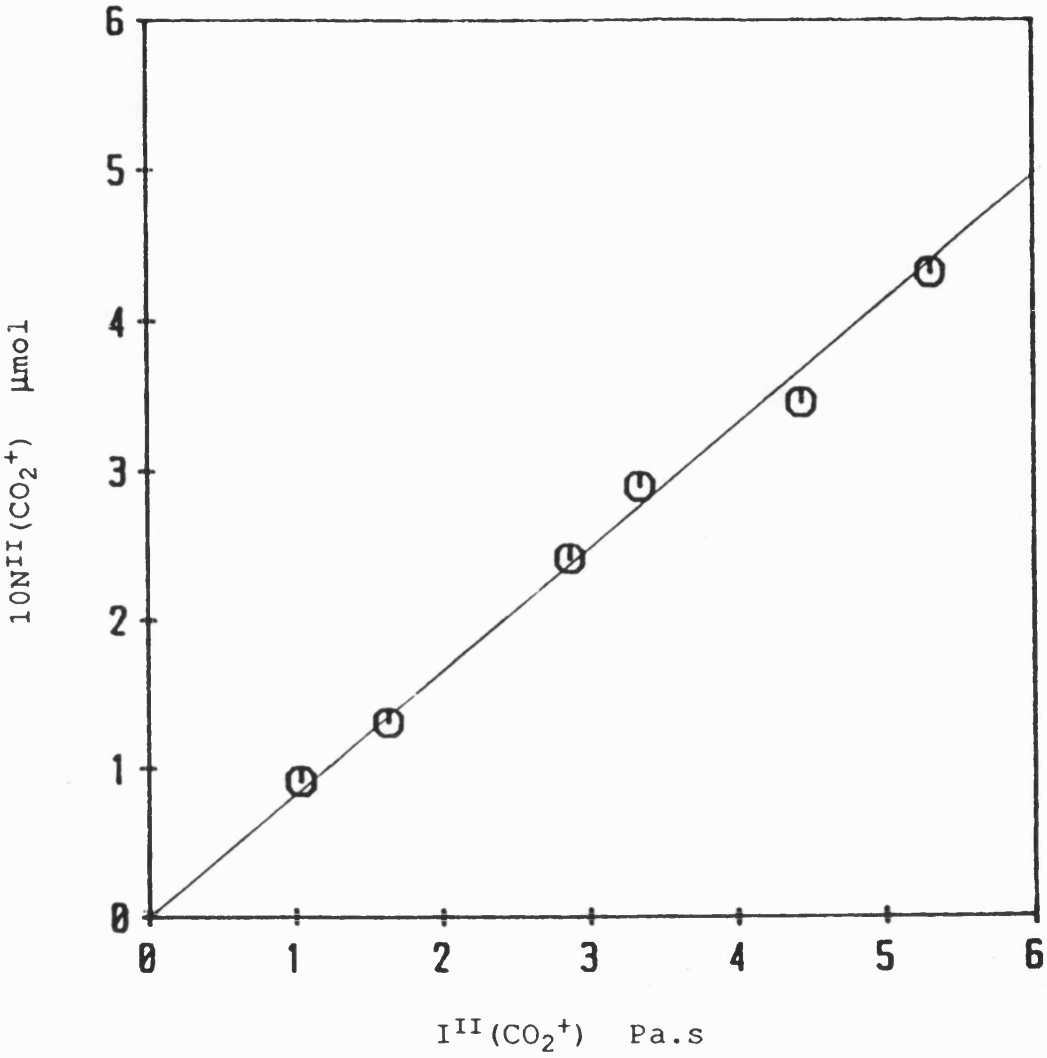

Figure 3.7 Calibration results with CaC_2O_4 (Stage II). heating rate: 150K/h

Chapter 4

QUALITATIVE ANALYSIS OF TPD SPECTRA

Before a qualitative analysis of TPD spectra, it is necessary to consider the energies of the chemisorbed species on the substrate surface. Any chemisorbed species can only vibrate at the active surface site on which it was adsorbed until its kinetic energy is sufficient to overcome some energy barrier, *e.g.*, for surface migration. Under vacuum the kinetic energy of a chemisorbed species can be increased by heating the sample. Once its kinetic energy exceeds the desorption energy, the molecule can leave the substrate surface and enter the gaseous phase. The desorption sequence and the desorption rate of individual chemisorbed species at different temperatures depend mainly on the strength of the chemical bond between the chemisorbed molecule and the substrate atom, however, the distribution of surface functional groups also has some contribution. A TPD spectrum reveals the changes of the partial pressures of various gases desorbed during a temperature profile. The partial pressure of a gas in a TPD spectrum can be related to the desorption rate of the molecules of that gas desorbed from various states of surface complexes and various types of active surface sites. Therefore, a qualitative analysis

of the TPD spectrum can yield information of the stabilities of various states of surface complexes and the variety of active surface sites.

4.1 TPD Spectra before Gasification

In this section the TPD spectra of PVDC char and the six coal chars before gasification are analysed. Normally, a sample was first outgassed at 1273 K for 15 h and then saturated with 1 atm oxygen at 523 K for 12 h. Subsequently, the char was heated from the initial temperature 523 K to 1273 K at a heating rate of 150 K/h and held at 1273 K for sometime. All of the TPD spectra presented in this thesis of later chapters are corrected for ion fragmentation of CO_2^+ and background gases as discussed in Chapter 2.

4.1.1 TPD Spectra of PVDC Char before Gasification

Figure 4.1 shows a typical TPD spectrum of PVDC char before gasification. It consists of a CO_2 desorption curve and a CO desorption curve. In the initial stages of TPD the desorption rate of CO_2 increases faster than that of CO. After reaching a maximum at around 693 K, the desorption rate of CO_2 decreases and gradually approaches zero. However, when CO_2 desorption reaches the maximum and starts to decline the desorption rate of CO continues increase

until reaches a maximum at around 953 K. Since both the maximum and the duration of CO desorption are much bigger than those of CO_2, the main component of the gas evolved, especially at higher temperatures, is CO. At around 1083 K the declining rate of CO desorption becomes slower and a shoulder occurs. Note that an important feature of this figure is that CO desorption does not stop at 1273 K and its partial pressure is still significant even after dwelling at this temperature for as long as 5 h. The long tail of the CO desorption curve represents this 5 h dwelling period at 1273 K. It indicates that the desorption cannot be completed if the sample is only heated to 1273 K and, therefore, it is necessary to heat the sample to a higher temperature to complete the desorption.

Unfortunately, the samples could only be heated to 1473 K and held at this temperature for some short time owing to the limitation of the maximum furnace temperature. A typical TPD spectrum is shown in Figure 4.2, which also consists of a CO_2 desorption curve and a CO desorption curve. The shapes and the peak (and shoulder) temperatures of the two desorption curves in the part up to 1273 K of Figure 4.2 are very similar to those in Figure 4.1, except that the partial pressures at the peak and the shoulder of the CO desorption curve of the former are smaller than those of the latter. Because the same sample amounts were used, this decreased

desorption of the same char heated to a higher temperature must be due to some change of surface conditions during heat-treatment. The char used for Figure 4.2 was outgassed at 1473 K for 5 h before oxygen chemisorption and TPD. This high temperature treatment will result in thermal annealing [4.1, 4.6, 4.7]. That is, the surface area of the char was reduced during high temperature treatment because some narrow pores were closed. This may explain the smaller CO desorption in Figure 4.2. The possibility of that the peak around 1473 K is due to reaction between carbon sample and the silica crucible in the reactor was ruled out by carrying out a similar TPD experiment using a platinum crucible which yielded a similar high temperature peak as under normal conditions.

The most important feature of Figure 4.2 is that, as expected, another CO desorption peak at around 1473 K or above occurs. Because this peak is so close to the maximum temperature, *i.e.*, the maximum furnace temperature, neither an accurate peak temperature nor a complete peak could be obtained.

4.1.2 Designation of Adsorbed States of C-O Complexes

Marchon *et al* [4.2] recently measured TPD spectra after exposing a clean surface of polycrystalline graphite to various doses of O_2 at 523 K. They reported two maxima at 1093 and 1253 K and a shoulder at 973 K on the CO desorption curves and two maxima at 463 and 693 K on the CO_2 desorption curves. They also reported that the O_2 chemisorption could be enhanced by raising the adsorption temperature and three other CO_2 peaks at 573, 793 and 923 K were observed when higher adsorption temperatures were used.

Comparing with their results, the peak temperature at 953 K and the shoulder temperature at 1083 K of CO desorption in Figure 4.1-4.2 are close to the shoulder at 973 K and the peak at 1093 K reported by them, but their other CO desorption peak at 1253 could not be distinguished. In another respect, the peak temperature at 693 K of CO_2 desorption observed in this work is also coincident with their peak temperature at 693 K, although the other three peaks at 573, 793 and 923 K could not be distinguished. Because the initial TPD temperature used in this work was 523 K, their CO_2 desorption peak at 463 K was not observed.

The shapes and temperatures of the peaks (shoulders) reported by them differ to some extent from those obtained

in this work. It may be due to the differences of materials and experimental conditions being used.

Different C-O surface complexes should have different thermal stabilities. From the above TPD spectra, several adsorbed states of C-O complexes can be distinguished. That is, there are at least one adsorbed state of C-O complex leading to CO_2 desorption and at least three adsorbed states of C-O complexes leading to CO desorption from the surface of PVDC char. The latter three are designated as α-state, β-state, and δ-state of C-O surface complexes corresponding to the maximum desorption temperatures at 953, 1083 and 1473 K, respectively. γ-state of C-O surface complex will be designated in Section 4.2.

4.1.3 TPD Spectra of Coal Chars before Gasification

Figures 4.3-4.8 show the typical TPD spectra to 1273 K of the six coal chars before gasification. A rough analysis of these spectra gave some fascinating information, *i.e.*, by displacing the pressure axes the TPD peaks of these coal chars could be superimposed on each other and also on those of PVDC char. Further analysis revealed the following similarities of these spectra with the spectrum of PVDC char:

i. Each of the spectra consists of a CO_2 desorption curve and a CO desorption curve;

ii. Each CO_2 desorption curve possesses a broad peak at around 693 K and the temperatures of these peaks for the different chars vary only in a small range, as shown in Table 4.1;

iii. Each CO desorption curve possesses a peak or a shoulder at around 953 K and another peak or shoulder at around 1083 K. The temperatures of the first peaks vary only in a small range, as shown also in Table 4.1;

iv. In all these TPD spectra the CO desorption does not stop at 1273 K and the partial pressures of CO are still significant even after dwelling at this temperature for some time.

In order to confirm the CO desorption peak at around 1473 K from these chars, a demineralized char of Baddesley coal was heated to 1473 K using the same heating program as that described for PVDC char. The TPD spectrum obtained shown in Figure 4.9 verifies the existence of the CO desorption peak at around 1473 K; in addition the peaks at lower temperatures are similar to those for chars heated only to 1273 K.

The above consistency between the TPD spectra of PVDC char and the six coal chars indicates that all of the

adsorbed states of C-O complexes which exist on the surface of PVDC char also exist on the surface of coal chars. In other words, the desorptions of C-O surface complexes from the surface of coal chars follow the same pattern as that from the surface of PVDC char. Therefore, all the designations for the desorption of C-O complexes from the surface of PVDC char can be applied to coal chars. The minor differences of peak (and shoulder) temperatures from various chars may be due to chemical-physical variations of the surface functional groups of the different chars.

4.1.4 Designation of Active Surface Sites on Char Surface

From above discussion on a wide variety of TPD spectra, it is evident that the CO_2 desorption from PVDC and the six coal chars is correlated with at least one state of C-O complex and the CO desorption is correlated with at least three states of C-O complexes, *i.e.*, α-state, β-state and δ-state of C-O complexes. Because the variety of the adsorbed states of C-O complexes on the char surfaces is correlated with the variety of the active sites on the char surface, it is reasonable to propose that there are at least one type of active surface site correlated with CO_2 desorption and at least three types of active surface sites correlated with CO desorption from the surface of a char. The latter three are designated as α-type, β-type and δ-type active surface

sites, correspondingly. Further evidence will be provided and discussed in the later sections of this chapter.

4.2 TPD Spectra of Chars Quenched during Gasification

Typically, the chars used for the discussion in this section were first gasified with 1 atm CO_2 at 1123 K for 1 h and then quenched. In an attempt to "freeze" the situation on the char surface during gasification, the reactor chamber was quenched in cold water after the furnace was quickly removed. The cooling rate obtained in this approach was more than -350 K/min. Since CO_2 gasification is very slow at temperatures less than 973 K [4.3], the "freezing" of the surface of a char could be obtained in less than 1 minute. Subsequently, the char was cooled to 523 K and all the remaining CO_2 was pumped out until the vacuum in the reactor chamber reached 10^{-5} Pa. Normally, the char was finally heated at a heating rate of 150 K/h to 1273 K and held at this temperature for some time to obtain a TPD spectrum.

4.2.1 Spectrum of PVDC Char Quenched during Gasification

Figure 4.10 shows a typical TPD spectrum of PVDC char quenched at 1123 K during CO_2 gasification. Comparing with Figure 4.1, some significant features of Figure 4.10 can be found:

i. The CO_2 desorption curve almost disappears;

ii. The CO desorption peak of the α-state C-O complex disappears;

iii. Instead of the CO desorption shoulder of β-state C-O complex at 1083 K in Figure 4.1-4.2, a main peak of CO desorption occurs at around 1223 K;

iv. The areas under the TPD curves are much smaller than those in Figure 4.1-4.2.

v. The CO partial pressures at 1273 K even after dwelling at this temperature for 5 h are still significant, *i.e.*, the desorption of C-O complexes at 1273 K from PVDC char quenched during gasification is also incomplete.

In order to complete the desorption of C-O complexes, some PVDC chars quenched during CO_2 gasification were heated to 1473 K. A typical TPD spectrum obtained is shown in Figure 4.11. It also gives a desorption peak of δ-state C-O complex at around 1473 K or above in addition to the desorption peak at 1223 K.

It was assumed for a long time that the peak at 1223 K in Figure 4.10 corresponds to the desorption shoulder at around 1083 K of β-state C-O complex in Figure 4.1, although the temperature discrepancy is 140 K. This temperature discrepancy was attributed to different adsorption conditions. Note that Figure 4.1 was measured by the oxygen

saturation technique, thus, all of the active sites were occupied and the initial surface coverage by every state of C-O complex is 100%, including that by β-state C-O complex. However, Figure 4.10 was measured by quenching the char during CO_2 gasification at 1123 K. Under such a condition the char surface might be far away from being saturated, *i.e.*, the initial surface coverage occupied by β-state C-O complex is less than 100%. This smaller initial surface coverage occupied by "β-state" C-O complex could lead to higher desorption peak temperature (see Chapter 6).

In order to verify the above assumption, a cleaned PVDC char was first exposed in CO_2 at 1123 K, then the temperature was decreased at a rate of -1 K/min to 523 K and held at 523 K overnight. After all of the remaining CO_2 was pumped out, the char was heated to 1473 K following the normal temperature program. The TPD spectrum to 1473 K obtained is shown in Figure 4.12. In contrast with previous assumption, the first peak temperature in Figure 4.12 is at 1223 K. This temperature is exactly the same as that in Figure 4.10.

Marchon *et al* [4.2] also studied the TPD spectra of the polycrystalline graphite after CO_2 adsorption at various temperatures, although they did not quench their samples. They observed a peak of CO desorption at 1093 and a shoulder

near 1223 K and that the latter became the prominent peak when adsorption was carried out at 973 K. These two maxima were coincident with those they observed in the spectra after O_2 chemisorption.

The peak temperature at 1223 K in Figure 4.10-4.12 is coincident with the prominent peak temperature reported by Marchon *et al* when polycrystallite graphite was exposed to CO_2 at 973 K. It indicates that the main CO desorption peaks at 1223 K in Figure 4.10-4.12 are other CO desorption peaks rather than that of β-state C-O complex. It is designated as the desorption peak of γ-state C-O complex.

These TPD spectra reveal that only two of the states of C-O complexes distinguished by TPD are present on carbon surfaces during CO_2 gasification and most active sites revealed by the oxygen chemisorption technique are not involved in CO_2 gasification, except the γ- and δ-type of active sites. These results provide clear evidence for the proposition in the Introduction, *i.e.*, that only a small part of classical ASA and only some states of C-O surface complexes take part in the gasification process.

These results are consistent with those of Hermann and Huttinger [4.5]. In a study on the water vapour gasification of PVC char, they reported that the water vapour

gasification only took place by some "extremely stable" C-O surface complexes. However, they only reported one desorption peak, although the partial pressures of many CO desorption peaks reported by them were also significant even at 1373 K.

Additionally, it is noted in Figure 4.10-4.12 that a small desorption peak of CO_2 occurs at around 1123 K. However, it is hard to explain the mechanism of formation of this peak from our present knowledge, although it may be due to the disproportionation of CO, as discussed in Section 3.5.

4.2.2 Spectra of Coal Chars Quenched during Gasification

The TPD spectra of the six coal chars quenched during gasification are shown in Figures 4.13-4.18. They are also similar in many respects to the spectra of PVDC char quenched during gasification in Figures 4.10-4.12, *i.e.*, the CO_2 desorption curves almost disappear and the CO desorption peaks of α-state and β-state C-O complexes disappear and the desorption peaks of γ-state C-O complex become the main peaks. These figures show that the conclusion above, *i.e.*, only the γ-state and δ-state of C-O complexes are involved in CO_2 gasification of PVDC char extends also to the coal chars.

From these TPD spectra it is easier to measure the maximum desorption temperatures of γ-state C-O complex, because no desorption peak of α- or β-state of C-O surface complexes interferes. The results are tabulated in Table 4.2. These values vary about 1223 K in a range less than ±50 K, similar to that of α-state C-O complex tabulated in Table 4.1. The range of the peak temperature is probably related to the variety of surface functional groups of various coal chars and also probably related to the extent of the initial surface coverage, as discussed in Chapter 6.

Figure 4.13 is the TPD spectrum of the demineralized char of Baddesley coal quenched during gasification and Figure 4.14 is the spectrum of the corresponding undemineralized char. It is significant that the area under the curve of the former is smaller than that under the latter. The bigger area under TPD curve in Figure 4.14 is believed due to the catalytic effect of the mineral matter in the undemineralized char, as discussed in Section 4.6. The small CO_2 peak at 863 K is due to the decomposition reaction of carbonate in the impurity of this undimineralised coal char.

4.2.3 TPD Spectra of PVDC Char Quenched at Different Gasification Conditions

Some quenching experiments were carried out with PVDC char during CO_2 gasification at different temperatures and after different durations. The result TPD spectra are very similar to Figure 4.10-4.12. They further verify that only the γ-state and δ-state of C-O complexes are involved in CO_2 gasification under the present experimental conditions. The maximum desorption temperatures of γ-state C-O complex in these TPD spectra are tabulated in Table 4.3. They vary also to a small extent about 1223 K.

4.3 TPD Spectra after CO_2 Gasification

After measuring the TPD spectrum of a char quenched during CO_2 gasification, the char was cooled to 523 K and then saturated with oxygen again. Subsequent TPD was carried out from 523 K at a heating rate of 150 K/h to 1273 K and held at this temperature for sometime. Figures 4.19-4.25 show the TPD spectra of PVDC and six coal chars treated as above. Their shapes are very similar to the corresponding TPD spectra before gasification. Their peak temperatures of CO_2 desorption curves and peak temperatures of the desorption of α-state C-O complex are tabulated in Table 4.4. They both are close to those in Table 4.1.

The same is true for those TPD spectra of PVDC char after CO_2 gasification under different conditions. Their peak temperatures of CO_2 desorption curves and peak temperatures of the desorption of α-state C-O complex are tabulated in Table 4.5. They both are close to those in Table 4.1 and those in Table 4.4.

These experiments show that under the experimental conditions the desorption mechanism of various C-O complexes is little altered during gasification, although the amounts of the C-O complexes increase as a result of gasification.

4.4 TPD Spectra After CO adsorption

CO desorption is the most important step for gasification and some information about CO desorption from char surfaces has been obtained. Furthermore, it is reasonable to explore the effects of CO adsorption upon the TPD spectra of chars. To our knowledge, no work has been published on TPD spectra following CO adsorption on carbons when we did these experiments.

Figure 4.26 shows a TPD spectrum to 1323 K of PVDC char preheated to 1473 K under vacuum and then exposed in 1 atm CO at 1123 K for 1 h and quenched. This figure also only

consists of the CO desorption peaks of γ- and δ-state of C-O surface complexes, *i.e.*, CO desorption occurs on γ- and δ-type active surface sites. Another PVDC char sample was exposed in 1 atm CO at 1123 K for 1 h and then the temperature was reduced at a rate of -1 K/min to 523 K. The TPD spectrum obtained from this sample in Figure 4.27 shows CO desorption from α-, γ- and δ-type of active surface sites, however, CO desorption from α-type active surface sites under these conditions is far less than that of classical TPD. That is, most of CO desorption from α-type of active surface sites is irreversible or CO was not adsorbed on α-type of active surface sites. Figure 4.28 is a TPD spectrum of PVDC char after exposing in 1 atm CO at 523 K for 15 h. It gives similar result to Figure 4.27.

Marchon *et al* [4.4] recently reported that no ^{12}CO was observed in the TPD spectrum of polycrystallite graphite after exposure to ^{13}CO. They concluded that CO does not dissociate on the carbon surface, but rather it inserts onto some five-membered ring in the graphite lattice to form some stable six-membered ring. This aspect of the interaction of CO with carbon surface will be discussed in Chapter 7.

4.5 Development of Active Surface Sites during Progressive Gasification

From both a scientific or a technological point of view, it is important to elucidate the development of various types of active surface sites during progressive gasification. It is particularly worthwhile when we have understood what type or types of active surface sites participate in CO_2 gasification. To measure the effects of progressive gasification more clearly a char with a low surface area and a more homogeneous surface was produced by heat-treating the normal PVDC char. The heat-treated PVDC char was gasified with 1 atm CO_2 at 1123 K for 10, 15 and 20 h, respectively. Before gasification and after each gasification the classical TPD was measured and the resulting TPD spectra are co-plotted in Figure 4.29 for convenience of comparison.

It is surprising to find that the TPD spectrum before gasification only consists of one single sharp CO desorption peak at around 1390 K, which is higher than the normal peak temperature at 1223 K of γ-state of C-O complex and lower than the normal temperature at around 1473 K of the desorption peak of δ-state C-O complex. This peak was never distinguished in all of the TPD spectra discussed above. The sharpness of this peak may be due to the homogeneity of this

char; however, it is hard to explain why this peak disappears after a certain amount of gasification. This peak is probably due to the desorption of another state of C-O complex.

The classical TPD spectra after CO_2 gasification of this PVDC char show only three desorption peaks of α-state, γ-state and δ-state of C-O complexes at 953, 1223 and 1473 K, respectively. It is unexpected that the desorption peak of β-state C-O complex at 1083 K disappears. However, it can be seen clearly that the desorptions of α-state, γ-state and δ-state of C-O complexes are enhanced following the progressive CO_2 gasification, *i.e.*, the amount of α-type, δ-type and γ-type of active surface sites increase following the increase of the duration of CO_2 gasification.

Figure 4.30 shows a similar co-plots from the TPD spectra of Electrode carbon 706 before gasification and after gasification with CO_2 at 1123 K for 10, 15, 25 h subsequently. Although Electrode carbon 706 is a completely different kind of carbon with high-temperature treated PVDC char as explained in Chapter 2, it shows similar behaviour during gasification.

Co-plots the TPD spectra of the heat-treated PVDC char quenched during CO_2 gasification at 1123 K for 10, 15 and 20

h are in figure 4.31. As expected, only the desorption peaks of C-O complexes from the γ-type and the δ-type of active surface sites are shown and the amounts of these two types of active sites increase with the progressive gasification.

Thus far, it is evident that all of the amount of the α-type, δ-type and γ-type of active surface sites increase following the progressive gasification with CO_2, except we are unable to explain the sharp CO desorption peak in the TPD spectrum in the initial period of gasification and why the CO desorption shoulder at around 1083 K disappears.

4.6 Catalytic Effect of Mineral Matter on CO_2 Gasification

The catalytic effect of mineral matter on gasification with CO_2 is an interesting research field and thousands of studies have been reported on this topic. However, only limited experiments were able to be carried out in this research, because of the damaging effect of K_2CO_3 on the quartz reactor at high temperature.

In order to study this topic, some PVDC char was impregnated with 10 wt% of K_2CO_3 and preheated to 1473 K under vacuum before subsequent TPD measurements. The classical TPD spectrum to 1473 K of this char is shown in

Figure 4.32. It also consists of a CO_2 desorption curve and a CO desorption curve.

The CO_2 desorption curve in Figure 4.39 consists of one peak at 693 K and two shoulders at 793 and 923 K; among them only the peak at 693 K was distinguished in the spectra of unimpregnated chars. However, all three peak temperatures are coincident with those reported by Marchon *et al* [4.2].

The CO desorption curve consists of a smooth shoulder at 953 K and two sharp peaks at 1223 K and 1423 K. One important feature of this curve is that the desorptions of γ-state and δ-state C-O complexes are significantly enhanced by the presence of K_2CO_3. It provides strong evidence that K_2CO_3 can increase the amount of γ-type and δ-type active surface sites. This is also coincident with the comparison of the TPD spectra of demineralized and undemineralized chars of Baddesley coal discussed in Section 4.2.2.

However, it should be noted that the sharp and asymmetric shape of the desorption peaks of γ-state and δ-state C-O complexes in Figure 4.29 are very different from those discussed above. This difference of peak shape may give important information about the different mechanisms of catalytic and uncatalytic gasifications (see Chapter 6).

4.7 Summary

From all of above TPD spectra, one broad CO_2 desorption peak (which was resolved into three desorption peaks (shoulders) in the case of K_2CO_3 impregnated PVDC char only) and four CO desorption peaks (shoulders) were distinguished. These four CO desorption peaks are designated as the desorption of α-state, β-state, γ-state and δ-state of C-O surface complexes. Accordingly, there are possibly up to three types of active site on char surface correlated with CO_2 desorption and at least four types of active sites correlated with CO desorption on the char surface. The latter four are designated as α-type, β-type, γ-type and δ-type of active surface sites, respectively. For the great majority of chars the CO_2 peaks (if present) were not resolved and a single broad peak of CO_2 desorption was obtained. Among the CO desorption peaks only γ-type and δ-type of active surface sites are present during CO_2 gasification. Mineral matter and added K_2CO_3 catalyst can enhance the amount of these two types of active sites.

It is interesting to note that most desorption peaks obtained from polycrystalline graphite in a previous study are also observed in the TPD spectra of PVDC char and various coal chars in the present work. This suggests that although the structure of the chars are much more disordered

than that of the polycrystallite graphite, there are very similar surface sites in the two classes of carbon.

Similarly, if they are measured by the classical oxygen saturation technique, no matter before or after gasification under various gasification conditions, the peak temperature of CO_2 desorption curve and the peak temperatures of CO desorption of α-state and γ-state C-O complexes only vary in a small range for the PVDC char and the six coal chars.

Based on the above analysis and the kinetic analysis of TPD spectra in Chapter 6, we have proposed a hypothesis for the structure of C-O complexes on the active surface sites which is presented in Chapter 7.

References

[4.1] F. Boulangier, X. Duval and M. Letort, *Proc. Third Carbon Conf.*, Pergamon Press, p.257(1959).

[4.2] B. Marchon, J. Carrazza, H. Heinemann and G. A. Somorjai, *Carbon*, **26**, 507(1988).

[4.3] M. Mentser and S. Ergun, *U.S. Bur. Mines Bull*, **No.644**, 1973, pp.22-26.

[4.4] B. Marchon, J. Carrazza, H. Heinemann and G. A. Somorjai, *J. Phys. Chem.*, **92**, 5744(1988).

[4.5] G. Hermann and K. J. Huttinger, *Carbon*, **24**, 705(1986).

[4.6] P. L. Walker, Jr. and O. P. Mahajan, "*Analytical Method for Coal and Coal Products, Vol. 1*", (ed. C. Karr), Academic Press, New York, pp.125-163(1978)

[4.6] M. R. Khan, *Fuel*, **66**, 1626(1987).

Table 4.1 Peak temperatures of CO_2 desorption curves and CO desorptions of α-state C-O complex from the surfaces of PVDC char and the six coal chars before gasification

Sample	Peak Temperature of CO_2 desorption	Peak temperature of CO desorption of α-state of C-O complex
PVDC	685 - 704	923 - 952
Baddesley (Dem)	676 - 749	950 -1017
Baddesley (Undem)	685 - 740	952 - 962
Cynheidre (Dem)	691 - 739	895 - 985
Bagworth (Dem)	694 - 706	923 - 956
Longannet (Dem)	685 - 709	948 - 952
Tilmanstone (Dem)	652 - 706	939 - 953
Possible peak temperature	694 - 701	947 - 952

Table 4.2 Peak temperatures of CO desorption of γ-state C-O complex from the surfaces of PVDC char and the six coal chars quenched during CO_2 gasification at 1123 K

Sample		Peak temperature (K)
PVDC		1194 - 1251
Baddesley	(Undem)	1228 - 1232
Baddesley	(Dem)	1226 - 1236
Cynheidre	(Dem)	1207 - 1253
Bagworth	(Dem)	1199 - 1230
Longannet	(Dem)	1205 - 1219
Tilmanstone	(Dem)	1213 - 1269

Table 4.3 Peak temperatures of CO desorption of γ-state C-O complex from the surface of PVDC Char quenched during CO_2 gasification under different conditions

Gasification temperature (K)	Duration (h)	Peak temperature (K)
1223	1	1241 - 1255
1123	1	1194 - 1251
1123	2	1214 - 1253
1123	5	1255
1023	1	1166 - 1240
1023	5	1192 - 1202
1023	10	1216

Table 4.4 Peak temperatures of CO_2 desorption curves and CO desorptions of α-state C-O complex from the surfaces of PVDC char and the six coal chars after CO_2 gasification

Sample	Peak Temperature of CO_2 desorption	Peak temperature of CO desorption of α-state C-O complex
PVDC	682 - 700	941 - 955
Baddesley (Dem)	674 - 748	953 - 966
Baddesley (Undem)	685 - 702	947 - 995
Cynheidre (Dem)	691 - 739	891 - 985
Bagworth (Dem)	685 - 715	925 - 981
Longannet (Dem)	682 - 698	918 -1013
Tilmanstone (Dem)	489 - 710	935 - 972
Possible peak temperature	691 - 698	953 - 955

Table 4.5 Peak temperatures of CO_2 desorption curves and CO desorptions of α-state C-O complex from the surfaces of PVDC char after CO_2 gasification under different conditions

Gasification condition	Peak Temperature of CO_2 desorption	Peak temperature of CO desorption of α-state C-O complex
1223 K 1 hr	694 - 703	948 - 959
1123 K 1 hr	682 - 700	941 - 955
1123 K 2 hr	681 - 704	943 - 962
1123 K 5 hr	657 - 719	947 - 963
1023 K 1 hr	676 - 708	937 - 954
1023 K 5 hr	674 - 703	933 - 956
1023 K 10 hr	659 - 715	932 - 974
Possible peak temperature	694 - 700	948 - 956

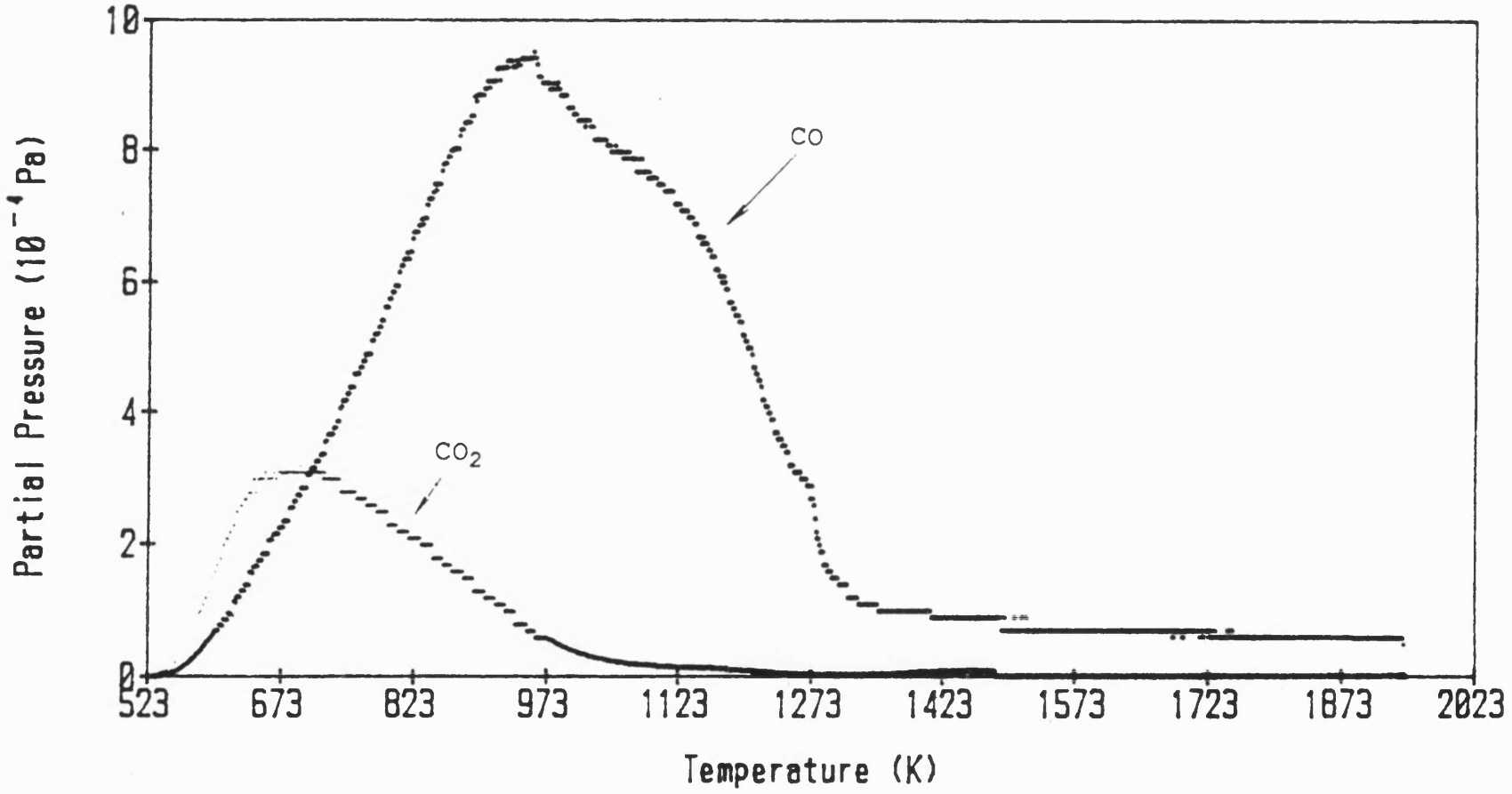

Figure 4.1 Classical TPD spectrum of PVDC char before gasification, maximum temperature 1273 K.

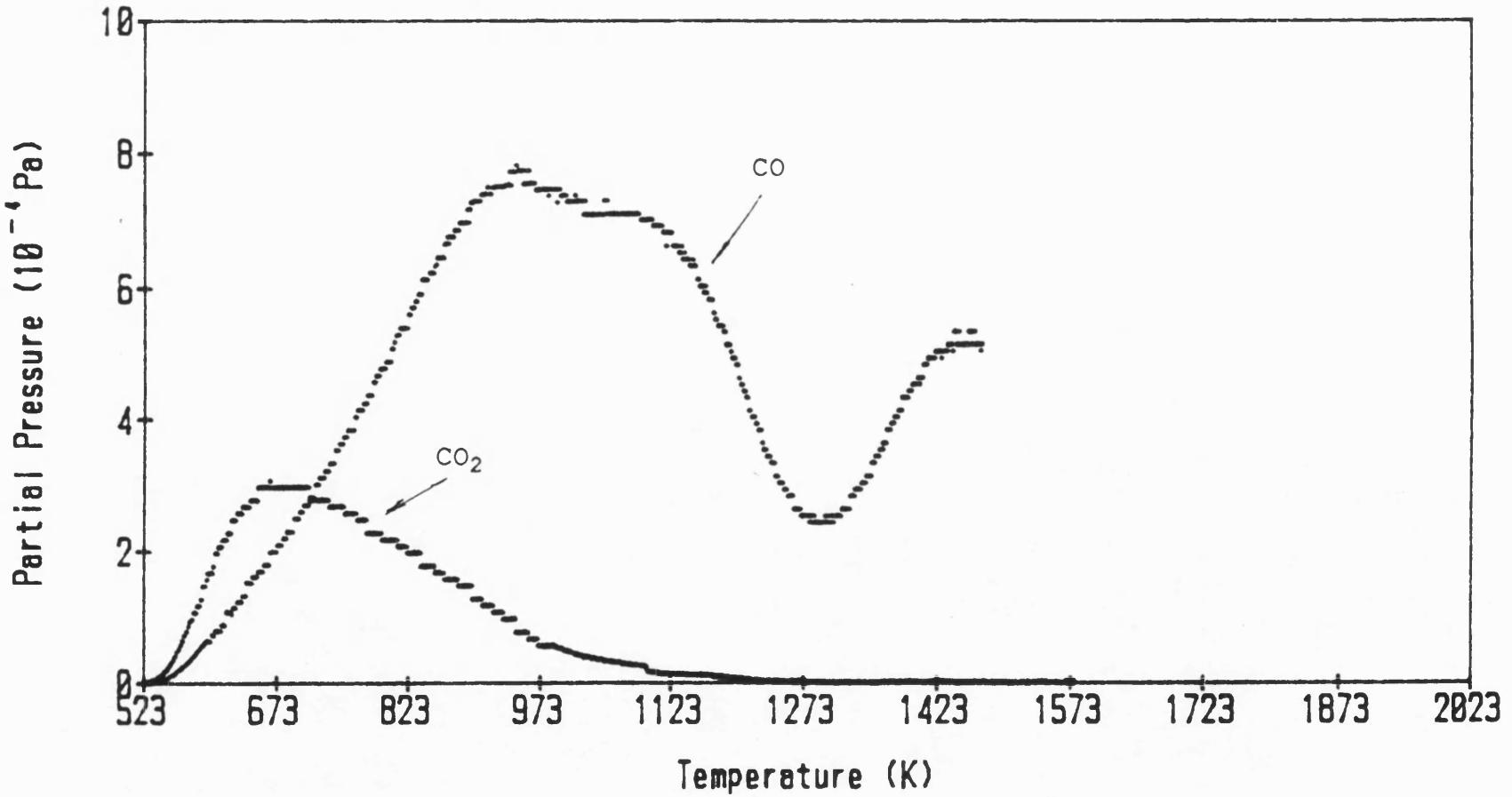

Figure 4.2 Classical TPD spectrum of PVDC char before gasification, maximum temperature 1473 K.

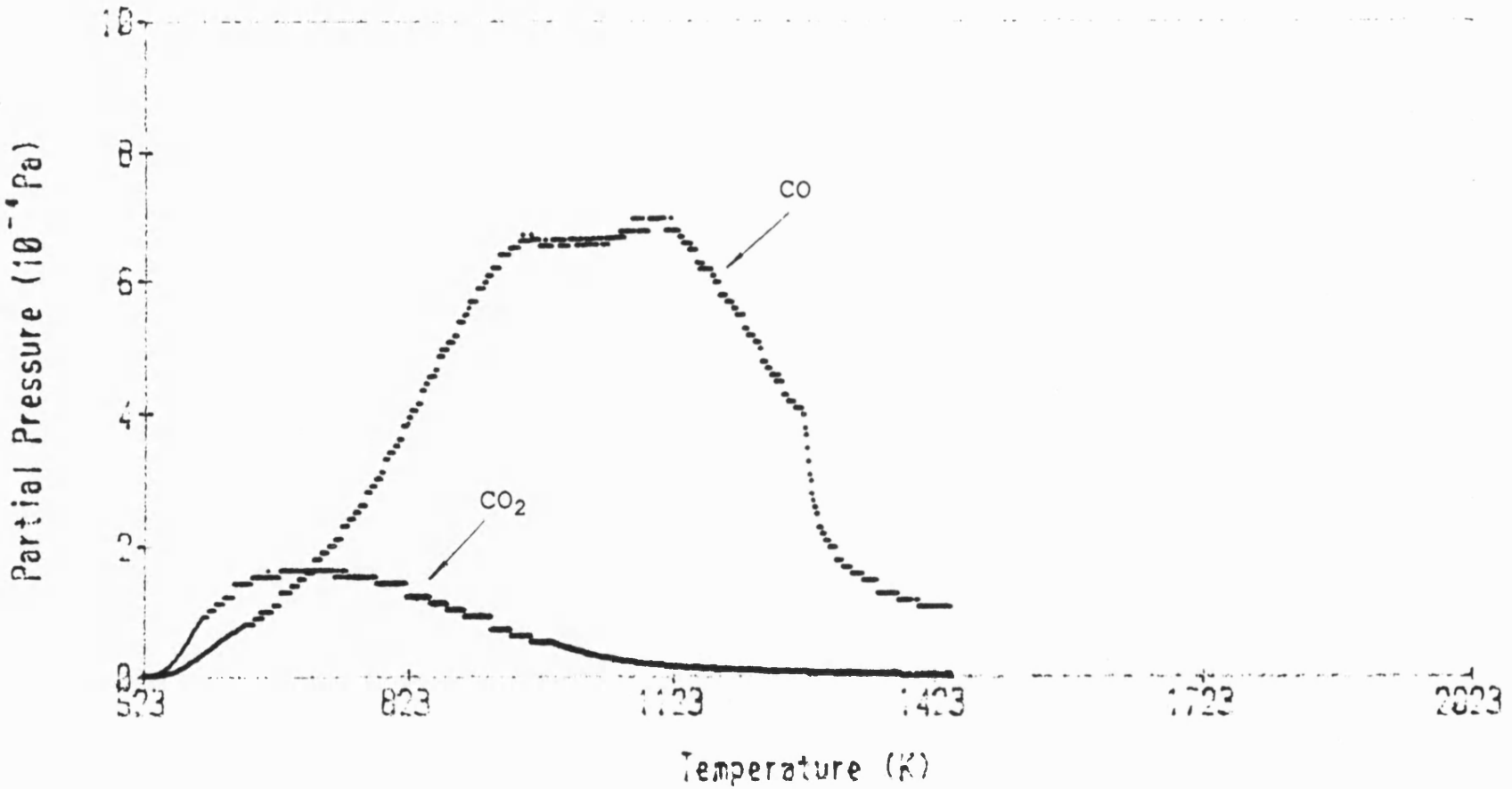

Figure 4.3 Classical TPD spectrum of Baddesley coal char (Dem) before gasification, maximum temperature 1273 K.

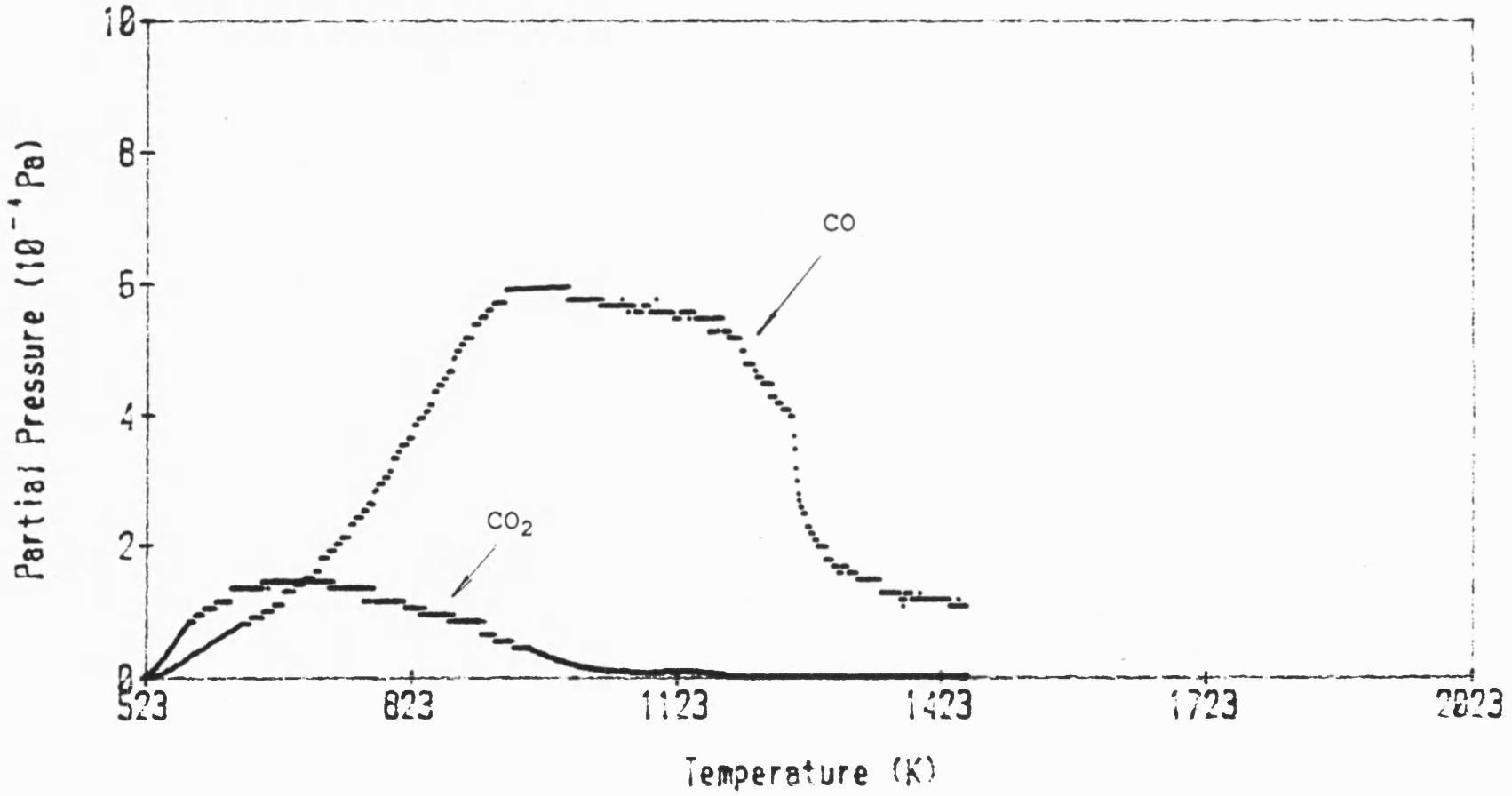

Figure 4.4 Classical TPD spectrum of Baddesley coal char (Undem) before gasification, maximum temperature 1273 K.

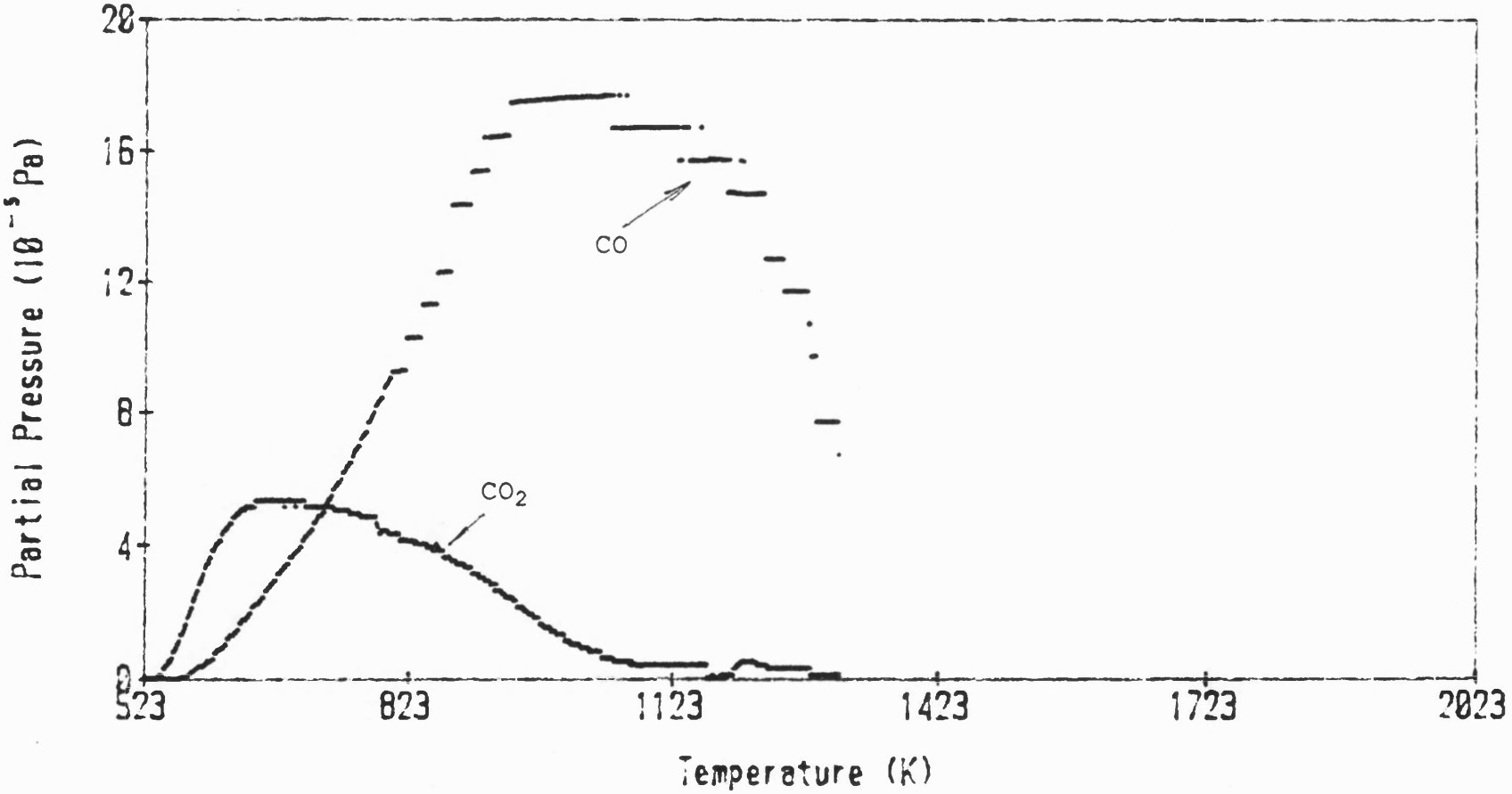

Figure 4.5 Classical TPD spectrum of Tilmanstone coal char (Dem) before gasification, maximum temperature 1273 K.

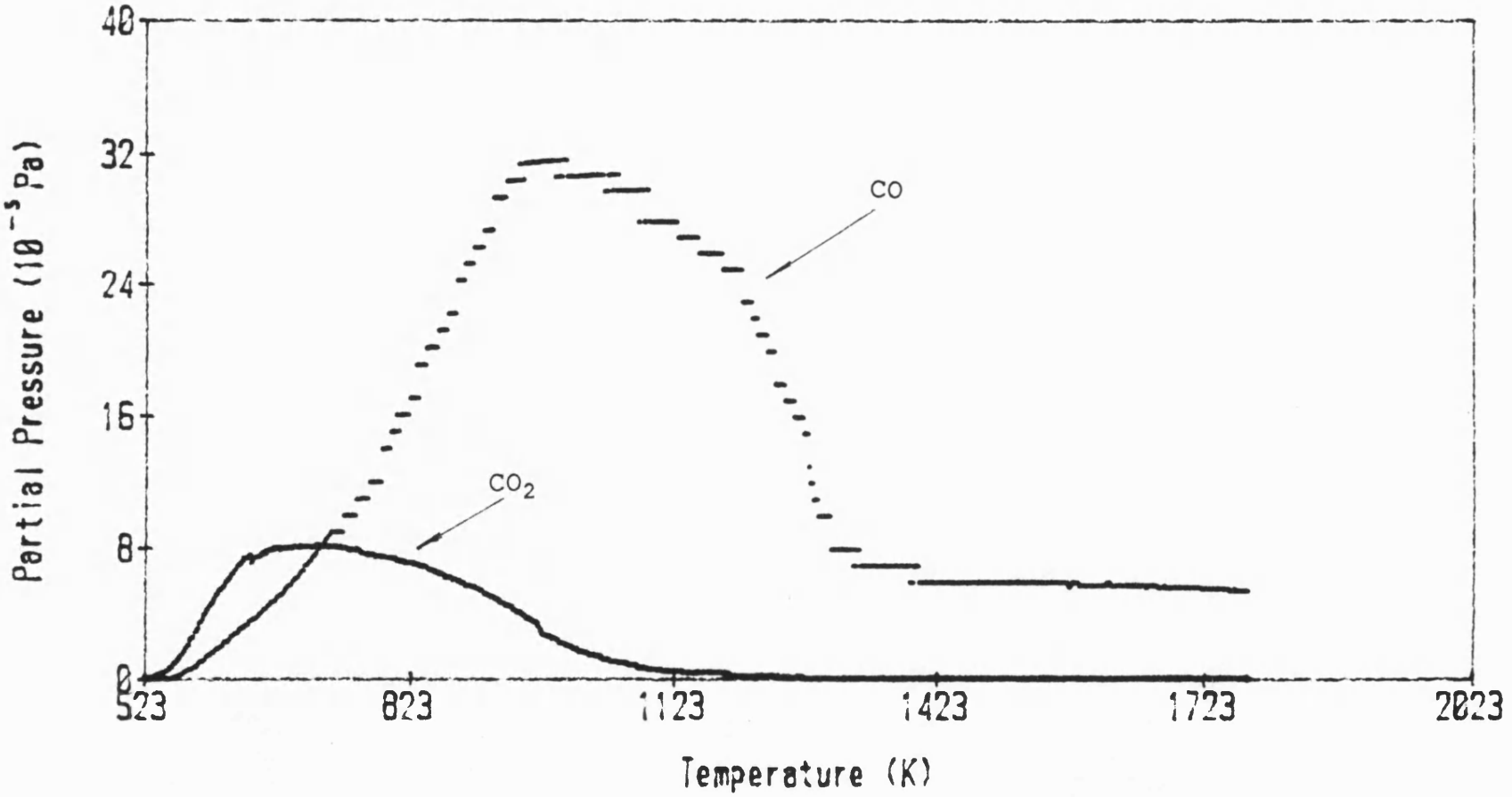

Figure 4.6 Classical TPD spectrum of Cynheidre coal char (Dem) before gasification, maximum temperature 1273 K.

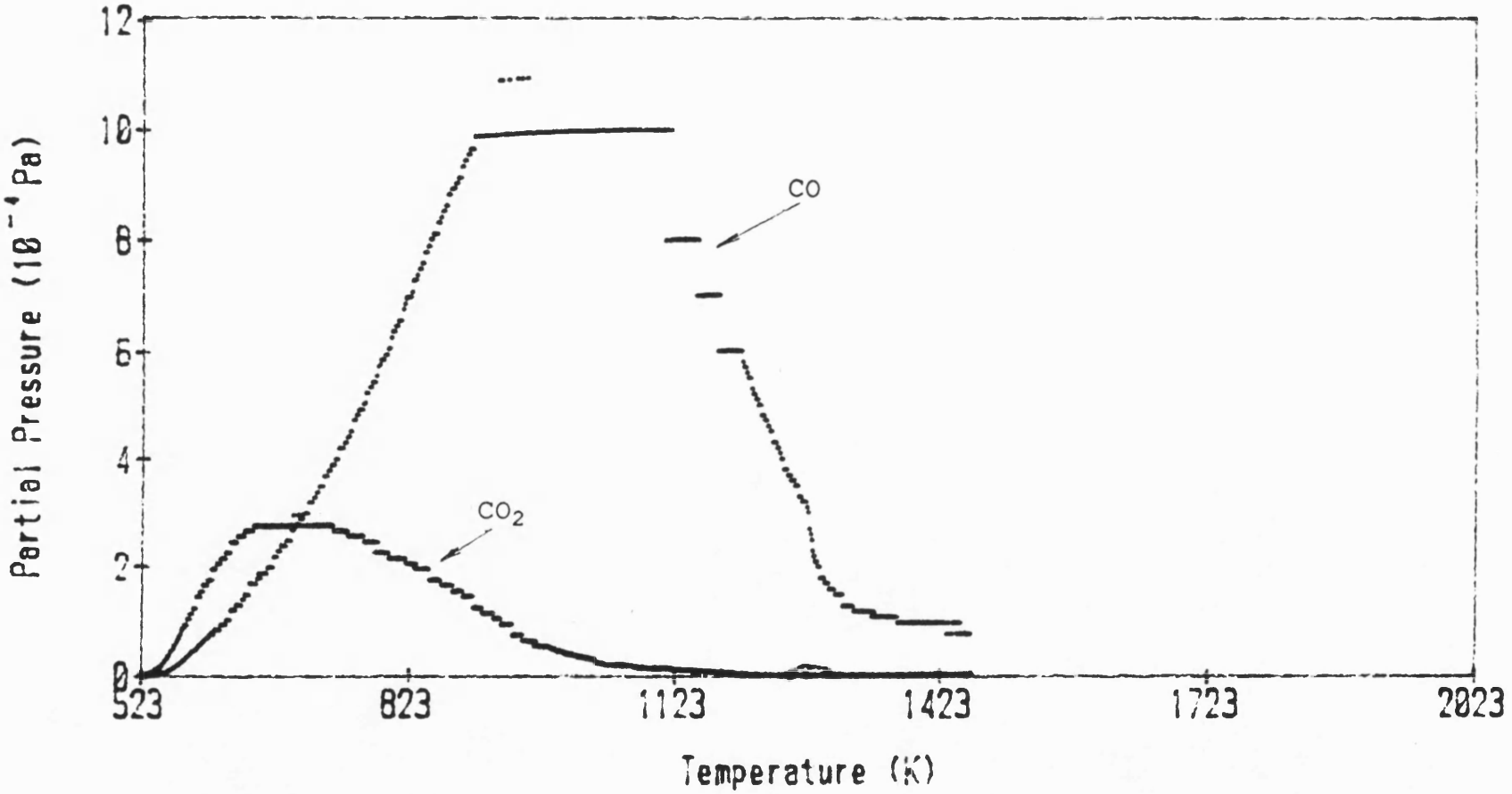

Figure 4.7 Classical TPD spectrum of Bagworth coal char (Dem) before gasification, maximum temperature 1273 K.

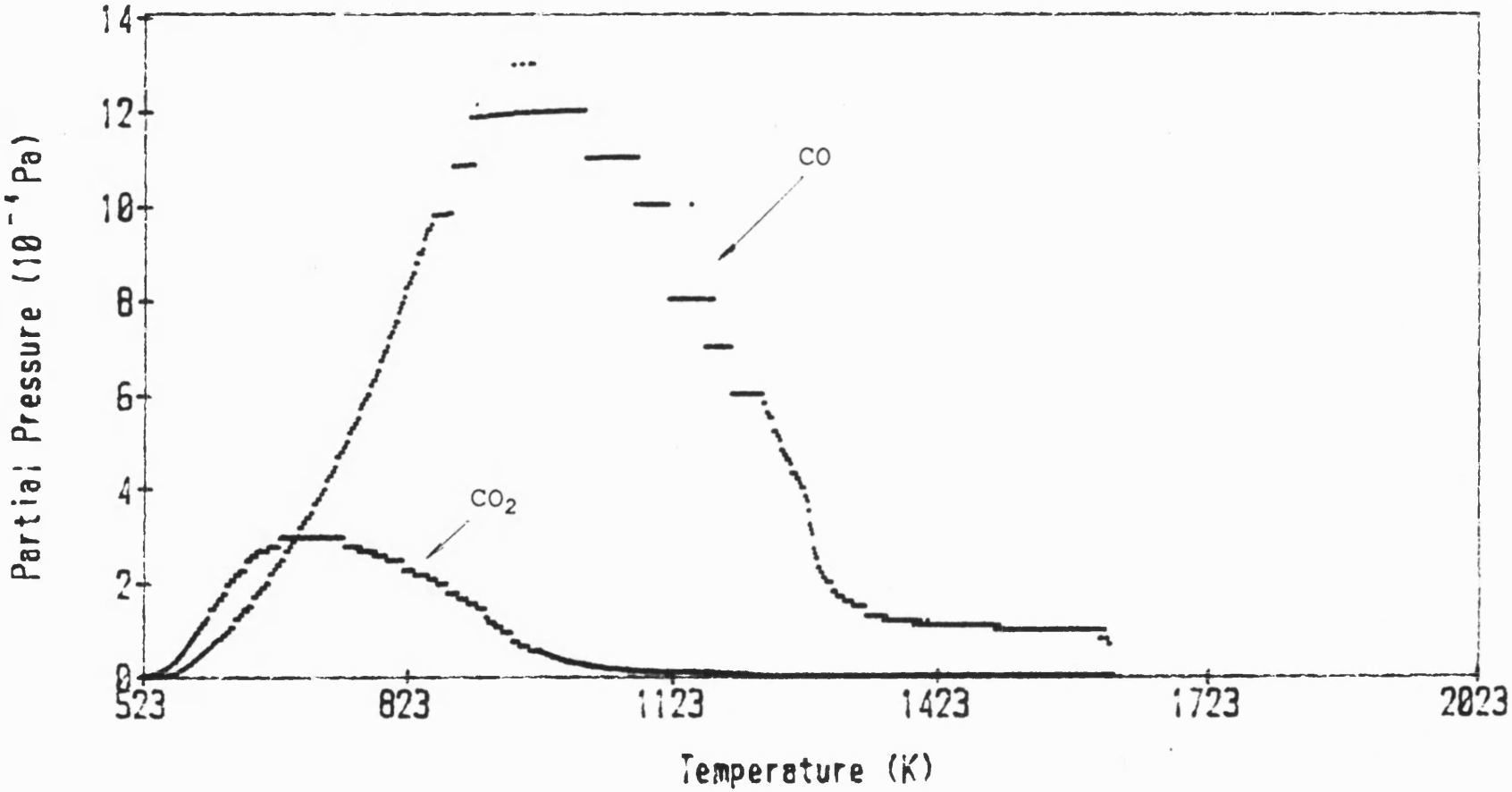

Figure 4.8 Classical TPD spectrum of Longgannet coal char (Dem) before gasification, maximum temperature 1273 K.

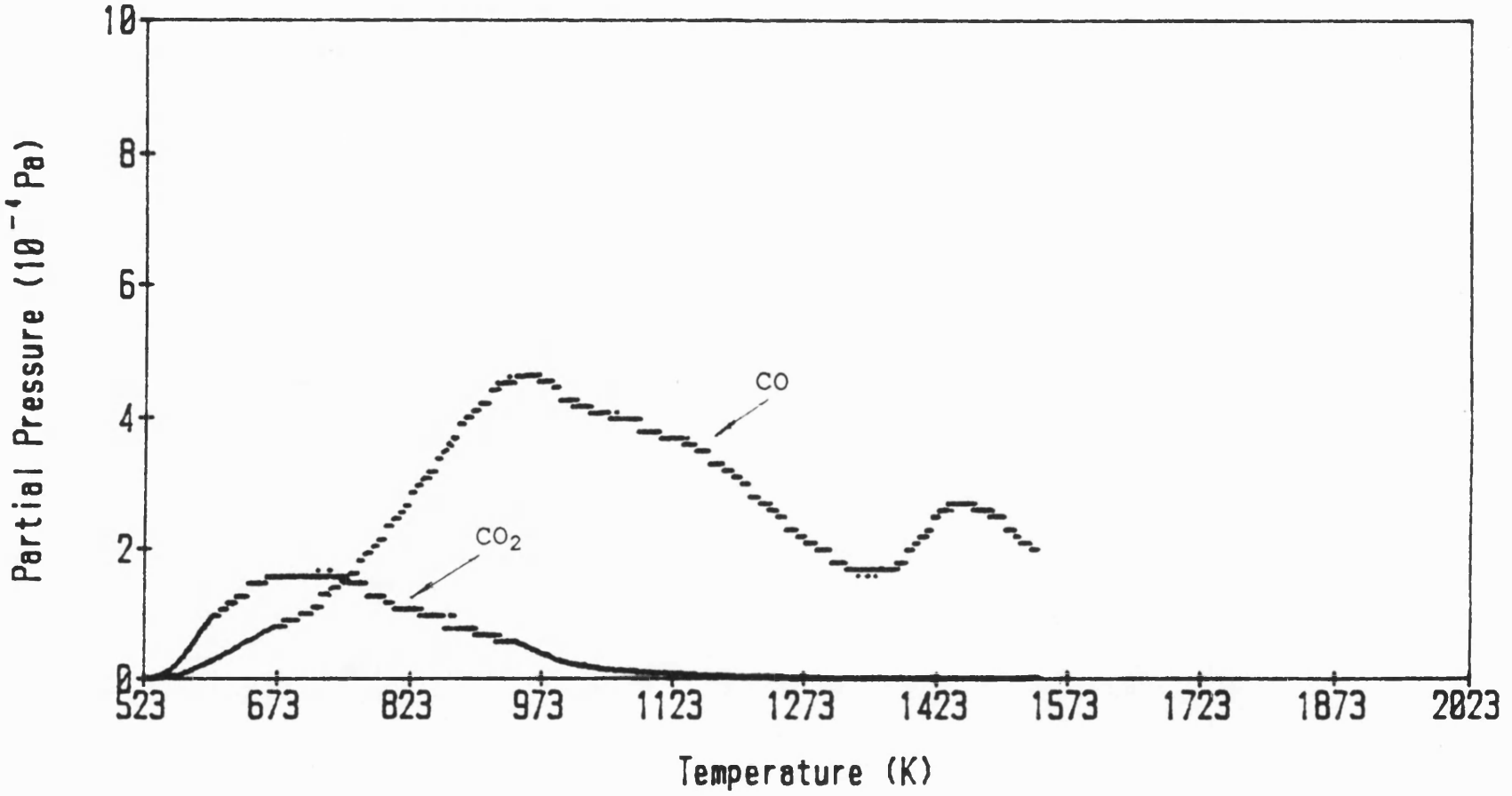

Figure 4.9 Classical TPD spectrum of Baddesley coal char (Dem) before gasification, maximum temperature 1473 K.

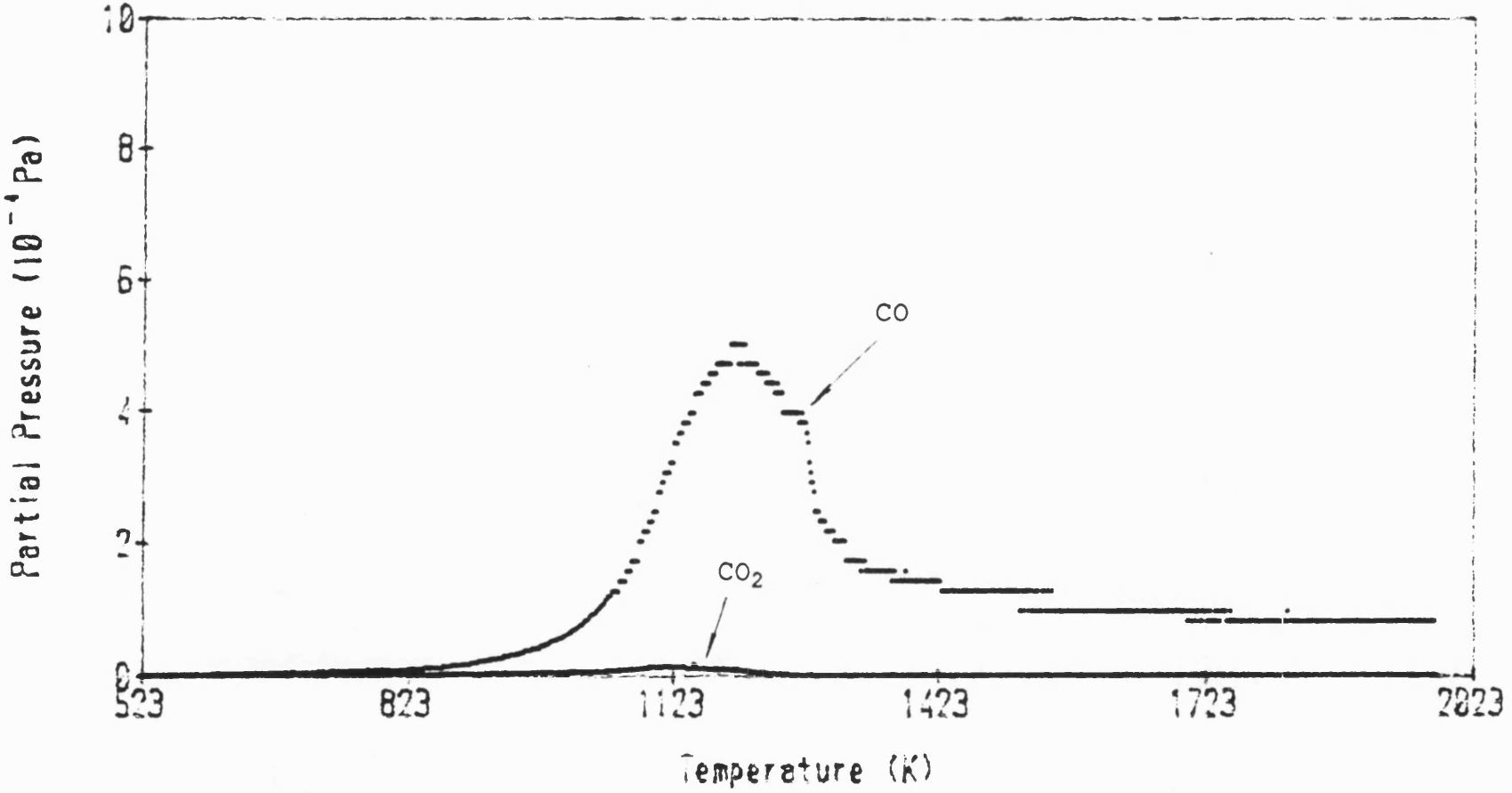

Figure 4.10 TPD spectrum of PVDC char quenched during CO_2 gasification, maximum temperature 1273 K.

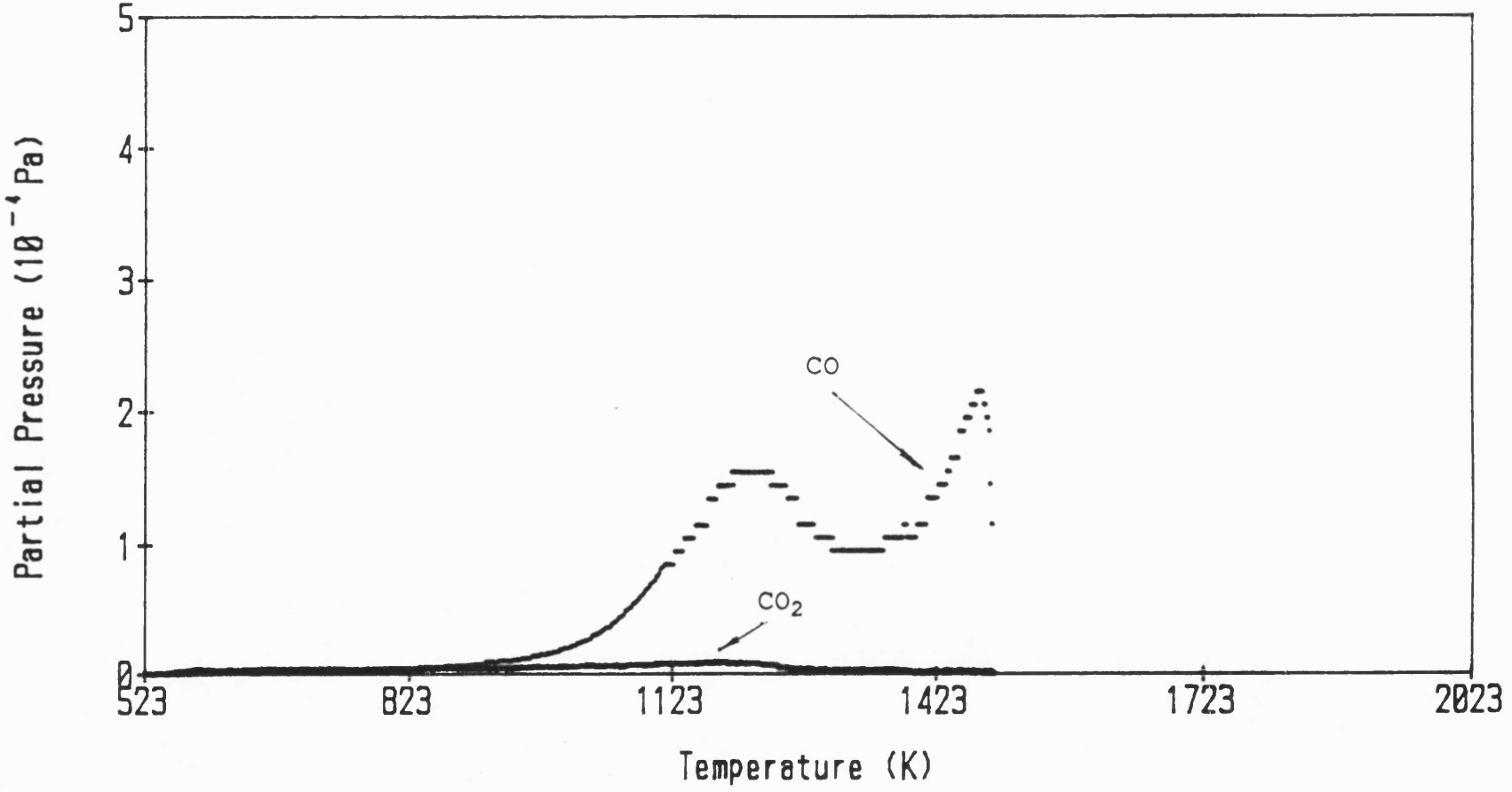

Figure 4.11 TPD spectrum of PVDC char quenched during CO_2 gasification, maximum temperature 1473 K.

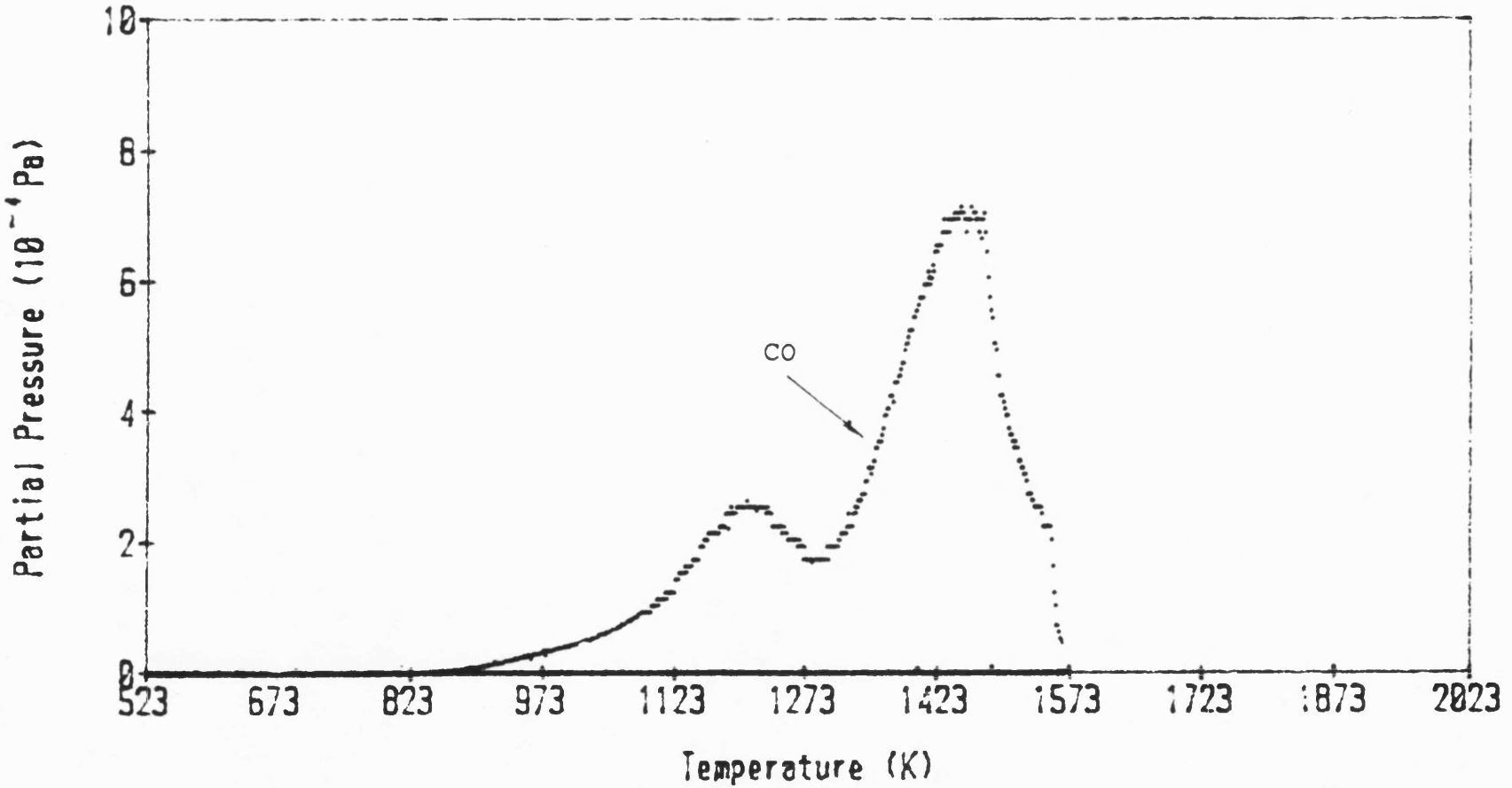

Figure 4.12 Classical TPD spectrum of PVDC char saturated with CO_2, maximum temperature 1473 K.

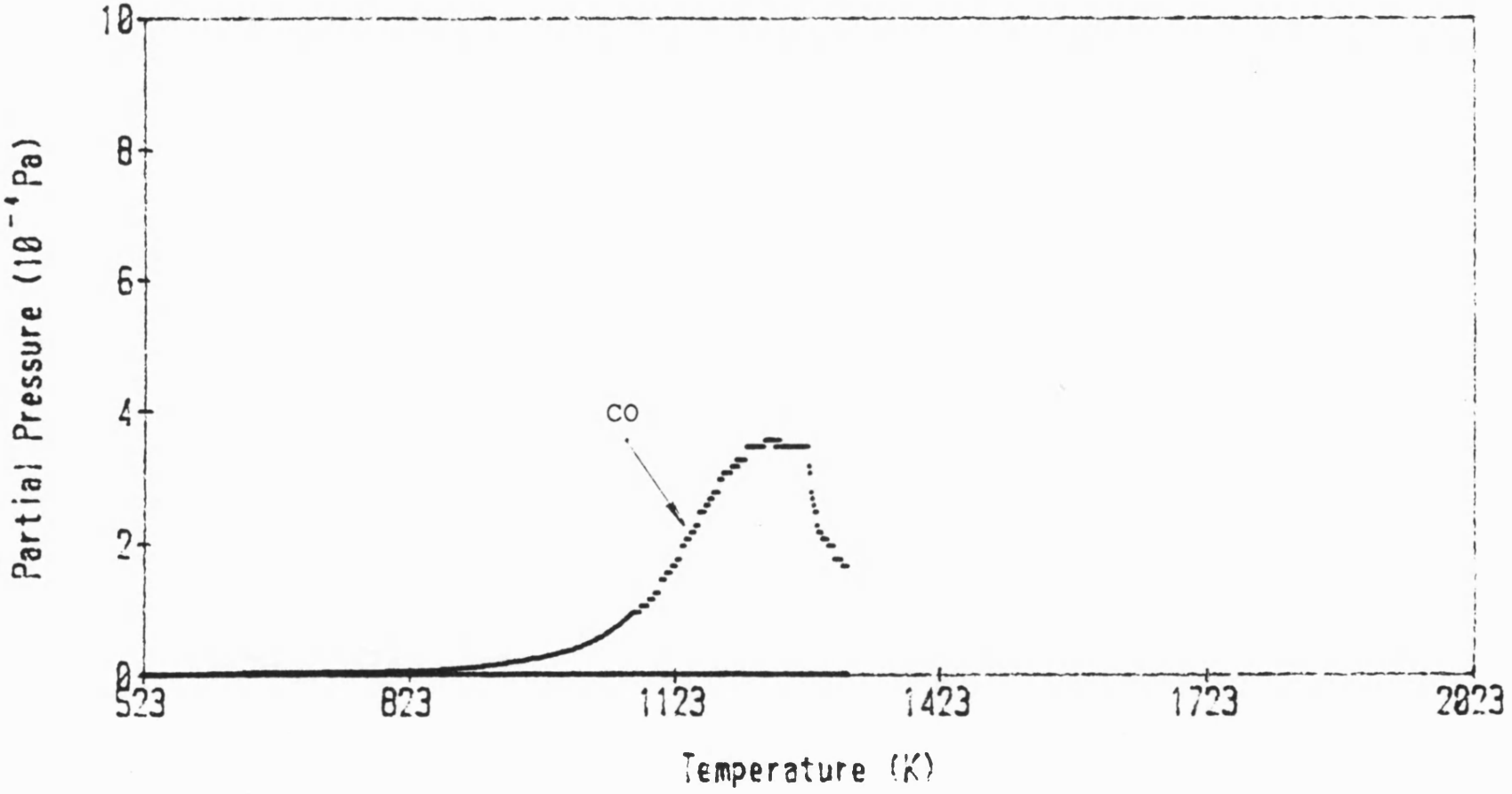

Figure 4.13 TPD spectrum of Baddesley coal char (Dem) quenched during CO_2 gasification, maximum temperature 1273 K

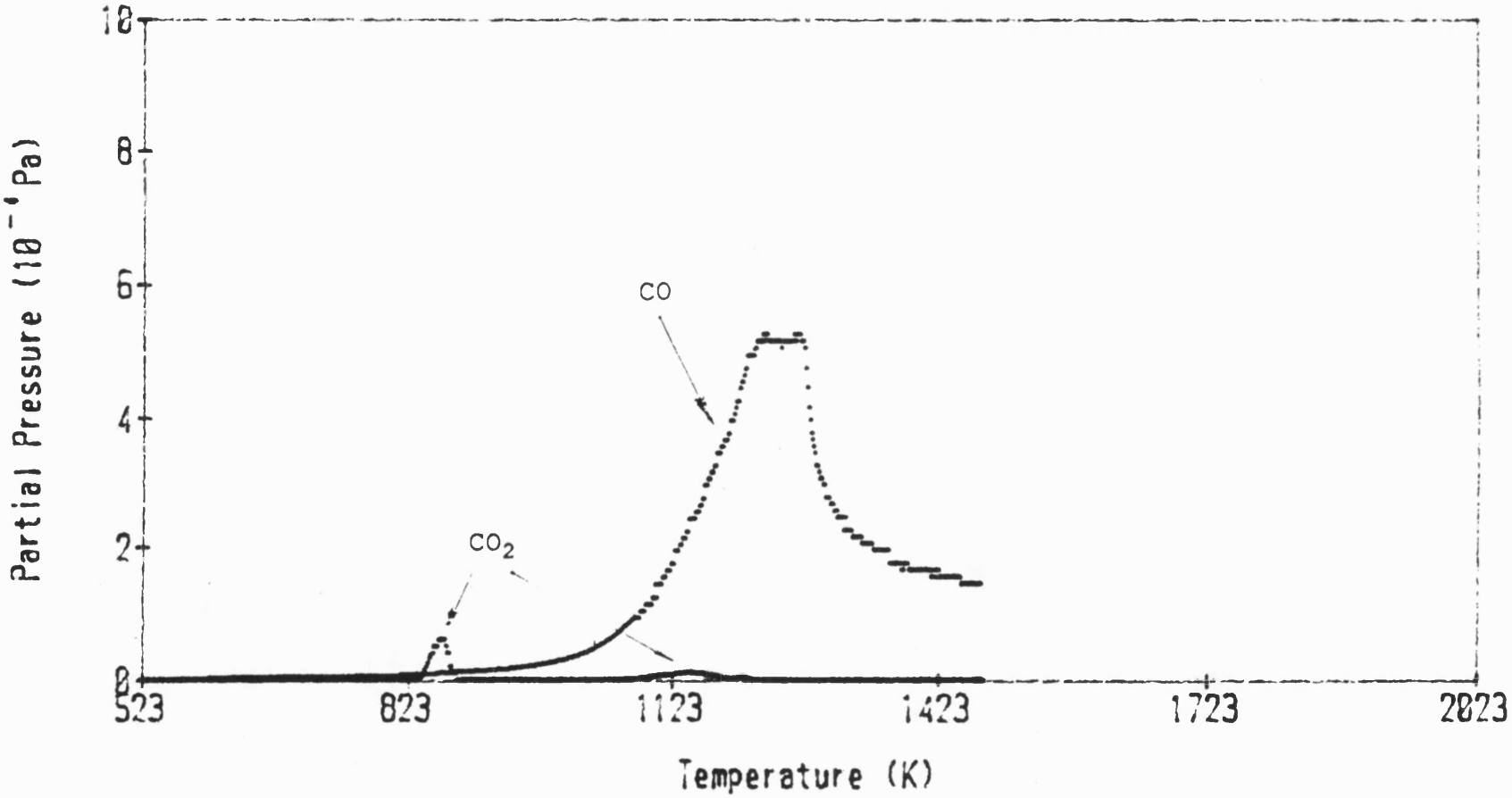

Figure 4.14 TPD spectrum of Baddesley coal char(Undem) quenched during CO_2 gasification, maximum temperature 1273 K

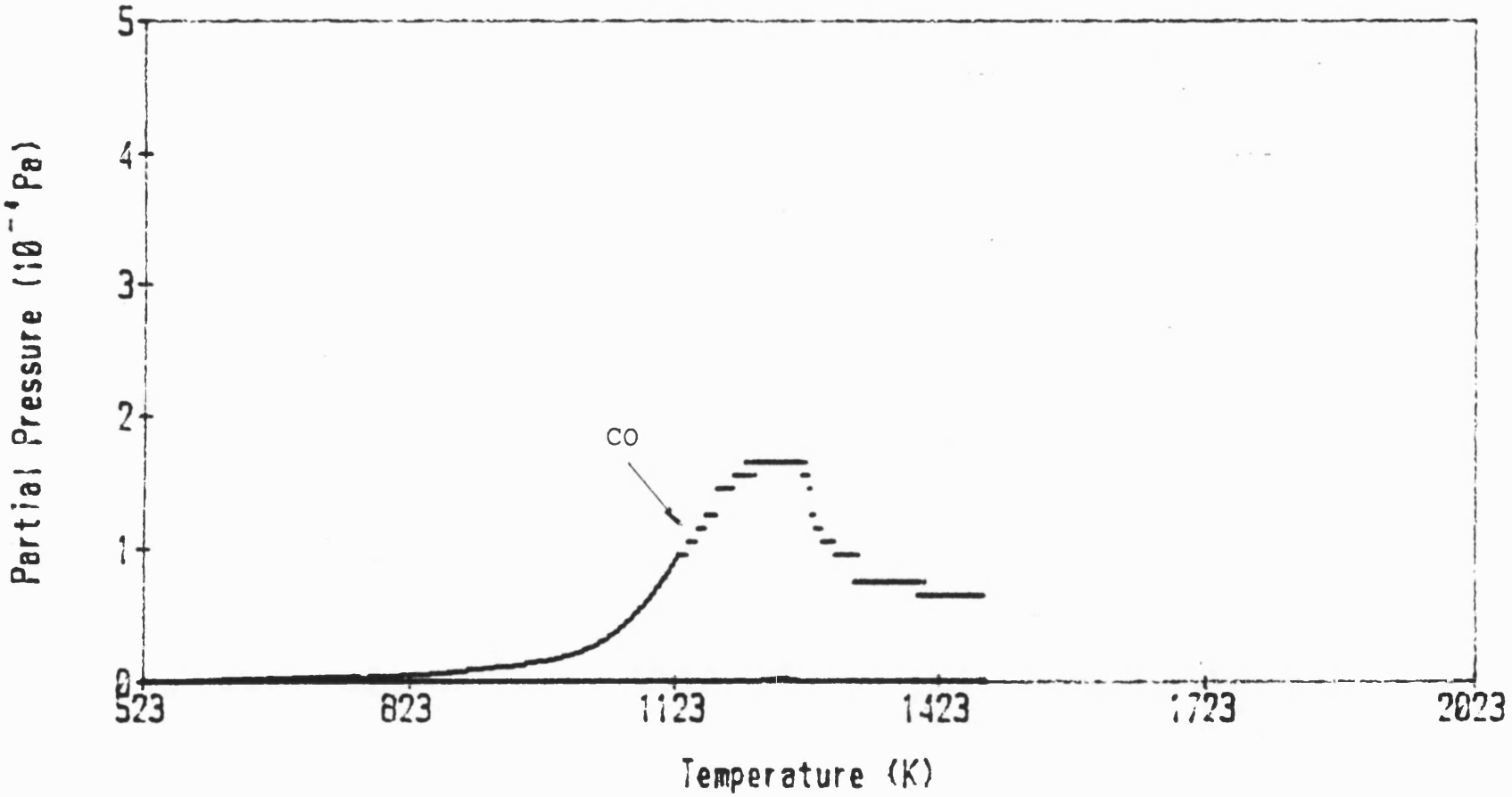

Figure 4.15 TPD spectrum of Tilmanstone coal char (Dem) quenched during CO_2 gasification, maximum temperature 1273 K

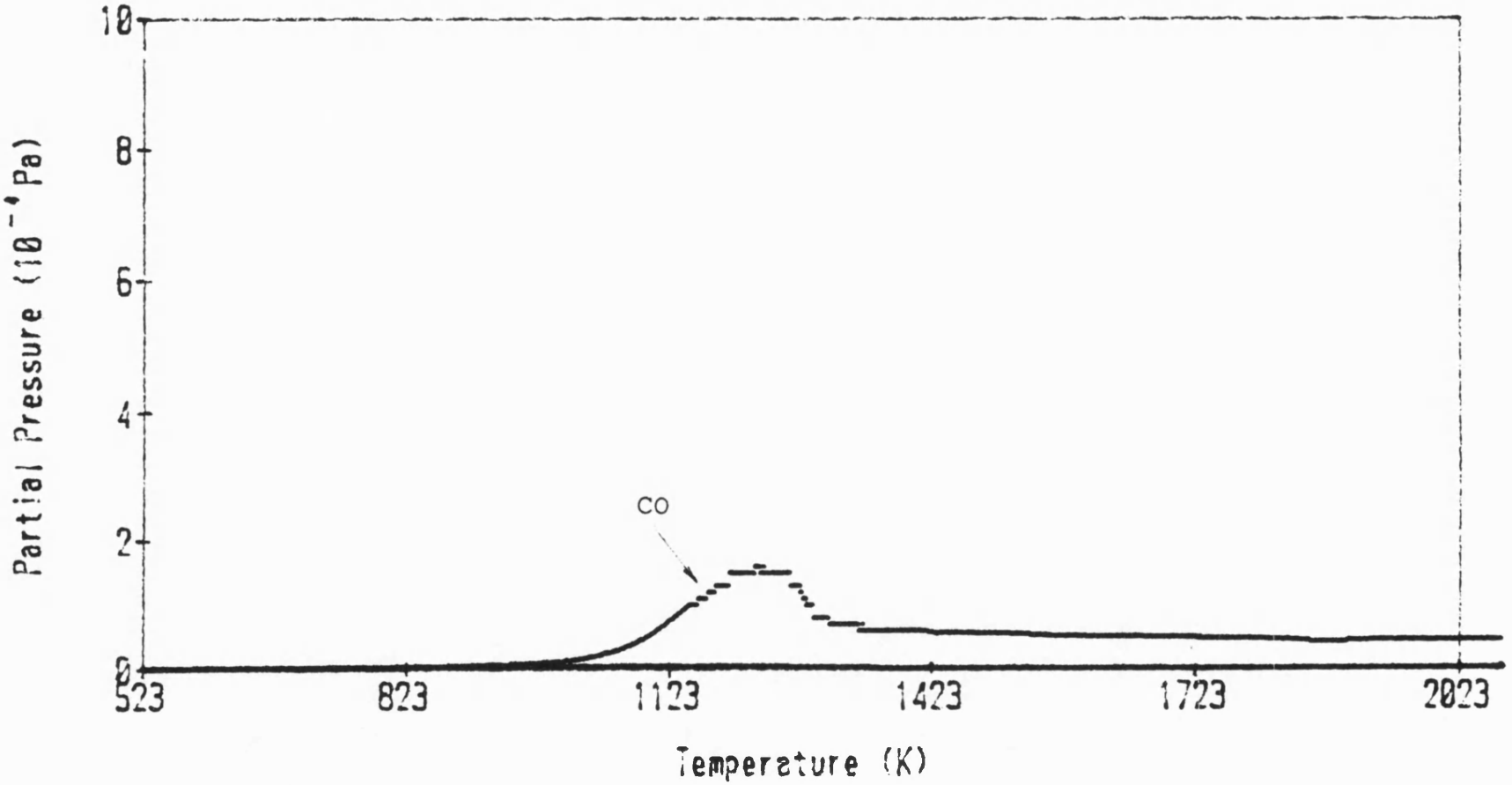

Figure 4.16 TPD spectrum of Cynheidre coal char (Dem) quenched during CO_2 gasification, maximum temperature 1273 K

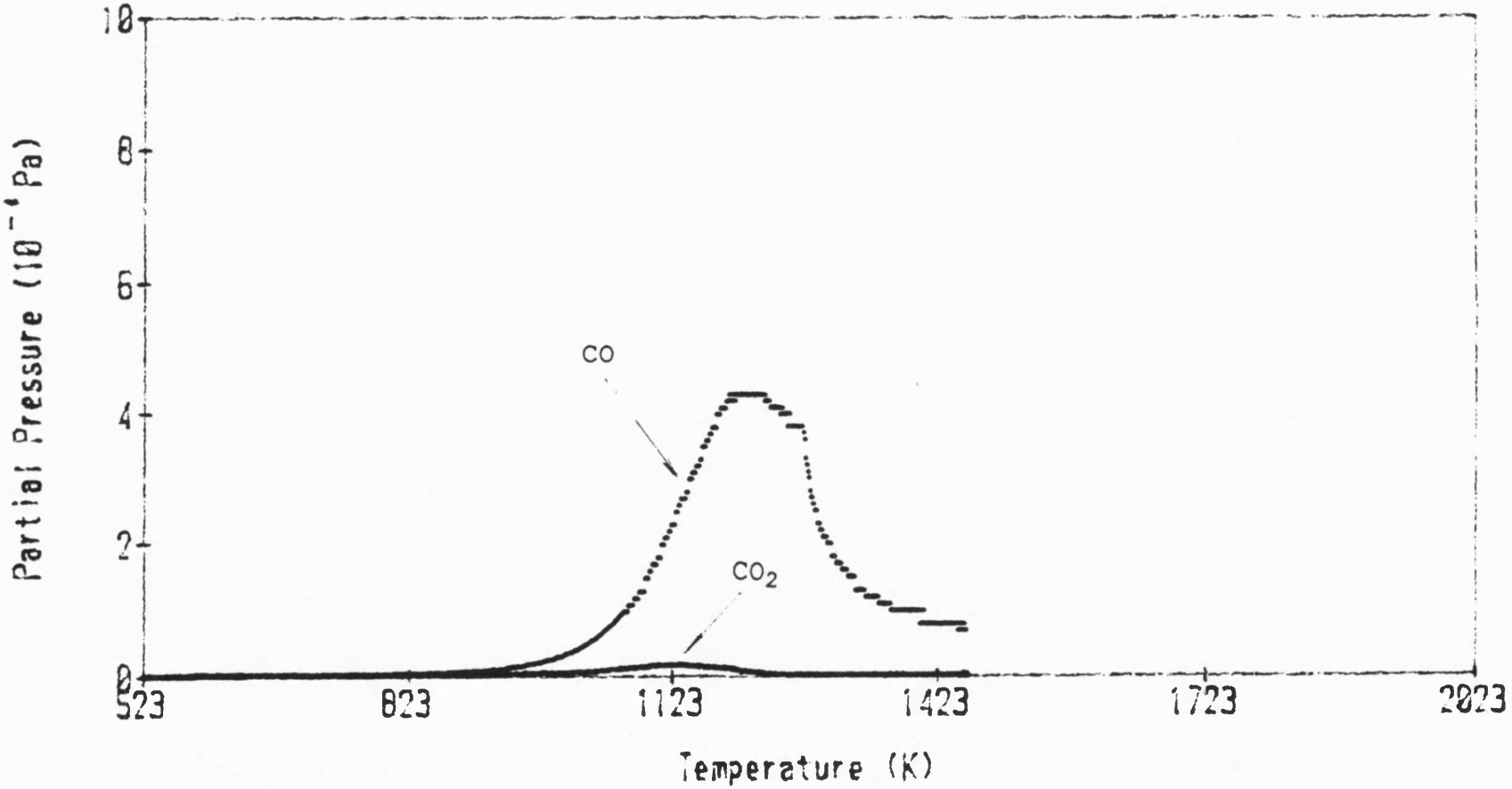

Figure 4.17 TPD spectrum of Bagworth coal char (Dem) quenched during CO_2 gasification, maximum temperature 1273 K

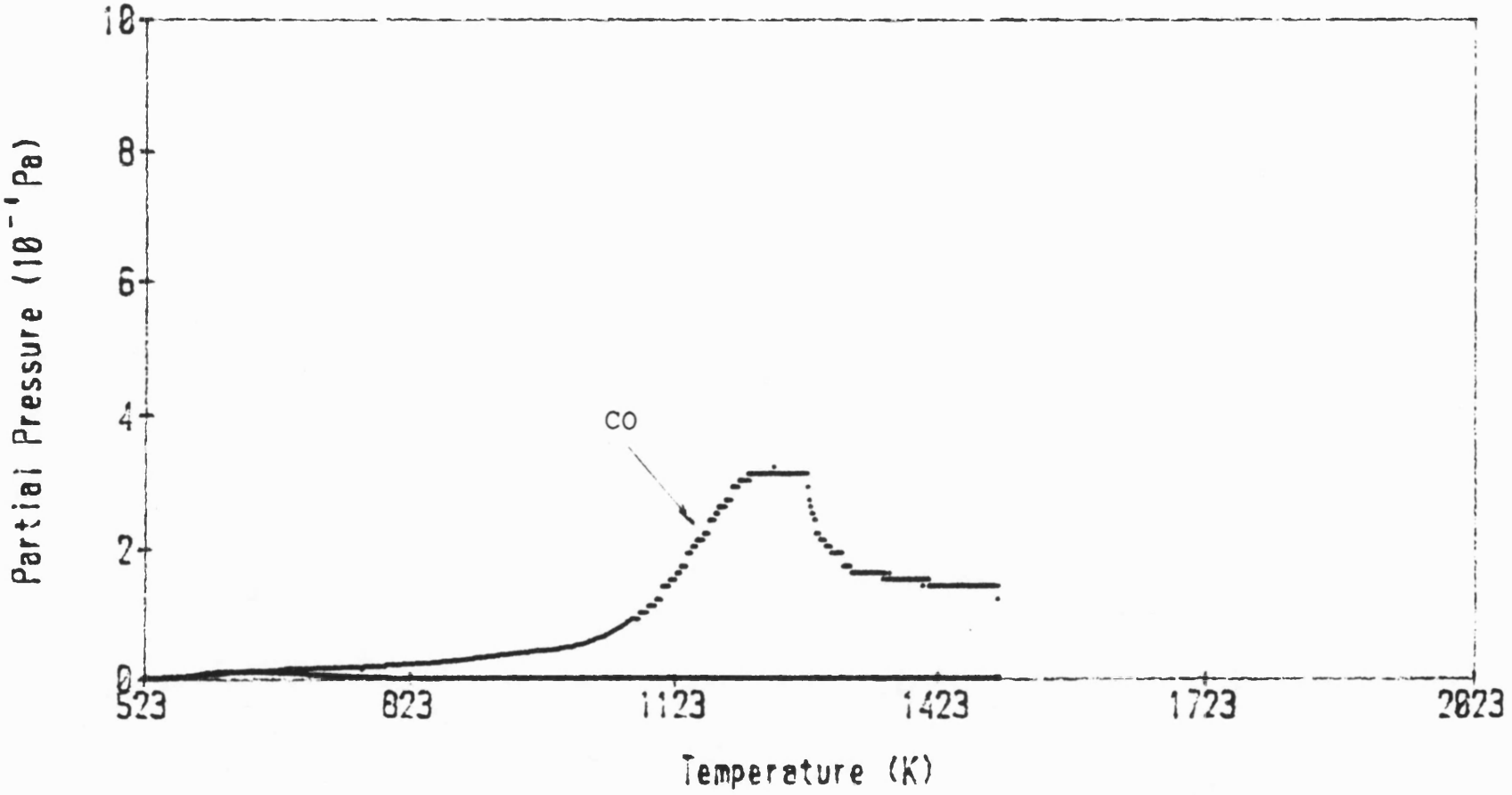

Figure 4.18 TPD spectrum of Longgannet coal char (Dem) quenched during CO_2 gasification, maximum temperature 1273 K

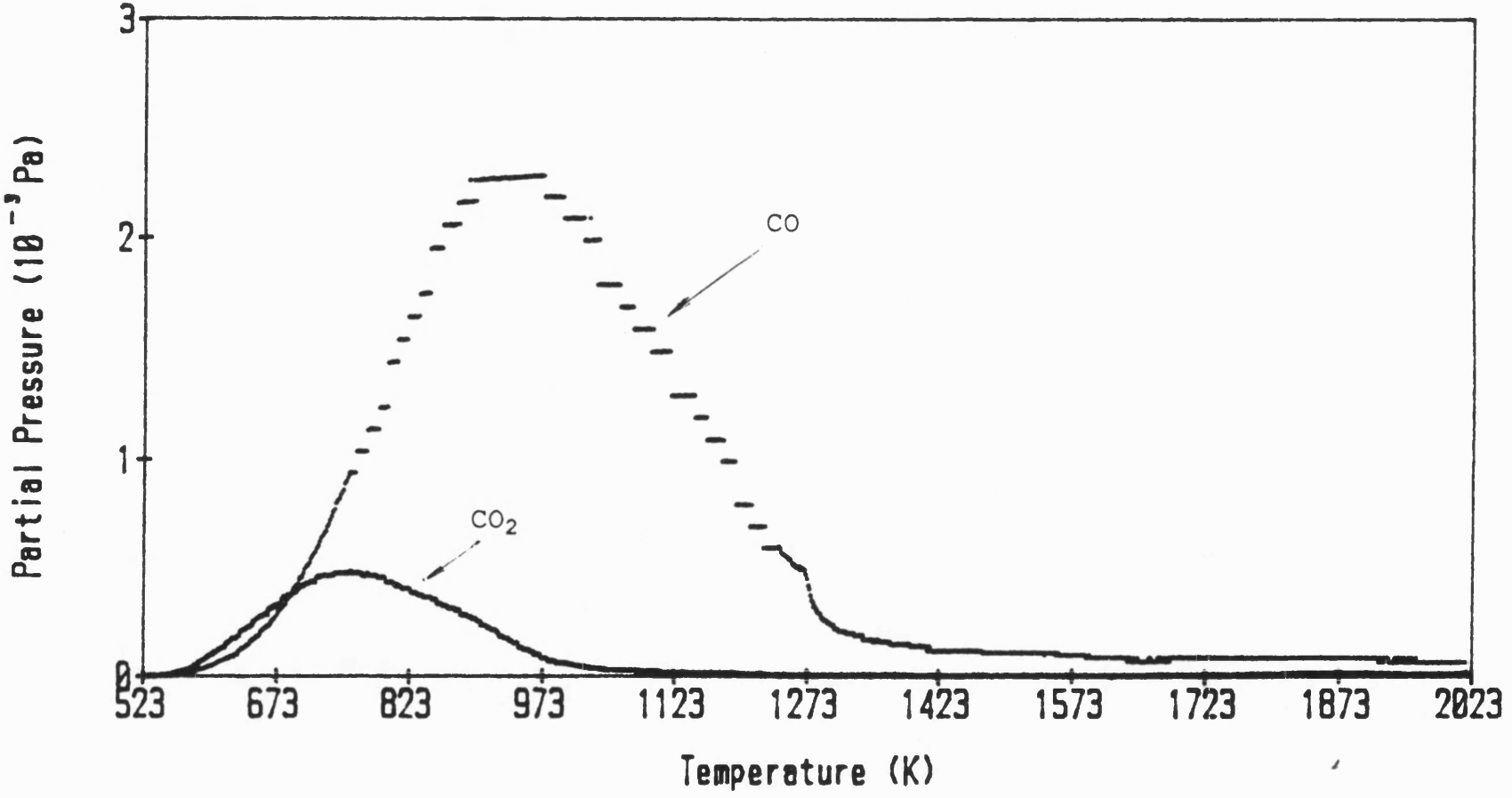

Figure 4.19 Classical TPD spectrum of PVDC char after CO_2 gasification, maximum temperature 1273 K.

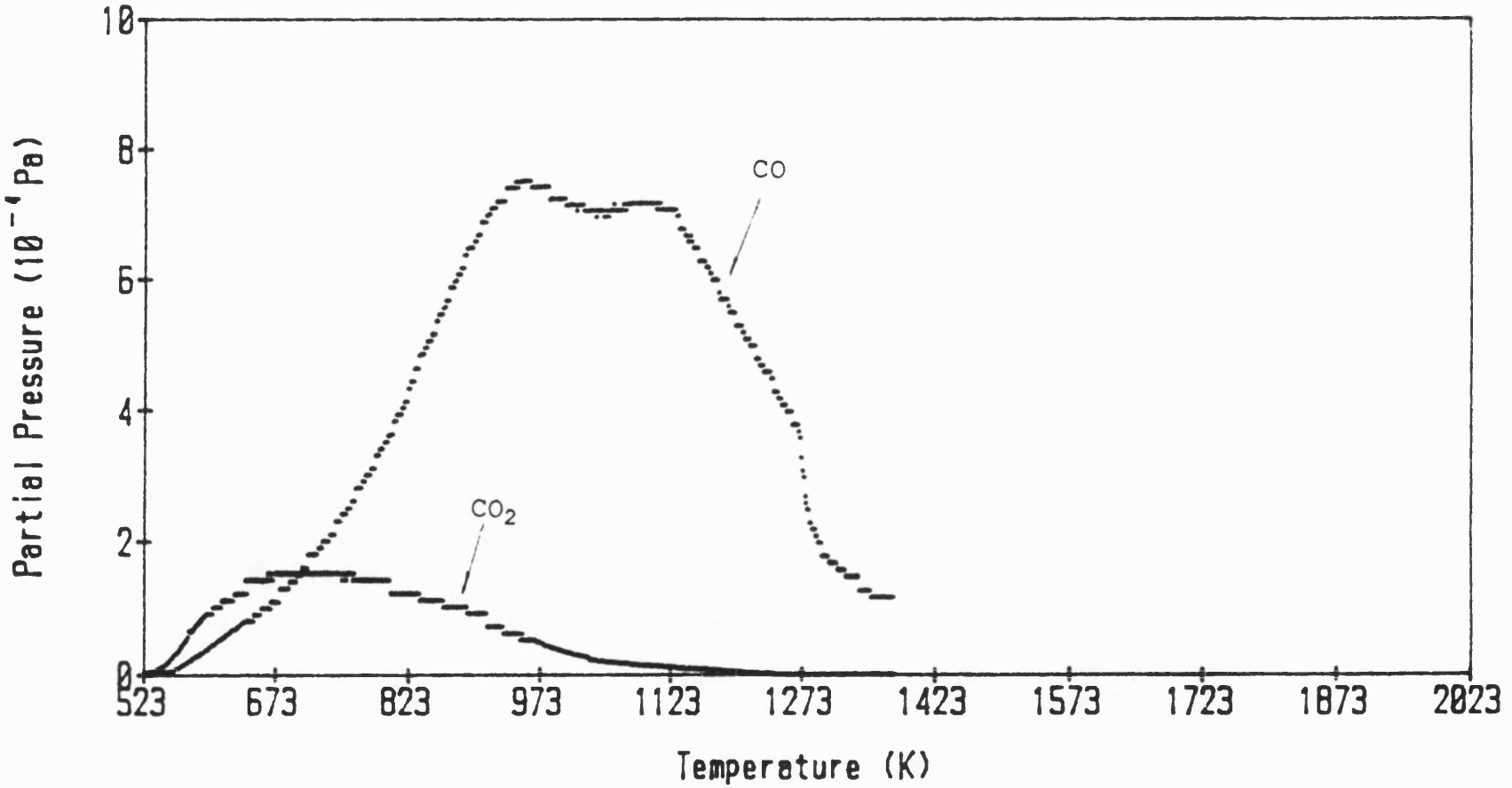

Figure 4.20 Classical TPD spectrum of Baddesley coal char (Dem) after CO_2 gasification, maximum temperature 1273 K.

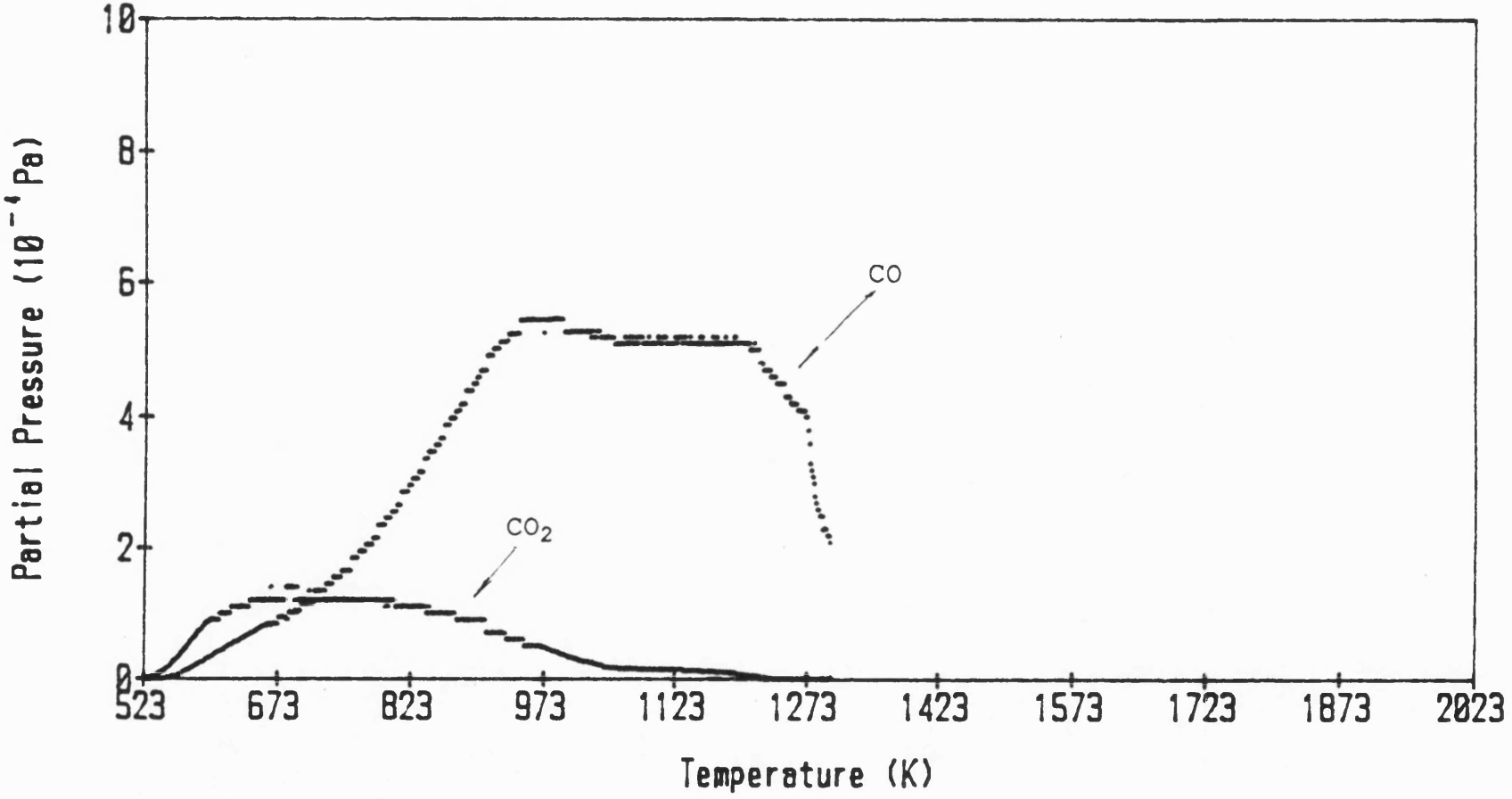

Figure 4.21 Classical TPD spectrum of Baddesley coal char (Undem) after CO_2 gasification, maximum temperature 1273 K.

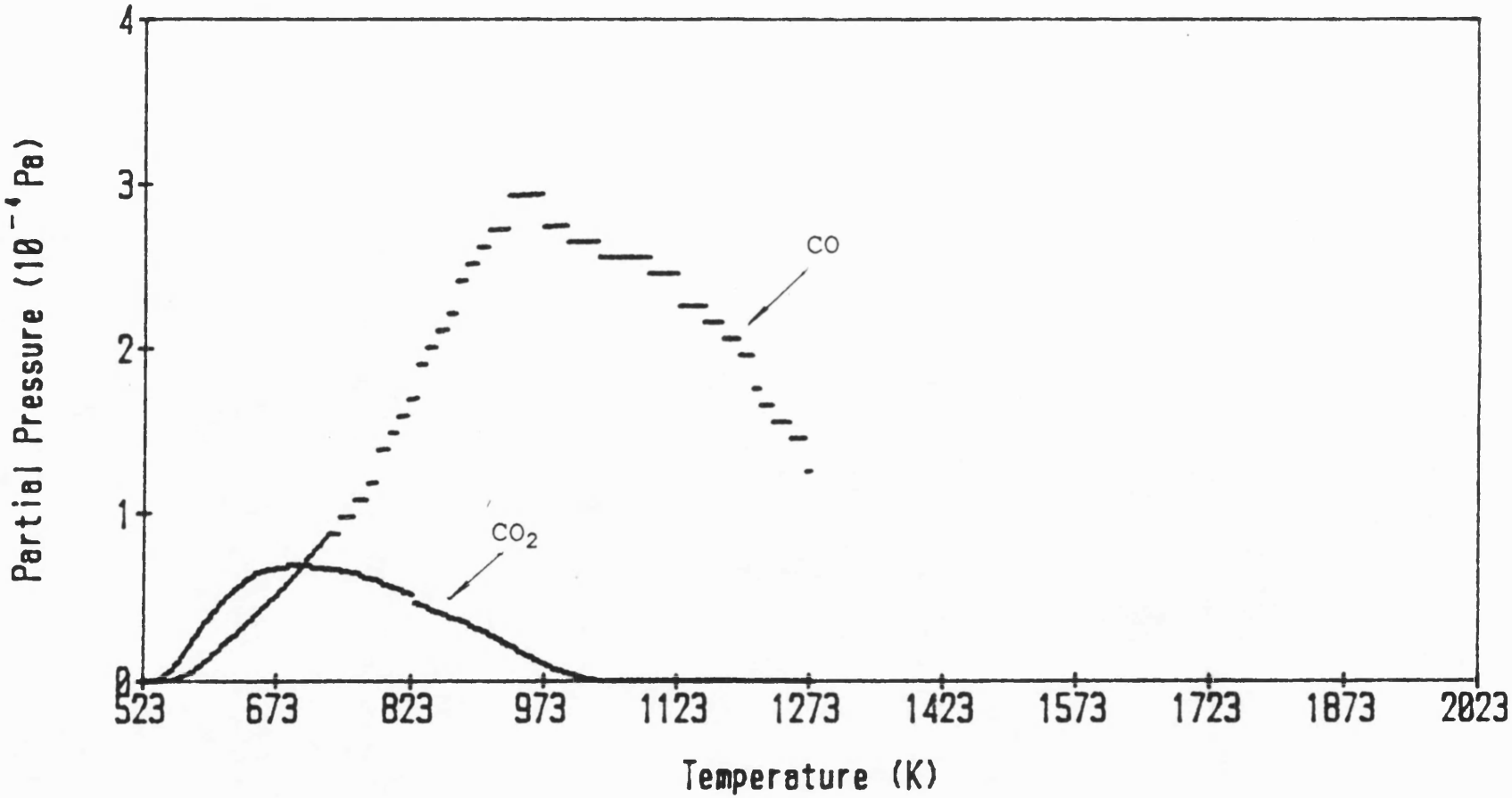

Figure 4.22 Classical TPD spectrum of Tilmanstone coal char (Dem) after CO_2 gasification, maximum temperature 1273 K.

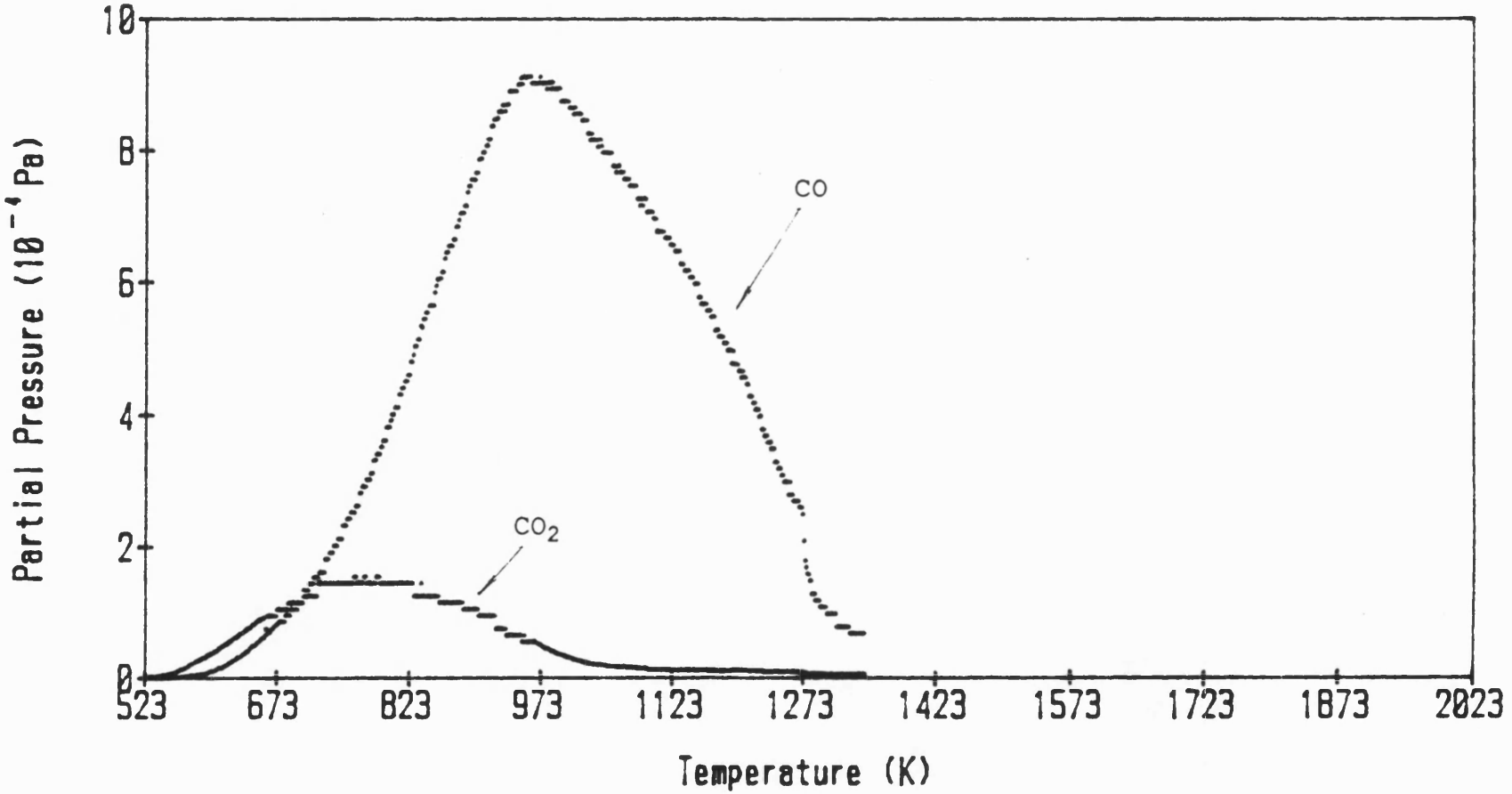

Figure 4.23 Classical TPD spectrum of Cynheidre coal char (Dem) after CO_2 gasification, maximum temperature 1273 K.

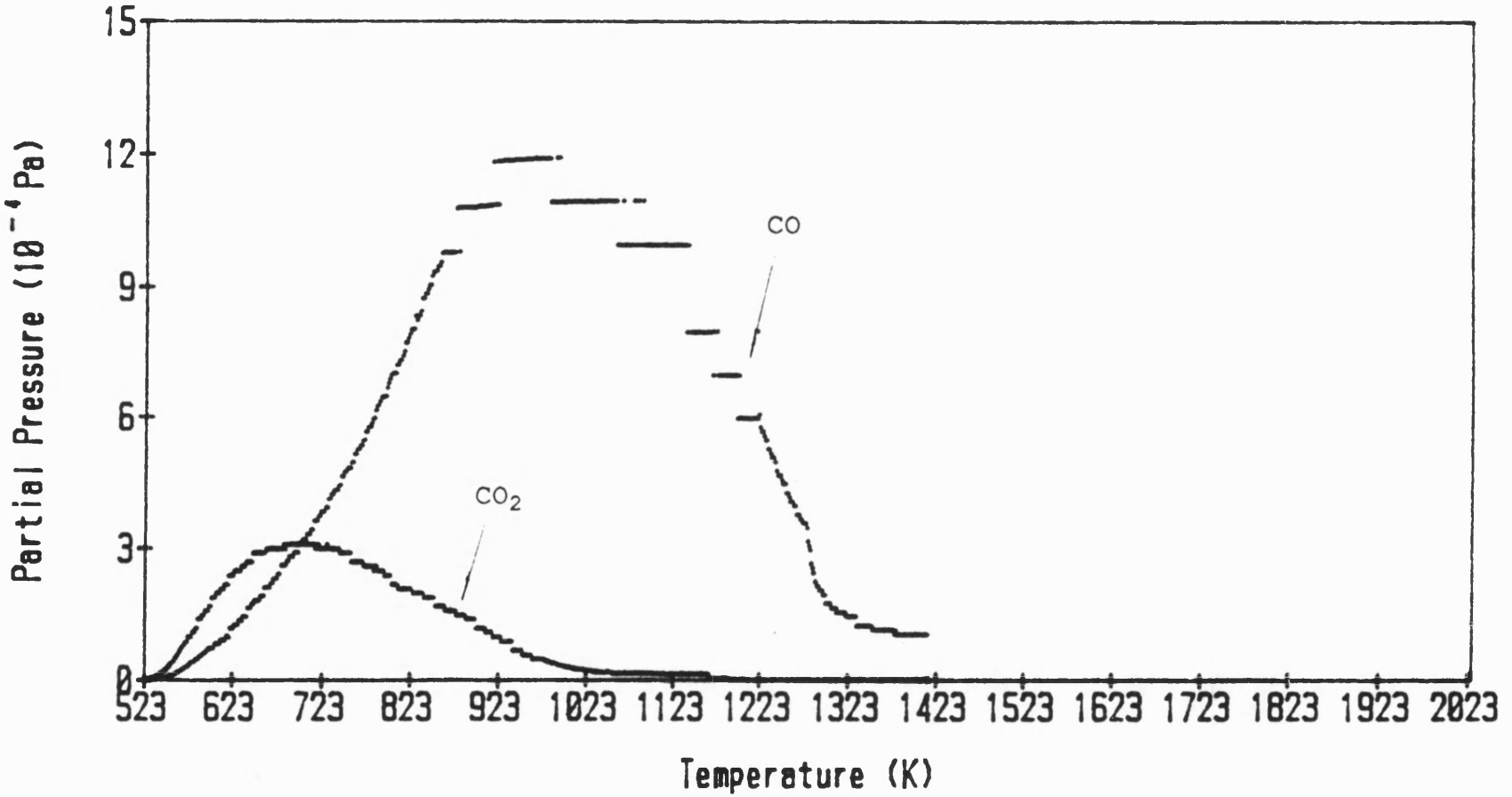

Figure 4.24 Classical TPD spectrum of Bagworth coal char (Dem), after CO_2 gasification, maximum temperature 1273 K

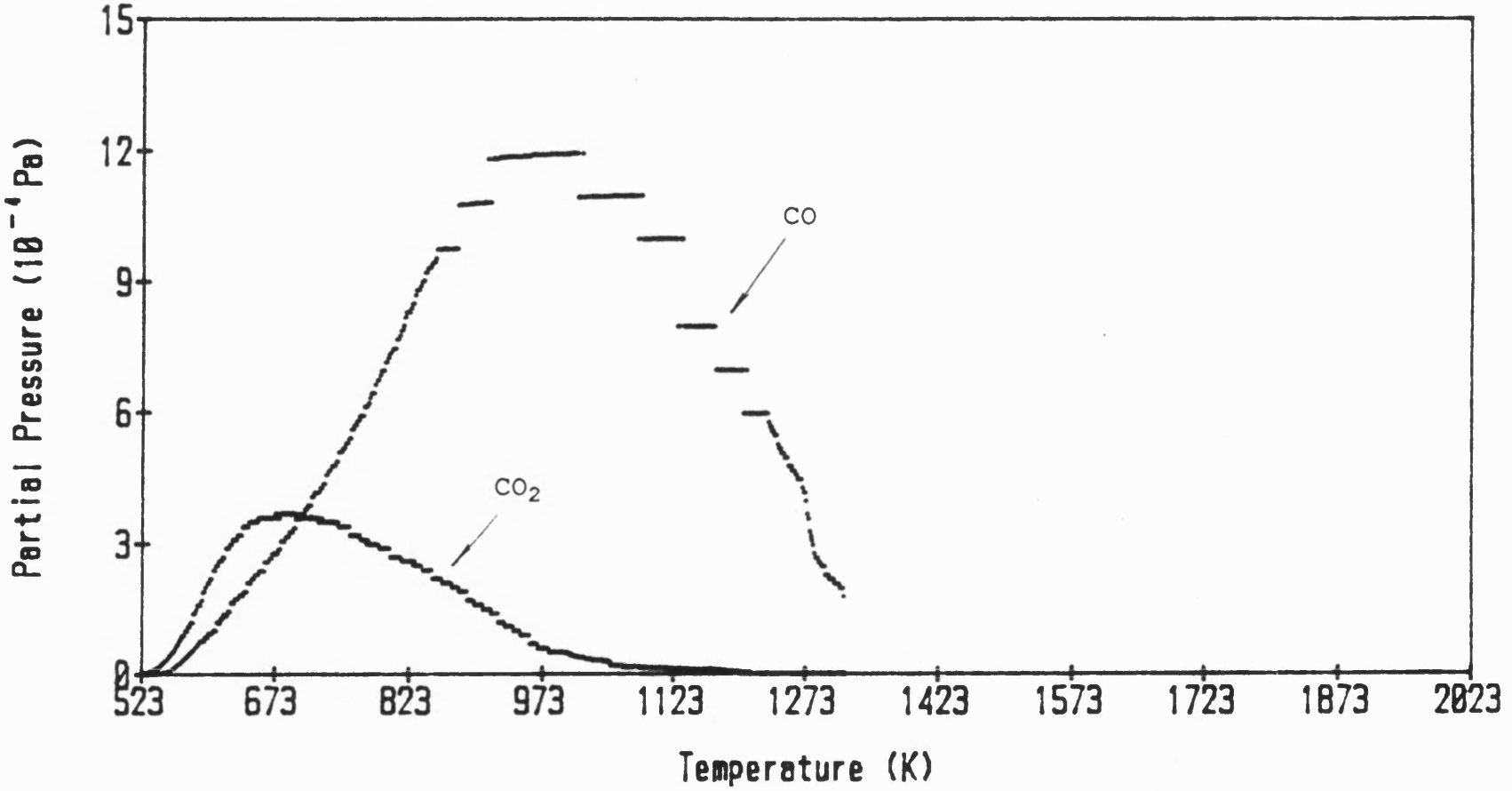

Figure 4.25 Classical TPD spectrum of Longgannet coal char (Dem) after CO_2 gasification, maximum temperature 1273 K.

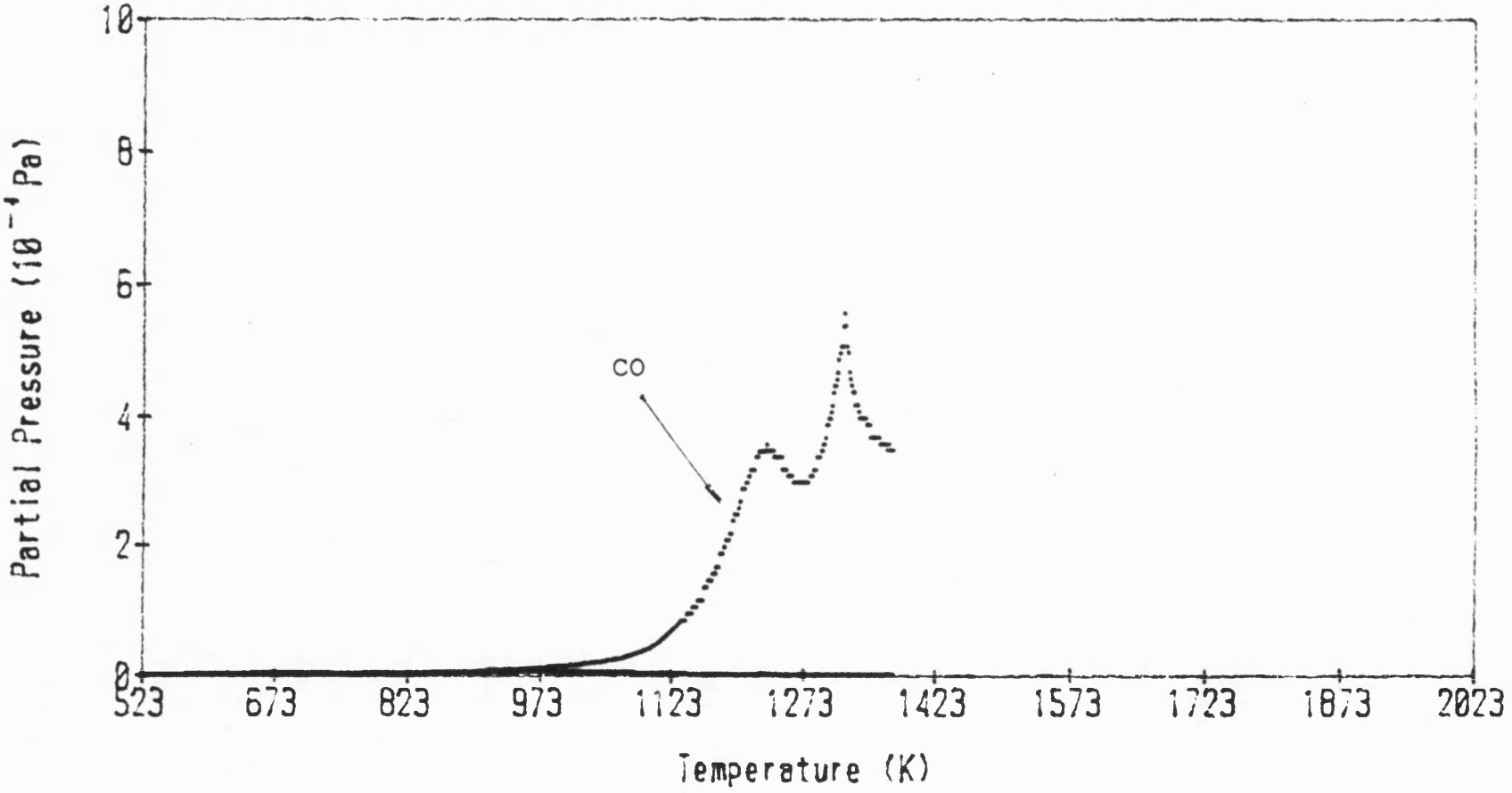

Figure 4.26 TPD spectrum to 1323 K of PVDC char after exposing in 1 atm CO at 1123 K for 1 h and quenching.

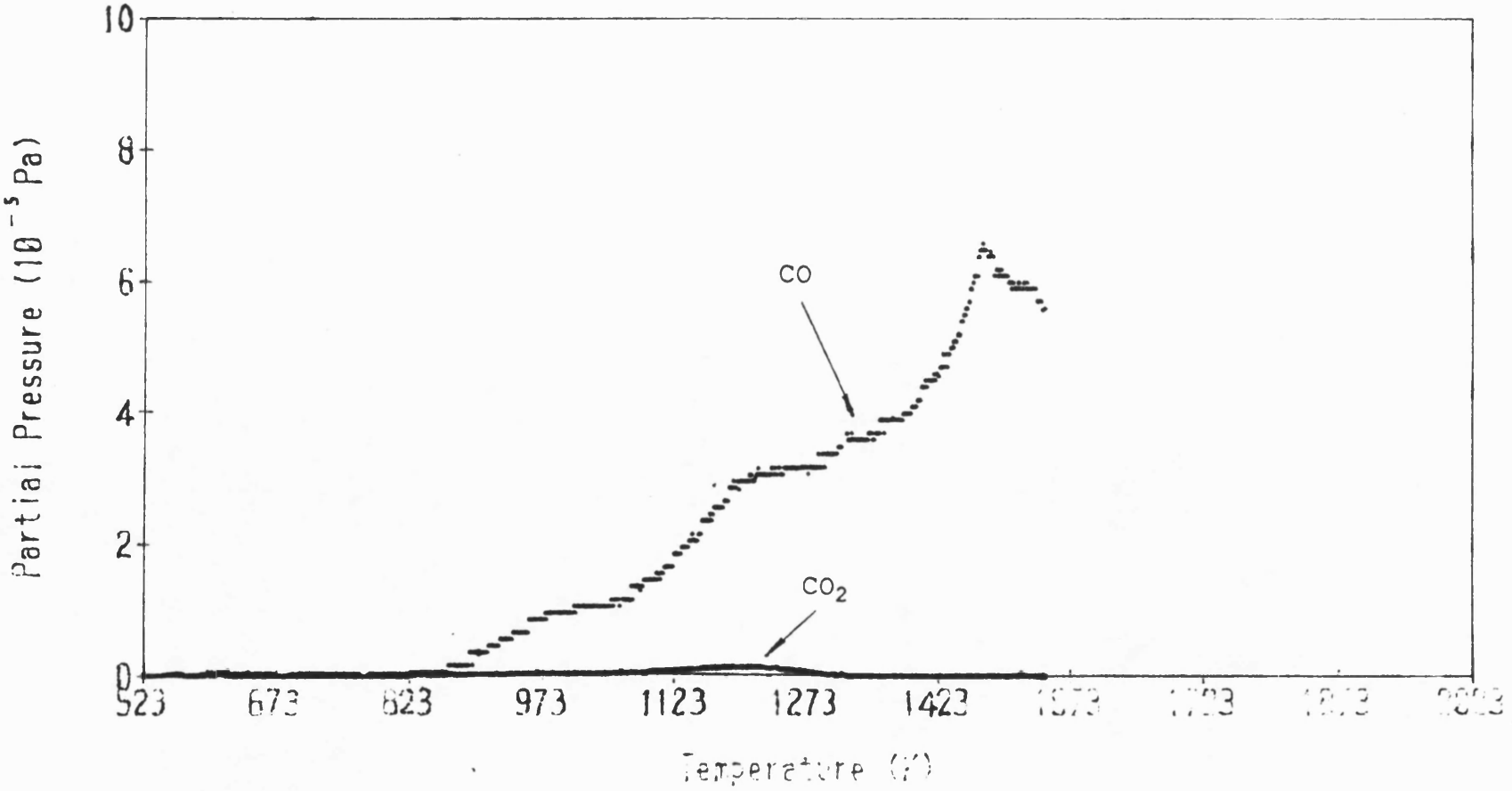

Figure 4.27 TPD spectrum to 1473 K of PVDC char after exposing in 1 atm CO at 1123 K for 1 h and then the temperature was reduced at the rate of -1 K/min to 523 K.

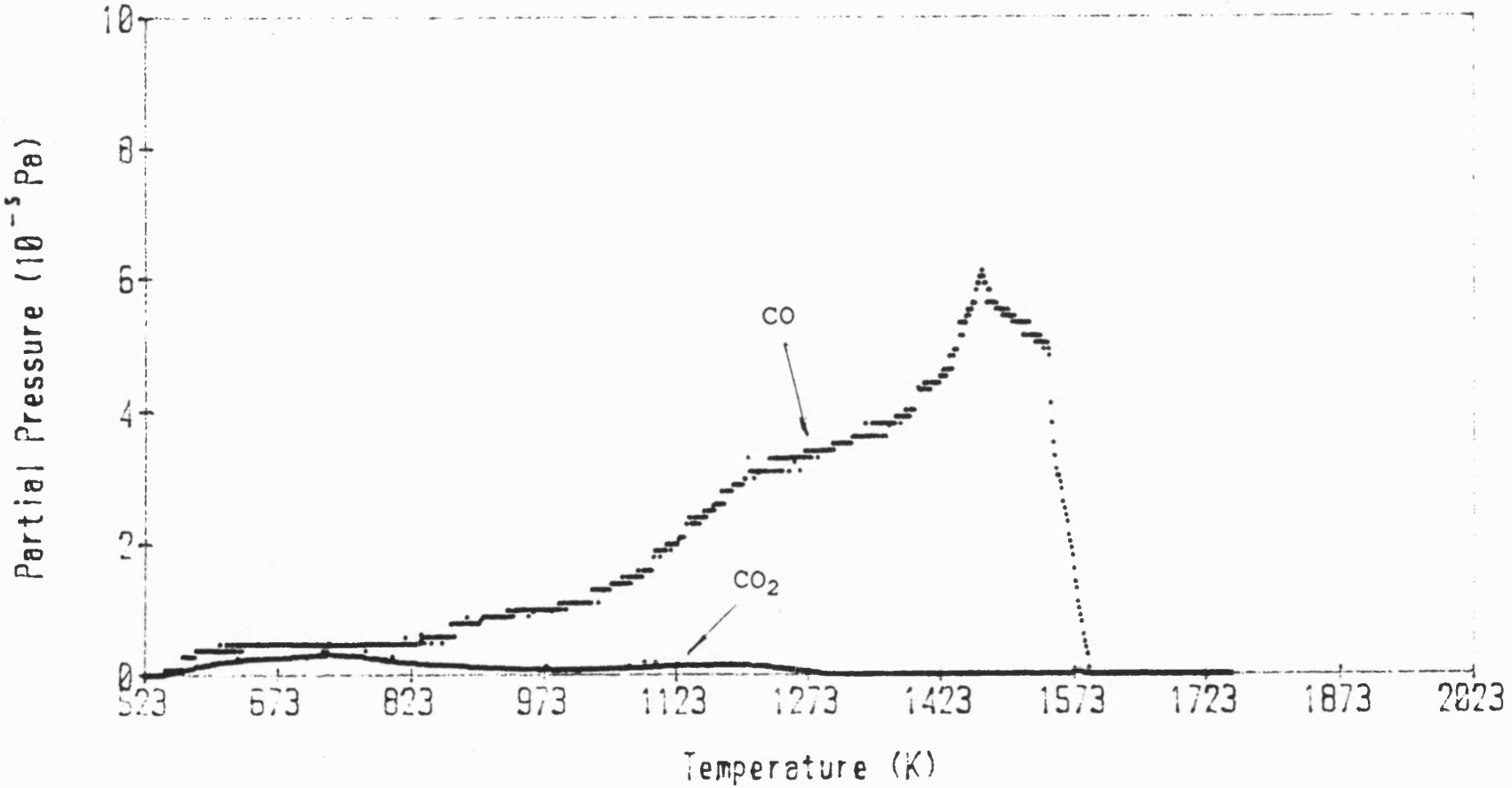

Figure 4.28 TPD spectrum to 1473 K of PVDC char after exposing in 1 atm CO at 523 K for 15 h.

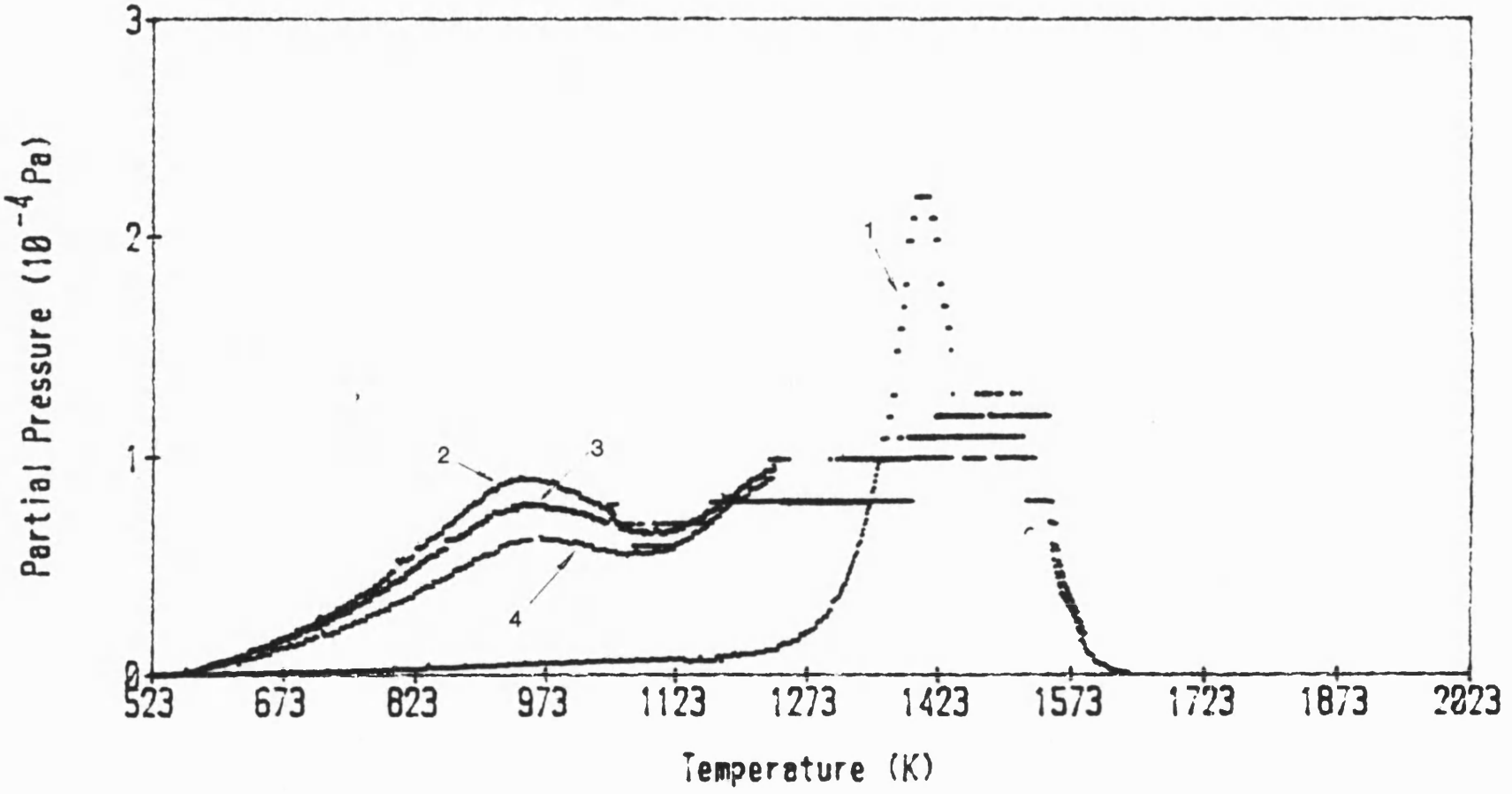

Figure 4.29 The development of active surface sites on PVDC char heat-treated at 1973 K after progressive CO_2 gasification at 1123 K. 1. before gasification, 2. 10 h, 3. 15 h, 4. 20 h.

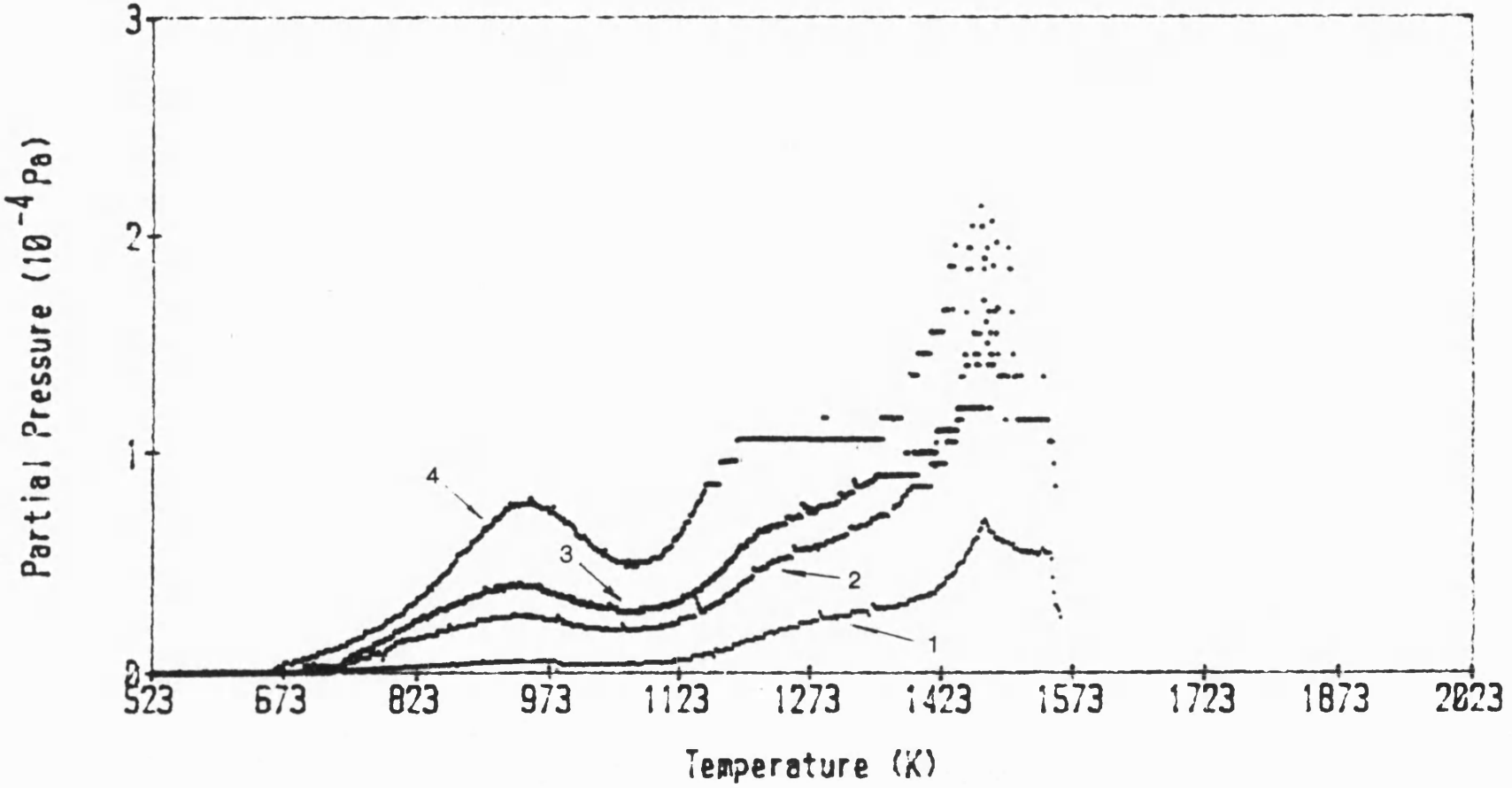

Figure 4.30 The development of active surface sites on Electrode 706 after progressive CO_2 gasification at 1123 K. 1. before gasification, 2. 10 h, 3. 15 h, 4. 20 h.

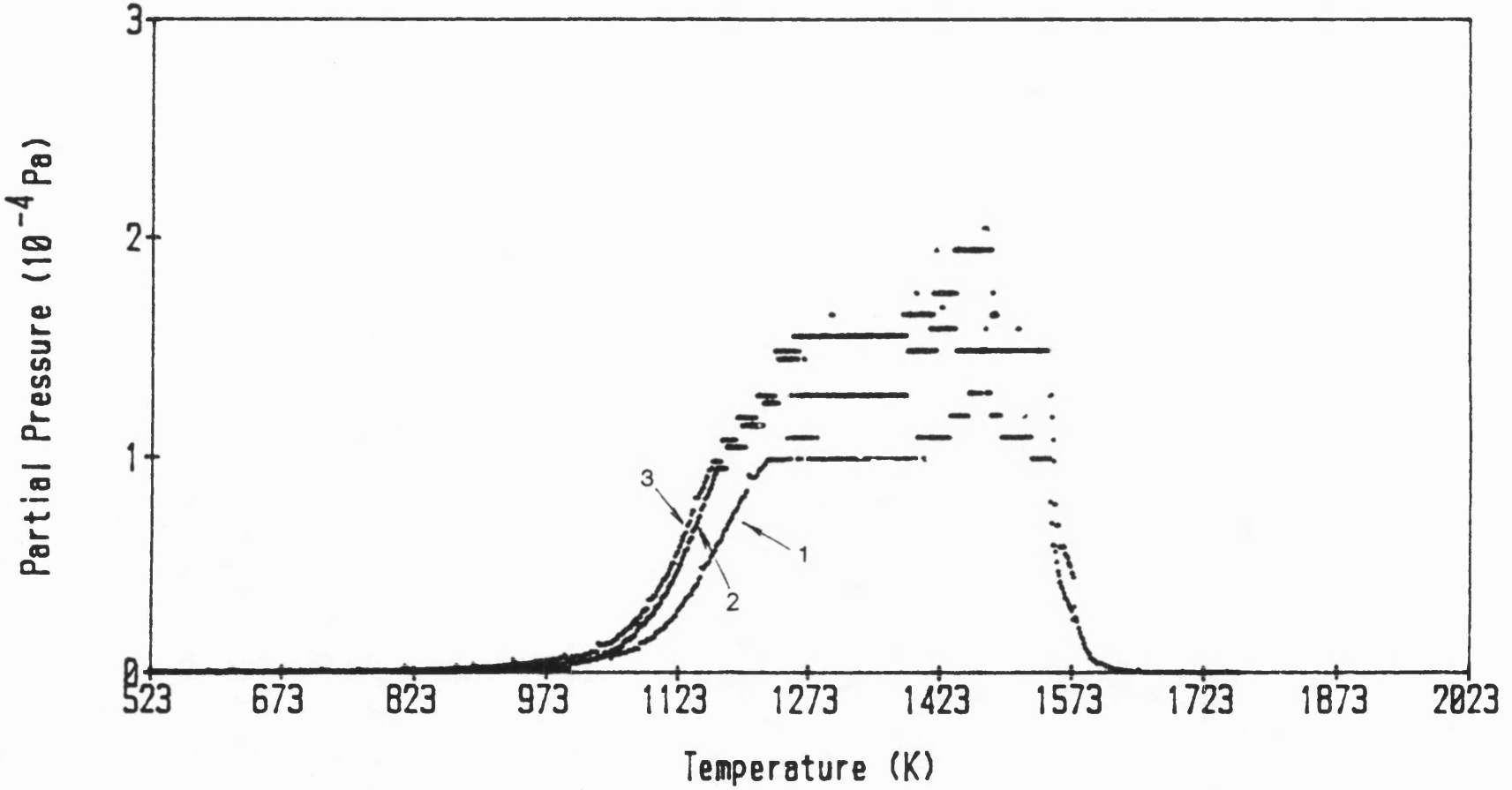

Figure 4.31 The development of active surface sites on PVDC char heat-treated at 1973 K quenched during CO_2 gasification at 1123 K. 1. 10 h, 2. 15 h, 3. 20 h.

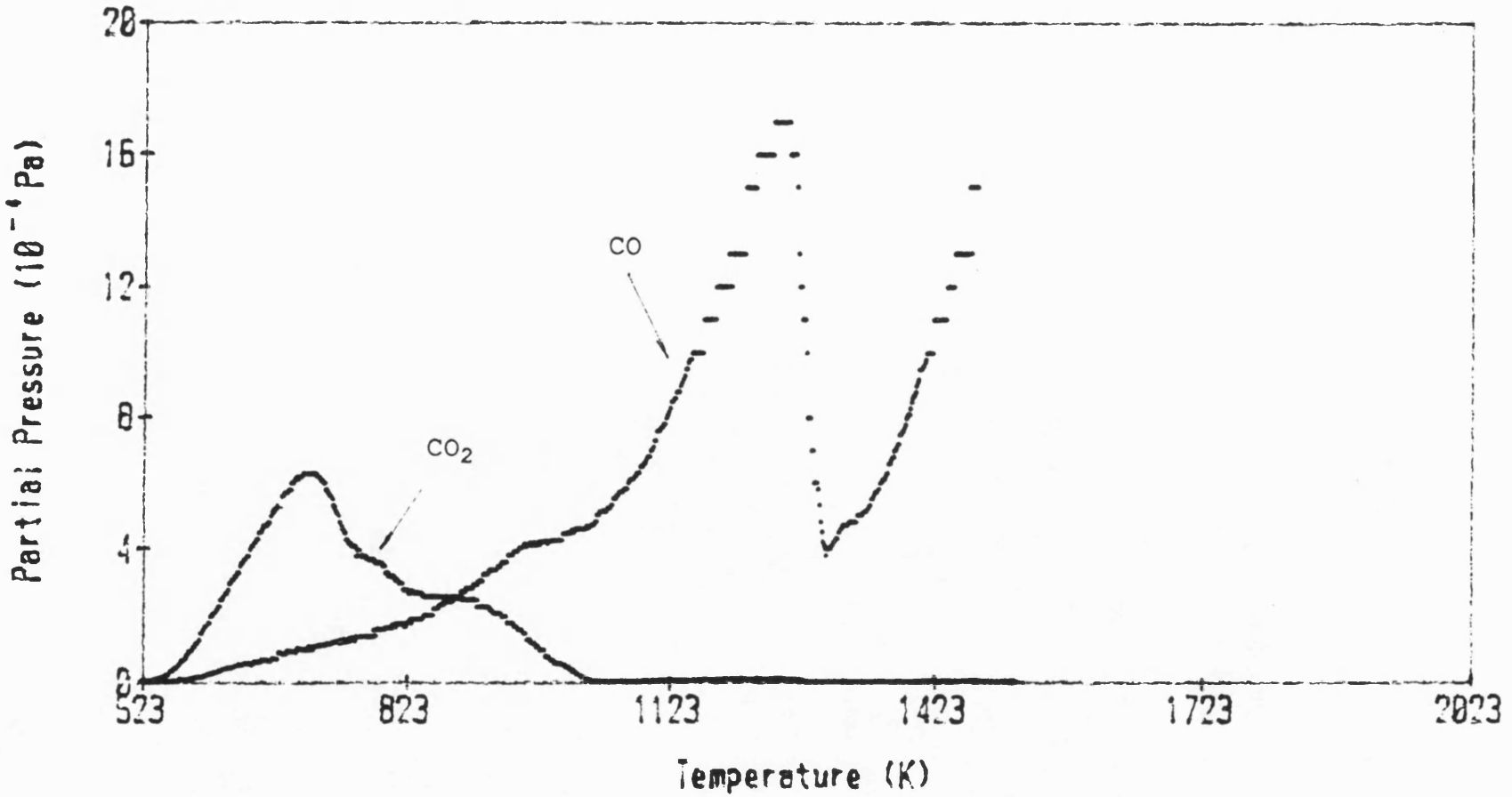

Figure 4.32 Typical TPD spectrum of PVDC char impreganated with 10% K_2CO_3

Chapter 5

ACTIVE SURFACE AREA AND REACTIVITY OF COAL CHARS

Many models of char gasification kinetics have been proposed, particularly so in the last decade of intensive coal research [5.1-5.8]. Considering the following fundamental expression for the kinetics of char (carbon) gasification,

$$C + \text{gas(A)} \longrightarrow \text{products}$$

its reaction rate can be described as:

$$\frac{dX_C}{dt} = kC_t(1 - X_C) \qquad (5.1)$$

where X_C is carbon conversion or burn-off,

k is the rate constant,

C_t is total concentration of carbon active sites (active surface area).

In the absence of kinetic limitations of pore diffusion, the pore structure is relevant only to the amount of surface area available for reaction. In that case, the rate constant in Equation (5.1) should be a function only of temperature and not also of carbon type or pyrolysis history [5.1]. It should also be independent of carbon conversion [5.2]. Only then can the time required for complete (or partial)

gasification be obtained by integration of Equation (5.1), *i.e.*,

$$t = -\frac{1}{k}\int_{0}^{1}\frac{d[\ln(1 - X_C)]}{C_t} \qquad (5.2)$$

The necessary condition for the evaluation of the above integral is the functional relationship between C_t and X_C. Its nature has not been extensively investigated. Early work of Walker and coworkers was done with highly ordered carbons [5.2-5.4]. More recently, more disordered carbons, including coal chars, have been used [5.5-5.8]. However, the picture that has emerged from these studies is complex and incomplete because the definitions of active surface area in these models include active sites other than those practically participating gasification, as discussed in Chapter 4. In this investigation, therefore, particular attention was paid to the role of γ-type and δ-type active surface sites in gasification and attempts were made to find the relationship between the surface area covering γ-type and δ-type active sites and gasification reactivity of coal chars.

5.1 Definition of Active Surface Area

Causton and McEnaney [5.7] first proposed the calculation method of ASA from the areas under the TPD curves of a char using Equation (5.3),

$$ASA = \frac{N_O \, A_O \, N_{Avo}}{W} \qquad (5.3)$$

where N_O is the number of oxygen atom desorbed,

A_O is the cross-sectional area of oxygen atom,

N_{Avo} is Avogadro's number,

W is the weight of sample in gram.

A value of 0.083 nm^2 was used for A_O [5.5]. N_O is calculated from the relationship:

$$N_O = N_{CO} + N_{CO_2} \qquad (5.4)$$

where N_{CO} and N_{CO_2} are obtained from the integration of the areas under CO and CO_2 curves of TPD spectrum and the calibration curves. Because the gas desorbed from a char surface is a mixture of CO and CO_2, the analysis in Chapter 3 for a gas mixture should be applied and Equation (5.4) should be modified with Equations (3.12) and (3.13).

Because the classical definition of active surface area measured by oxygen chemisorption technique apparently includes more active surface sites than those practically participating in CO_2 gasification, it is suggested that the ASA obtained from classical method is defined as total

active surface area (TASA) and the ASA during CO_2 gasification as reactive active surface area (RASA) to distinguish the two measuring procedures.

Theoretically, the TASA of a char measured by the dynamic method should include all the active sites on its surface. In order to obtain such a complete ASA, the char should be heated over 1473 K or held at 1473 K for a long time until all of the δ-state C-O complex were desorbed. Additionally, it is also necessary to heat the char over 1473 K and held for a long time at high temperature to ensure complete outgassing before subsequent oxygen saturation. Both are hardly feasible, not only due to the limitation of the maximum furnace temperature, but also due to the thermal annealing effect on the char. As discussed in Section 4.1, this effect can change the porous structure of the char and thus change its surface area during high-temperature treatment. Similar considerations apply for the measurement of RASA. This problem applies especially to ASA measurement using a dynamic technique and its only solution is using some arbitrary definition of ASA.

Toward this objective, some experiments were carried out and the results are listed in Table 5.1, which shows that the areas under the TPD curves of CO_2 desorption and the TPD curves of CO desorption of PVDC chars heated to 1273 K are

reasonably reproducible. That is, TPD up to 1273 K does not introduce a significant effect of thermal annealing. Therefore, in this investigation ASA is arbitrarily defined as the areas occupied by the C-O complexes which can be desorbed under 1273 K. That is, most of the δ-type of active sites are not included.

5.2 Definition of Reactivity

For the study in this section, each of PVDC char and the six coal chars underwent the measurements of TASA before gasification, RASA and TASA after gasification sequentially. Gasification was carried out for 1 h at 1123 K in flowing CO_2 (50 ml/min) at 1 atm. Afterwards, the sample bucket was taken out of the reactor and the weight percentage of the char burn-off during gasification was assessed. The reactivity of the char is defined as this burned-off (BO). Under these conditions, 10% BO equals to 0.1 $gg^{-1}h^{-1}$. The weight losses during ASA measurements are negligible when compared to the burn-off of the samples.

5.3 Relationship between Reactivity and ASA

It is well-known that the reactivity of a char is correlated with its ASA. As ASA is divided into TASA and

RASA, it is reasonable to discuss which of them correlates with the reactivity better.

The TASA before gasification, RASA and TASA after gasification of PVDC char and the six coal chars were calculated from the corresponding TPD spectra. These three ASA values and the corresponding reactivities are tabulated in Table 5.2. In this table all of the ASA values fall between those of the electrode carbon 706, whose ASA values ($\approx$1 m^2/g) are at the limit of detection of the apparatus, and those of PVDC char which is the most reactive of the chars. This table shows that (i) all the RASA are much smaller than the correspondent TASA either before gasification or after gasification; and (ii) all of the three measurements of ASA increase with increasing reactivity.

In order to further elucidate the relationship between reactivity and ASA, the above results are plotted in Figures 5.1-5.3. These figures show that, all three measures of ASA increase almost linearly with burn-off, although there is a great deal of scatter for the TASA values. Simple linear correlations of the data yield the following equations:

Before gasification	TASA=6.37+4.86BO,	χ = 0.9163
During gasification	RASA=1.88+0.733BO,	χ = 0.9774
After gasification	TASA=10.2+5.90BO,	χ = 0.8989

where χ is the correlation coefficient.

Reyes and Jensen [5.9] proposed a linear model between carbon conversion and internal surface area per unit volume accessible to oxidant, *i.e.*, TSA. Considering that ASA/TSA is almost constant in a wide range of burn-off [5.7], their model is consistent with the above results, although other kinds of functional relations between X_C and C_t were also reported [5.10-5.16].

Comparing the slopes of these linear correlations shows that RASA values are about 15% of the TASA values before gasification. Note that Causton and McEnaney [5.7] showed for PVDC char that TASA/TSA ≈ 30% for a wide range of burn-off. This suggests that RASA/TSA ≈ 5% for this char. Judged by the correlation coefficients the RASA measurements give the best linear correlation with burn-off. Thus we may conclude that RASA gives a better and more relevant correlation with the reactivity for CO_2 of a wide range of chars than does TASA before or after gasification. This is an encouraging result since from theory it is expected that reactivity is directly related to ASA. However, the proportion of these sites participating in gasification has not been yet established. It appears from this result that RASA and to a lesser extent the oxygen chemisorption capacity, i.e., TASA, are related to the number of active

sites participating in gasification, rather than being absolute measures of active surface area.

References

[5.1] L. R. Radovic, P. L. Walker, Jr. and R. G. Jenkins, *Fuel*, **62**, 849(1983).

[5.2] N. R. Laine, F. J. Vastola and P. L. Walker, Jr., *J. Phys. Chem.*, **67**, 2030(1963).

[5.3] R. O. Lussow, F. J. Vastola and P. L. Walker, Jr., *Carbon*, **5**, 591(1967).

[5.4] F. Rodriquez-Reinoso, P. A. Thrower and P. L. Walker, Jr., *Carbon*, **12**, 63(1974).

[5.5] P. L. Taylor and P. L. Walker, Jr., *Extended Abstracts*, 15th Biennial Conference on Carbon, Philadelphia, PA, p.437(1981)

[5.6] S. B. Tong, P. pareja and M. H. Back, *Carbon*, **20**, 191(1982)

[5.7] P. Causton and B. McEnaney, *Fuel*, **64**, 1447(1985).

[5.8] R. Cypres, D. Planchon and C. Braekman-Danheux, *Fuel*, **64**, 1375(1985).

[5.9] S. Reyes and K. F. Jensen, *Chem. Eng. Sci.*, **41**, 333(1986)

[5.10] N. M. Laurendau, *Prog. Energy Combust. Sci.*, **4**,

221(1978).

[5.11] E. Chornet, J. H. Baldasano and H. T. Tarki, *Fuel*, **58**, 395(1979).

[5.12] S. K. Bhatia and D. D. Perlmutter, *AIChE J.*, **26**, 379(1980).

[5.13] G. R. Gavalas, *AIChE J.*, **26**, 577(1980).

[5.14] G. A. Simons, *Carbon*, **20**, 117(1982).

[5.15] A. Cheng and P. Harriott, *Carbon*, **24**,143(1986).

[5.16] L. R. Radovic and A. A. Lizzio, *Proceedings of the 4th Annual Conference of Coal Science*, Pittsburgh, PA, p.440(1987).

Table 5.1 TASA of PVDC char before gasification of different runs, heated to 1273 K.

Samples	TASA (m^2/g)
880715	157
880819	186
880821	177
880926	194
881010	160
Mean value± standard deviation	175±12

Table 5.2 The relationship between ASA and reactivity of PVDC char and coal chars

Chars	B.O. (%)	1st TASA (m^2/g)	RASA (m^2/g)	2nd TASA (m^2/g)
Electrode 706	1.31	1.0	1.8	1.4
Tilmanstone (Dem)	3.13	19.5	4.9	27.7
Cynheidre (Dem)	5.75	26.4	4.7	39.0
Bagworth (dem)	11.2	102	10.2	130
Longannet (Dem)	14.6	103	14.6	127
Baddesley (Dem)	16.0	69.9	11.4	86.6
Baddesley (Undem)	21.1	70.7	20.8	78.0
PVDC	37.2	175	27.5	243

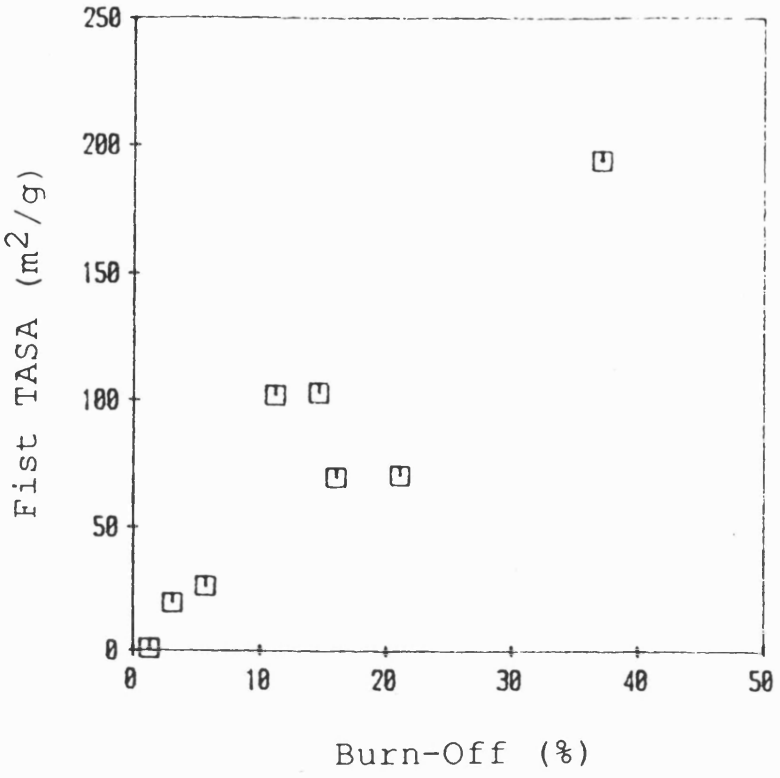

Figure 5.1 Plot of first TASA *vs* burn-off of chars (from left to right): Electrode carbon 706, Tilmanstone coal char, Cynheidre-pumpquart coal char, Bagworth coal char, Longannet coal char, Beddesley coal char (demineralized), Baddesley coal char (undemineralized), PVDC char.

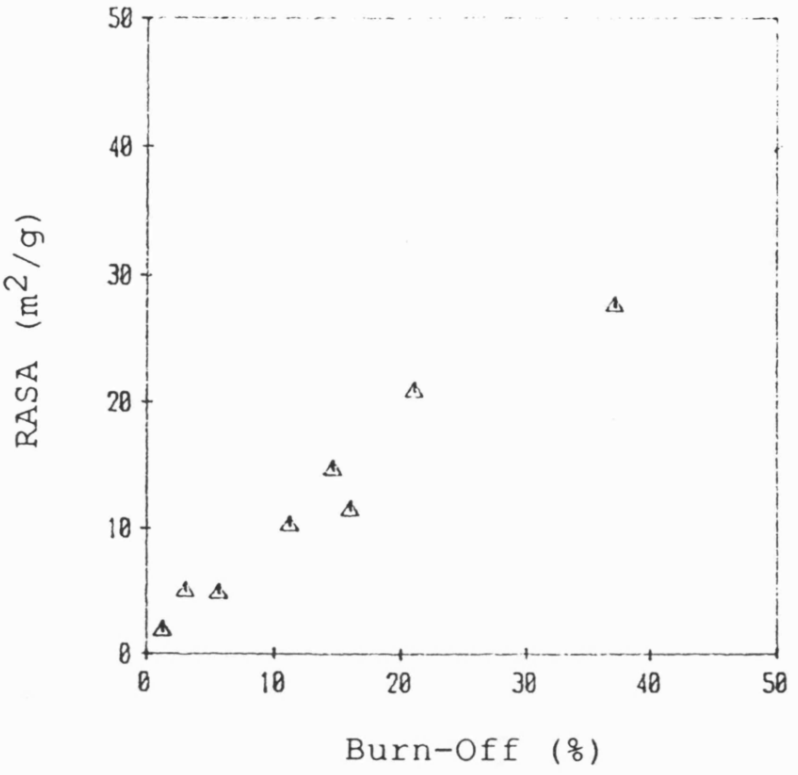

Figure 5.2 Plot of second TASA *vs* Burn-Off of chars (from left to right): Electrode carbon 706, Tilmanstone coal char, Cynheidre-pumpquart coal char, Bagworth coal char, Longannet coal char, Beddesley coal char (demineralized), Baddesley coal char (undemineralized), PVDC char.

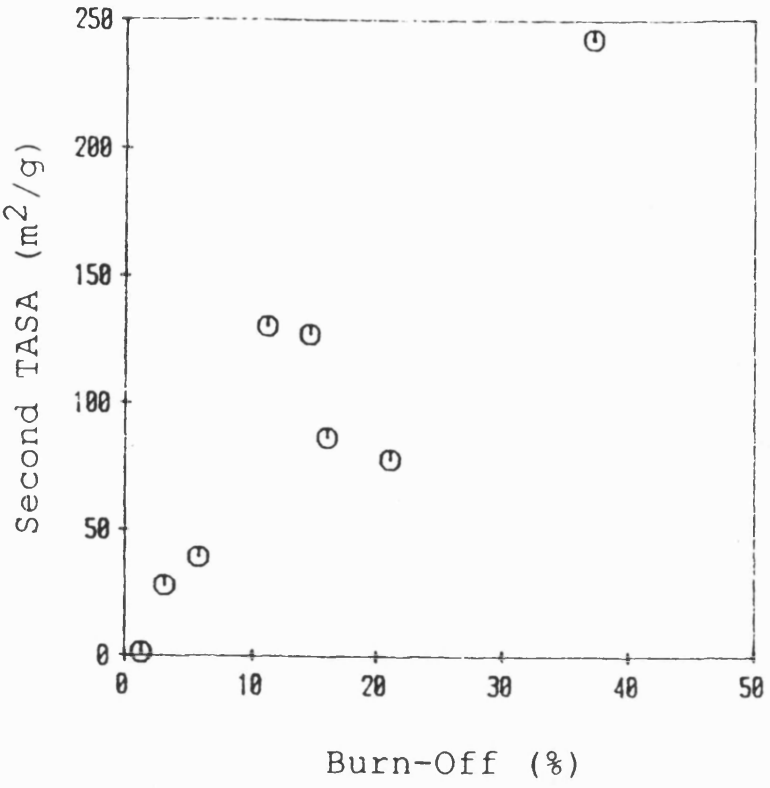

Figure 5.3 Plot of RASA *vs* Burn-Off of chars (from left to right): Electrode carbon 706, Tilmanstone coal char, Cynheidre-pumpquart coal char, Bagworth coal char, Longannet coal char, Beddesley coal char (demineralized), Baddesley coal char (undemineralized), PVDC char.

Chapter 6

KINETIC STUDY OF TPD SPECTRA

To understand the gasification mechanism, it is necessary to elucidate the structure and stability of various states of C-O complexes on the surfaces of coal chars formed after adsorption of O_2, CO_2, and H_2O. This elucidation can be reached in the two experimental approaches of chemisorption and desorption. A volumetric MS technique is mainly used for chemisorption studies and the data obtained can be analysed with Elovich equation. Some progress has been made with this approach [6.1-6.4]. In another approach, the desorption of C-O complexes from char surface may lead more directly to improved understanding of the gasification mechanism. However, little is known so far from the TPD-MS technique [6.5-6.8], probably owing to the absence of a suitable calibration method and theory for the desorption kinetics. As the calibration of the TPD-MS system has been realized in this work, attempts to further the elucidation of desorption kinetics are discussed in this chapter by the analysis and the synthesis of TPD curves of C-O surface complexes using flash desorption theory. Some results are really fascinating for the understanding of the chemistry of C-O surface complexes.

6.1 Theory of Desorption Kinetics

The theory of first-order and second-order kinetics of TPD was studied by Cvetanovic and Amenomiya [6.9] and Konvalinka *et al* [6.10], respectively. If the readsorption is negligible, their theory is exactly the same as the flash desorption theory [6.11]. The latter has been investigated in detail by Redhead [6.11, 6.12] and Ehrlich [6.13-6.15], and reviewed by Lyo and Gomer [6.16], Menzel [6.17, 6.20], Madix [6.18], Somorjai *et al* [6.19]. The following discussion is mainly based upon Readhead's work [6.12].

If the linear heating rate is constant, flash desorption theory can be easily used to analyse TPD-MS spectrum to yield following information:

i. the amount of the adsorbed state and the population of each state;

ii. the order of the desorption reaction of the individual state;

iii. the desorption activation energy of the individual state.

6.1.1 Readsorption

In a gas-solid system, the gas evolved from the solid surface may be readsorbed on the surface. It is necessary to

avoid or minimize this phenomenon, because it greatly complicates the analysis. At a given temperature, the possibility of readsorption of a gas evolved depends upon its flow rate, *i.e.*, the pumping speed of the TPD-MS system. The higher the pumping speed, the smaller is the possibility of readsorption. Konvalinka *et al* [6.10] calculated the critical flow rate on the basis of Eyring's reaction-rate theory [6.21]. They concluded that readsorption is negligible in a system in which the flow rate of hydrogen is more than 10^4 liters/g of sample/h. The pumping speed for CO employed in this work, Q_{CO}, can be calculated from Equation (3.11):

$$Q_{CO} = K_{CO}(T)RTS_{CO} = 28.21 \text{ l/s}$$

where $K_{CO}(T)$ is from the calibration result with calcium oxalate in Section 3.5.2 and the sensitivity of carbon monoxide relative to nitrogen, S_{CO}, is from the manual of the mass spectrometer. After correcting this value for difference in molecular weights of carbon monoxide and hydrogen according to Equation (3.24), the effective flow rate of hydrogen in the TPD-MS system used in the present study is 7.539 l/s. Because the sample size was about 50 mg, the pumping speed for hydrogen employed in the present TPD-MS system is about 5.5×10^5 litres/g of sample/h, *i.e.*, much higher than the above critical value. This indicates that it is reasonable to apply flash desorption theory to analyse TPD spectra obtained in this work.

To further verify this judgement, some experiments were carried out with only 5 mg of a PVDC char, where the effective flow rate of hydrogen in the system is 5.5×10^6 litres/g of sample/h. The TPD spectrum obtained is shown in Figure 6.1 which is very similar to that of the normal sample, thus, indicating that the readsorption of the evolved gases are negligible under the present condition. The parameters for TPD from porous solids were also discussed by Gorte *et al* [6.22, 6.23]. In particular, they pointed out that readsorption can easily change the desorption temperature by several hundred K. However, the temperature differences of desorption peaks of each state of surface oxides on a wide range of carbonaceous materials only vary in a small range as discussed in Chapter 4. These experimental results indicate that readsorption is not significant for TPD of surface oxides on carbons as discussed by Gorte *et al* [6.22, 6.23].

6.1.2 Flash Desorption Theory

According to Polanyi and Wigner's theory [6.13], the desorption of a molecule will occur if the kinetic energy of the molecule adsorbed is equal to or greater than the desorption energy E_d. If the desorption rate of the gas, R_d, is proportional to the nth power of the surface coverage,

θ^n, as in Equations (1.3) and (1.4). Then from the transition state theory, the desorption rate from unit active surface area may be written as:

$$R_d = - d\theta/dt = \nu_n \theta^n \exp(- \frac{E_d}{RT}) \qquad (6.1)$$

where n is the desorption order,

θ is the surface coverage,

ν_n is the frequency factor,

E_d is the activation energy of the desorption (kcal/mol).

A method to determine the desorption order can be derived from the temperature at which the desorption rate is maximum T_p. Note that the heating rate η of the TPD-MS system used in this work is linear, *i.e.*, $\eta = dT/dt$ and $T = T_0 + \eta t$, and that the second derivative of the surface coverage $d^2\theta/dt^2$ is zero at T_p. Assuming E_d is independent of θ, Equation (6.1) can be solved to find T_p,

$$\frac{E_d}{RT_p^2} = \frac{\nu_1}{\eta} \exp(- \frac{E_d}{RT_p}) \qquad \text{for n=1} \qquad (6.2a)$$

$$= \frac{\theta_0 \nu_2}{\eta} \exp(- \frac{E_d}{RT_p}) \qquad \text{for n=2} \qquad (6.2b)$$

where θ_0 is the initial surface coverage.

Equation (6.2a) shows that T_p is independent of the initial surface coverage, θ_0, for a first-order desorption with a fixed E_d and, Equation (6.2b) indicates that T_p

increases following the decrease of θ_0 for a second-order desorption with a fixed E_d. Because the relations of T_P to the linear heating rate η differ for first-order and second-order desorptions, by using a series of η these two cases can be distinguished by plotting $\log(\theta_0 T_P^2)$ against $1/T_P$ at different linear heating rates. A second-order desorption with a fixed activation energy yields a straight line as from Equation (6.2b). From its slope the activation energy of the second-order desorption can be calculated.

The shape of the TPD curve can also be used to determine the desorption order and whether the activation energy is constant or a function of surface coverage. For the case of a linear heating rate the integration of Equation (6.1) leads to:

$$-\int_{\theta_1}^{\theta_2} \frac{d\theta}{\theta} = \frac{\nu_n}{\eta} \int_{T_1}^{T_2} \exp\left(-\frac{E_d}{RT}\right) dT$$

$$= \ln(\theta_1/\theta_2) \qquad \text{for } n=1 \qquad (6.3a)$$

$$= 1/\theta_2 - 1/\theta_1 \qquad \text{for } n=2 \qquad (6.3b)$$

The integral may be evaluated by using the substitution $u = -E_d/RT$, integrating by parts, developing the integral into power series and using the identity:

$$\int_{-\infty}^{u} \frac{\exp(t)}{t} = \frac{\exp(u)}{u} H(u) \qquad \text{for } u >> 1$$

where $H(u) = 1 + (1!/u) + (2!/u^2) + (3!/u^3) + \ldots$ (6.4)

Because the smallest E_d calculated in this work is 17 kcal/mol, *i.e.*, $E_d/2RT \gg 1$, taking only the first two terms in the expansion of H(u), one obtains:

$$\frac{\nu_n}{\eta}\int_{T_1}^{T_2}\exp\left(-\frac{E_d}{RT}\right) =$$

$$-\frac{\nu_n R}{\eta E_d}\left[T_2^2\exp\left(-\frac{E_d}{RT_2}\right) - T_1^2\exp\left(-\frac{E_d}{RT_1}\right)\right] \qquad (6.5)$$

Then for the first-order cases, using Equation (6.2a) leads to:

$$\ln\left(\frac{\theta_0}{\theta_P}\right) = 1 - \left(\frac{T_0}{T_P}\right)\exp\left[\frac{E_d}{R}\left(\frac{1}{T_0} - \frac{1}{T_P}\right)\right] \approx 1$$

or

$$\frac{\theta_0}{\theta_P} \approx e \qquad (6.6)$$

Thus, the surface coverage at T_P, θ_P, approximates to θ_0/e.

Substituting Equation (6.3a) and Equation (6.4) into Equation (6.1), the equation describing the shape of the desorption rate curve is obtained.

$$\mathrm{Ln}\left(\frac{\theta_P}{\theta}\right) = \frac{E_d}{R}\left(\frac{1}{T_P} - \frac{1}{T}\right) +$$

$$+\left(\frac{T}{T_P}\right)^2\exp\left[-\frac{E_d}{R}\left(\frac{1}{T} - \frac{1}{T_P}\right)\right] + 1 \qquad (6.7)$$

It can be seen that the desorption rate curve is asymmetric about the maximum at T_p for first-order desorption.

Similarly for the second-order case it can be shown that

$$\theta_0/\theta_p \approx 2 \tag{6.8}$$

and

$$\frac{\theta_p}{\theta} = \frac{1}{4}\left\{\exp\left[-\frac{E_d}{2RT}\left(\frac{1}{T_p}-\frac{1}{T}\right)\right] + \left(\frac{T}{T_p}\right)^2\exp\left[-\frac{E_d}{2R}\left(\frac{1}{T}-\frac{1}{T_p}\right)\right]\right\}^2 \tag{6.9}$$

Near the maximum temperature, T_p, $(T/T_p) \approx 1$, then

$$\frac{\theta_p}{\theta} \approx \cosh\left[-\frac{E_d}{2R}\left(\frac{1}{T}-\frac{1}{T_p}\right)\right] \tag{6.10}$$

Thus the desorption rate curve is symmetric about the maximum temperature for a small $(T-T_p)$.

However, as the measured curve sometimes consists of several overlapping peaks caused by the presence of several adsorbed states with different activation energies, the usage of this approach is limited. In such cases the methods of the previous section must be applied since the only parameter that can be accurately measured is T_p.

For first-order desorption with a fixed E_d it can be deduced from Equation (6.7) that:

$$N = N_p F_1(T) \tag{6.11}$$

where

$$F_1(T) = \exp\left\{1 - \frac{E_d}{R}\left(\frac{1}{T_P} - \frac{1}{T}\right) - \left(\frac{T}{T_P}\right)^2 \exp\left[-\frac{E_d}{R}\left(\frac{1}{T} - \frac{1}{T_P}\right)\right]\right\}$$

Combining Equation (3.8) with Equation (6.11) gives:

$$P = \frac{N_P RT}{Q} F_1(T) = k_1 T F_1(T) \qquad (6.12)$$

where $k_1 = N_P R/Q$.

For second-order desorption with a fixed E_d, it can be deduced that from Equation (6.9) that:

$$N = 4N_P F_2(T) \qquad (6.13)$$

where

$$F_2(T) = \left\{\exp\left[-\frac{E_d}{2RT}\left(\frac{1}{T_P} - \frac{1}{T}\right) + \left(\frac{T}{T_P}\right)^2 \exp\left[-\frac{E_d}{2RT}\left(\frac{1}{T} - \frac{1}{T_P}\right)\right]\right\}^{-2}$$

Combining Equation (6.13) with Equation (3.8) gives:

$$P = \frac{4N_P RT}{Q} F_2(T) = k_2 T F_2(T) \qquad (6.14)$$

where $k_2 = 4N_P R/Q$.

According to Equations (6.12) and (6.14), the theoretical curves of partial pressure *versus* temperature of first-order desorption and second-order desorption with E_d in the range 12 - 22 kcal/mol and T_P at 973 K are plotted in Figure 6.2a and 6.2b. The width of the curves in both figures reduces following the increase of E_d, however, the curve width of the second-order desorption is bigger than that of the corresponding curve of the first-order desorption. It is

also noteworthy that the partial pressures of CO at 1273 K of the second-order desorption curves are still significant. It is consistent with the experimental results as in Figure 4.1 and indicates that CO desorption of α- and β-state of C-O surface complexes are very likely of second-order desorption with a fixed E_d.

6.1.3 Applying Flash Desorption Theory to TPD-MS System

From the discussion in above section it can be seen that it is first important to identify the desorption order of a state of C-O surface complex. However, because overlapping of different desorption peaks always occurs, peak shapes can only offer limited information and the method using the maximum desorption temperature T_P is the only reliable one. Equation (6.2a) shows that T_P is independent of the initial surface coverage θ_0 for a first order desorption with a fixed E_d. Therefore, if T_P increases with the decrease of θ_0 the desorption may be of second-order with a fixed activation energy or of first-order with an activation energy dependent on θ_0. The experiments using a series of heating rates can further distinguish these two cases. However, for reasonable accuracy η must be varied by at least two orders of magnitude [6.13], which is not feasible in the present heating system. Therefore, it is proposed to distinguish these two cases by measuring the activation

energies of samples with different initial surface coverages. That is, if T_p increases and E_d keeps constant for a series of the samples with decreasing initial surface coverage θ_0, the desorption can be verified as second-order with a fixed activation energy. Otherwise it should be verified as first-order.

Because the scanning period of the mass spectrometer used in this work is constant, the shape and the maximum desorption temperature of the curve of the desorption rate *versus* temperature is exactly the same as that of the partial pressure *versus* temperature. The molar amount of a gas evolved in a TPD-MS system can be calculated from the area under its TPD curve using Equation (3.11). For a first-order desorption, Equations (6.1) can be generally written as:

$$\frac{dN}{dt} = \nu_1 (N_0 - N) \exp\left(- \frac{E_d}{RT} \right) \qquad (6.15)$$

where N is the molar amount desorbed on the surface before time t;

N_0 is the total molar amount adsorbed on the surface at time t=0.

It is difficult to measure N_0 of a single adsorbed state of C-O surface complex in Equation (6.15) because of the overlapping of the peaks of different adsorbed states and

some uncompleted desorption peaks. It is necessary, therefore, to apply the approximation of Equation (6.6):

$$\frac{dN}{dt} = \nu_1 (eN_P - N) \exp\left(- \frac{E_d}{RT} \right) \qquad (6.16)$$

Combining Equation (6.16) with Equation (3.11) gives:

$$\frac{dI}{dt} = \nu_1 (eI_P - I) \exp\left(- \frac{E_d}{RT} \right) \qquad (6.17)$$

where I_P is the area under the part of the TPD curve from starting temperature to the temperature at which the desorption rate of the state studied is maximum. Taking natural logarithm of Equation (6.17) leads to:

$$\ln\left(\frac{dI}{dt} \right) - \ln\left[\nu_1 (eI_P - I) \right] = - \frac{E_d}{RT} \qquad (6.18)$$

Therefore, Plotting $\ln\left(\frac{dI}{dt} \right) - \ln\left[\nu_1 (eI_P - I) \right]$ against $\frac{1}{T}$ should leads to a straight line passing the origin for a first-order desorption and E_d can be calculated from its slope.

For a second-order desorption, Equations (6.1) can be generally written as:

$$\frac{dN}{dt} = \nu_2 \frac{(N_0 - N)^2}{N_0} \exp\left(- \frac{E_d}{RT} \right) \qquad (6.19)$$

For the reasons stated above, it is also difficult to measure N_0 in Equation (6.19) and it is necessary, therefore, to apply the approximation of Equation (6.8):

$$\frac{dN}{dt} = \nu_2 \frac{(2N_p - N)^2}{2N_p} \exp\left(- \frac{E_d}{RT} \right) \qquad (6.20)$$

Combining Equation (6.20) with Equation (3.11) gives:

$$\frac{dI}{dt} = \nu_2 \frac{(2I_p - I)^2}{2I_p} \exp\left(- \frac{E_d}{RT} \right) \qquad (6.21)$$

and

$$\ln\left(\frac{dI}{dt} \right) + \ln\left[\frac{2I_p}{(2I_p - I)^2} \right] = \ln\nu_2 - \frac{E_d}{RT} \qquad (6.22)$$

Therefore, plotting $\ln\left(\frac{dI}{dt} \right) + \ln\left[\frac{2I_p}{(2I_p - I)^2} \right]$ against $\frac{1}{T}$ leads to a straight line for a second-order desorption and ν_2 and E_d can be calculated from its interception and slope respectively.

6.2. CO_2 Desorption Kinetics of C-O Surface Complexes

The CO_2 desorption curve in the typical TPD spectrum of PVDC char in Figure 4.2 differs greatly from the theoretical curves in Figure 6.2a for a first-order desorption or Figure 6.2b for a second-order desorption. The extended second part and the asymmetric shape of CO_2 desorption curve in Figure 4.2 is probably due to the overlapping of more than one peak, as indicated in Figure 4.32.

6.2.1 Analysis of TPD Curve of CO_2

Following the discussion in Section 6.1, a series of PVDC chars with different initial surface coverage of C-O complexes were prepared. The chars were first saturated with oxygen and then preheated to different temperatures in vacuum before subsequent classical TPD measurement. The higher the temperature of a char was heated to, the smaller is the initial surface coverage. This can be seen in Figure 6.3 where the areas under the TPD curves and, therefore, the initial surface coverages, decrease following the increase of preheating temperature. It is clearly shown in this Figure that the maximum peak temperatures of CO_2 desorption increase with the decrease of the initial surface coverage. It suggests that CO_2 desorption is not of first-order desorption with a fixed activation energy. It can also be seen that the peak shapes change from asymmetric to symmetric following the reduction of the initial surface coverage. Therefore, it is reasonable to envisage that CO_2 desorption of C-O surface complexes is of second-order desorption with a fixed activation energy. This was further verified by the calculation of the activation energies of CO_2 desorption with second-order law of Equation (6.22).

The semi-log plots of Equation (6.22) for CO_2 desorption of PVDC chars with different initial surface coverages,

Figure 6.4, gives three groups of straight lines which are clearly distinguished by three distinct slopes. Plot 1 belongs to the first group with an E_d = 17 kcal/mol, which represents the samples in Table 6.1 heat-treated under 553 K. Plots 2, 3 and 4 belong to the second group with an E_d = 36 kcal/mol, which represent the samples in Table 6.1 heat-treated between 553 and 923 K. Plots 5 and 6 belong to the third group with the highest E_d, however, the value of E_d can not be calculated accurately because the partial pressure of CO_2 is too low compared to the other two groups of plots. However, these three slopes must represent three fixed activation energies of second-order desorptions. The alternative possibility of first-order desorption with variable E_d can be ruled out since this would result in curved plots in Figure 6.4. Therefore, there must be at least three states of C-O surface complexes corresponding to CO_2 desorption above 525 K. The results obtained using Equation (6.22), tabulated in Table 6.1, show that the activation energy values of the three groups are almost constant, although the initial surface coverages are very different. It indicates that the desorptions of the three states of C-O surface complexes corresponding to CO_2 evolution are second-order desorptions with fixed activation energies, 17, 36 and 41 kcal/mol, respectively.

These results are consistent with those reported recently by Marchon *et al* [6.8]. They observed five peaks of CO_2 desorption from polycrystalline graphite after oxygen chemisorption. These peaks could be distinguished at 463, 573, 693 793 and 923 K. The activation energies of desorption of these five states reported by them are 26, 33, 39, 46 and 53 kcal/mol, respectively. However, they did not report the desorption orders of these state of C-O complexes and did not report their calculation in detail. Comparing their results with the present work, the three states of C-O surface complexes observed here are similar to those at 693, 793 and 923 K in their work, respectively. The slight temperature difference may be due to different materials and techniques used.

6.2.2 Synthesis of TPD Curve of CO_2

Applying Dalton's law of partial pressures to Equation (6.14) gives:

$$P = \Sigma k_i F_i(T) \qquad (6.23)$$

where the subscript i denotes the ith adsorbed state of C-O complex which decomposes and evolves carbon oxide during TPD.

Figure 6.5 shows the theoretical curve (the continuous line) and the experimental curve (the dotted line). The

theoretical line is plotted according to Equation (6.23), in which $(T_p)_1$ = 693 K, $(T_p)_2$ = 793 K, $(T_p)_3$ = 923 K, $(E_d)_1$ = 14 kcal/mol, $(E_d)_2$ = 35 kcal/mol, $(E_d)_3$ = 45 kcal/mol. These two curves fitted with each other well except that at 523 K the pressure of CO_2 in experimental curve is much lower than that of the theoretical curve. This is because that the experimental curve is obtained after a long time outgassing at 523 K before TPD and a part of CO_2 which should desorb at temperatures under 523 K has desorbed.

6.3 CO Desorption Kinetics of C-O Surface Complexes

Merely observing the peak shapes in the typical TPD spectrum in Figure 4.2, it is difficult to identify the desorption order of anyone of the α-state, β-state and δ-state of C-O complexes. This is mainly due to the overlapping of the desorption peaks. In some experimental conditions this overlapping can be minimized and some information about the desorption order can be obtained from the peak shapes. For example, the symmetric shapes of the CO desorption peaks of α-state C-O complex in Figure 4.26 and Figure 4.27 suggest a second-order desorption with a fixed activation energy. Similarly, the symmetric shape of the desorption peak of γ-state C-O complex from PVDC char quenched during CO_2 gasification, as shown in Figure 4.10-4.12, provides some evidence that CO desorption of β-state

C-O complex is probably of second-order desorption with a fixed activation energy.

6.3.1 Analysis of TPD Curve of CO

More evidence is also given by the analysis of the TPD spectra of PVDC chars with different initial surface coverages of C-O complexes. It is clearly shown in Figure 6.6 that the maximum peak temperatures of both α-state and β-state of C-O complexes increase with the decrease of the initial surface coverage. It is also shown in this Figure that the peak shapes of CO desorption of β-state C-O complex change from asymmetric to symmetric. This is due to the reduction of the overlapping of β-state peak with that of α-state C-O complex. It indicates that the CO desorptions of both α-state and β-state C-O complexes are not of first-order desorptions with a fixed activation energy and are probably of second-order desorption with a fixed activation energy. This is further verified by the calculation of their activation energies.

Figure 6.7 shows the semi-log plots of the calculated results according Equation (6.22) for CO desorption curves of PVDC char with different θ_0. Although the θ_0 of α-state surface complex for these chars are different, the plots are clearly distinguished into two groups with two fixed E_d.

Plots 1 and 2 belong to the first group with a fixed E_d = 17 kcal/mol, which represents the samples in Table 6.2 heat-treated under 723 K. Plots 4, 5 and 6 belong to the second group with a fixed E_d = 40 kcal/mol. The E_d calculated from plot 3 is in the middle of the above two values. It is attributed to the interference of β-state C-O surface complex. The results in Table 6.2 shows that the activation energy of the second-order desorption of α-state C-O complex is almost constant, indicating that the desorption of α-state of C-O complex is of second-order reaction with a fixed activation energy. Same is true for the desorption of β-state C-O complex, which is also of second-order desorption with a fixed activation energy.

The kinetic parameters of γ-sate C-O complex can be analysed from TPD spectra of PVDC chars which were gasified with CO_2 at different temperatures and quenched. These chars obviously have different initial surface coverages of γ-state C-O complex. The results in Figure 6.8 and Table 6.3 shows the activation energy of second-order desorption of γ-state C-O complex is also of second-order desorption with a fixed activation energy of 55 kcal/mol.

Unfortunately, it is impossible to identify the desorption order of δ-state C-O surface complex from char surface either by the maximum temperature or by the peak

shape of its desorption curves, because its desorption peaks are always not completed. Thus, the calculation of its desorption activation energy is based upon the assumption of second-order desorption with a fixed activation energy and the curve has reached its peak. To minimize the interference of γ-state C-O complex, two PVDC chars were gasified with CO_2 and quenched then heat-treated to 1223 K before the classical TPD. The calculated result in Table 6.4 shows the activation energy of the second-order desorption of δ-state C-O complex is about 82 kcal/mol.

The activation energies of α-state, β-state and γ-state C-O complexes reported by Marchon *et al* [6.8] are 57, 64 and 74 kcal/mol, respectively. However, it is hard to compare the results obtained from this work with theirs because they did not give any detail of their calculation and the desorption order of these C-O surface complexes. Laurendau [6.24] reviewed the activation energy of CO desorption of C-O surface complexes in C-CO_2 system. The value varied from 49-88 kcal/mol. Johnson [6.25] also summarized the activation energies calculated on the basis of first-order desorption of C-O surface complexes by earlier workers on different forms of carbon and gave an intermediate value of 59 kcal/mol. This value is within the range of the values for desorption of the γ-state and δ-state C-O complexes obtained in this work. It is consistent with the

experimental evidence presented here that both γ-state and δ-state of C-O surface complexes are involved in CO_2 gasification.

Additionally, it is fascinating to note from Table 6.5 and Table 6.6 that the second-order activation energies of CO desorption of both α-state and γ-state C-O complexes for most of coal chars used in this work are also very close to each other, except the chars with very small RASA. In that case, the interference of δ-state C-O surface complex becomes more significant to the calculation of the activation energy of the second-order desorption of γ-state C-O complex. Therefore, the values calculated are bigger than the normal value and close to the value of δ-state C-O complex. This similarity of activation energies of various states of C-O complexes gives further evidence for the existence of some kind of structural homogeneity on the surfaces of coal chars.

6.3.2 Synthesis of TPD Curve

Figure 6.9 shows the theoretical curve (the continuous line) and the experimental curve (the dotted line). The theoretical line is plotted according to Equation (6.23), in which $(T_P)_\alpha$ = 973 K, $(T_P)_\beta$ = 1093 K, $(E_d)_\alpha$ = 14 kcal/mol, $(E_d)_\beta$ = 45 kcal/mol. These two curves fitted with each other

well and give clear evidence of second-order desorption of α-state and β-state of C-O surface complexes.

6.4 Summary

In the foregoing discussion a kinetic analysis method and an approximation method were proposed for the application of flash desorption theory to the present TPD-MS system. By these approaches the following kinetic information about the desorption of C-O complexes from char surface were successfully revealed:

i. At least three adsorbed states of C-O complexes existed amenable to CO_2 desorption from char surface; the overlapping of the desorption curves of these states of C-O complexes leads to the broad peak of CO_2 desorption in the TPD-MS spectra;

ii. The desorption of above states are of second-order desorption with a fixed activation energy and their second-order activation energies are 17, 36 and 41 kcal/mol, respectively;

iii. The desorptions of α-state, β-state, γ- and δ-state of C-O surface complexes are also of second-order desorption with a fixed activation energy and their second-order activation energies are 17, 45, 55 and 82 kcal/mol, respectively.

The surface of coal char is very complicated and it is very likely that above discussion oversimplifies the system. For example, the interactions between the adsorbed molecules and the surface migration of these molecules were not considered. Nevertheless, above analysis method and the results highlighted the way for kinetic analysis of TPD-MS spectrum and the results are still credible. The significance of these results to the understanding of gasification mechanism will be discussed in next chapter.

References

[6.1] R. C. Bansal, F. J. Vastola, and P. L. Walker, Jr., *Carbon*, 443(8), 1970.

[6.2] R. Phillips, F. J. Vastola, and P. L. Walker, Jr., *Carbon*, 197(8), 1970.

[6.3] R. C. Bansal, F. J. Vastola, and P. L. Walker, Jr., *J. Collid Interf. Sci.*, **32**, 187(1970).

[6.4] M. J. D. Low, *Chem. Rev.*, **60**, 267(1960).

[6.5] R. Phillips, F. J. Vastola and P. L. Walker, Jr., *Carbon*, **8**, 197(1970).

[6.6] R. C. Bansal, F. J. Vastola and P. L. Walker, Jr., *Carbon*, **8**, 443(1970).

[6.7] G. Hermann and K. J. Huttinger, *Carbon*, **24**, 705(1986).

[6.8] B. Marchon, J. Carrazza, H. Heinemann and G. A. Somorjai, *Carbon*, **26**, 507(1988).

[6.9] R. J. Cvetanovic and Y. Amenomiya, *Advances in Catalysts*, **17**, 108(1967).

[6.10] J. A. Konvalinka, J. J. F. Scholten and J. C. Rasser, *J. Catalysts*, **48**, 365(1977).

[6.11] P. A. Redhead, *Trans. Faraday Soc.*, **57**, 641(1961).

[6.12] P. A. Redhead, *Vacuum*, **12**, 203(1962).

[6.13] G. Ehrlich, *J. Chem. Phys.*, **34**, 29(1961).

[6.14] G. Ehrlich, *J. Chem. Phys.*, **34**, 39(1961).

[6.15] G. Ehrlich, *J. Appl. Phys.*, **32**, 4(1961).

[6.16] S. K. Lyo and R. Gomer in "*Interactions on Metal Surfaces*", (ed. R. Gomer), Springer-Verlag, NY, pp.102-142(1975).

[6.17] D. Menzel, in "*Interaction on Metal Surface*, Vol. 4", (ed. R. Gomer), Springer, NY, pp.101-142(1975).

[6.18] R. J. Madix, in "*Chemistry and Physics of Solid Surfaces*, Vol. II" (ed. R. Vanselow), CRC Press Inc, Boca Raton, p.63(1979).

[6.19] G. A. Somorjai, "*Chemistry in Two Dimensions Surfaces*", Cornell University Press, Ithaca, pp.77-79(1981).

[6.20] D. Menzel, in "*Chemistry and Physics of Solid Surfaces*, Vol. IV" (ed. R. Vanselow), Springer, Berlin, p.389(1982).

[6.21] S. Glasstone, K. J. Laidler and H. Eyring, "*The*

Theory of Rate Processes", McGraw-Hill, NY, p.347(1941).

[6.22] R. J. Gorte, *J. Catalysis*, **75**, 164(1982).

[6.23] R. D. Demmin and R. J. Gorte, *J. Catalysis*, **90**, 32(1982).

[6.24] N. M. Laurendau, *Prog. Energy Combust. Sci.* **4**, 221(1978).

[6.25] J. L. Johnson in "*Chemistry of Coal Utilization, Second Supplementary Volume*" (ed. M. A. Elliott), Wiley, NY, p.1571(1981).

Table 6.1 Kinetic parameters of CO_2 desorption of C-O complex from PVDC chars heat-treated to different temperatures

Sample	H-T Temperature(K)	$v_2(sec^{-1})$	E_d(kcal/mole)
881010	523	3.0×10^{2}	17.5
881012	573	5.3×10^{1}	16.9
881014	623	5.4×10^{7}	36.5
881017	523	3.4×10^{2}	17.5
881018	673	5.9×10^{7}	32.7
881019	773	1.8×10^{6}	35.1
881020	523	7.3×10^{0}	15.7
881021	623	2.2×10^{7}	35.5
881022	723	1.2×10^{6}	36.2
881023	823	1.9×10^{5}	36.7
881024	923	1.1×10^{10}	41.1
881025	1023	3.0×10^{9}	40.3

Table 6.2 Kinetic parameters of CO desorption of α-state and β-state C-O complexes from PVDC chars heat-treated to different temperatures

Sample	H-T Temperature(K)	$v_2(sec^{-1})$	E_d(kcal/mole)
881010	523	5.5×10^{0}	17.7
881012	573	5.8×10^{0}	17.6
881014	623	7.7×10^{0}	18.2
881017	523	2.1×10^{0}	15.9
881018	673	5.1×10^{0}	17.4
881019	773	1.6×10^{2}	35.1
881020	523	1.5×10^{1}	19.3
881021	623	4.3×10^{0}	17.2
881022	723	2.6×10^{3}	28.2
881023	923	2.9×10^{4}	40.9
881024	1023	7.0×10^{3}	41.1
881025	1123	1.8×10^{4}	40.3

Table 6.3 Kinetic parameters of CO desorption of γ-State C-O complex from PVDC chars after CO_2 gasification at different temperatures

Sample	Gasification Temperature(K)	$v_2(sec^{-1})$	E_d(kcal/mole)
881025	1023	4.6×10^6	56.3
881030	1123	5.5×10^6	53.7
881109	1223	5.6×10^7	58.9
890428	1023	1.4×10^6	51.3*

* Saturated with CO_2 at 1023 K.

Table 6.4 Kinetic parameters of CO desorption of δ-State C-O complex from PVDC chars after CO_2 gasification and preheated to 1223 K

Sample	$v_2(sec^{-1})$	E_d(kcal/mole)
881109	2.3×10^7	77.2
881110	1.0×10^{10}	86.3

Table 6.5 Kinetic parameters of CO desorption of α-State C-O complex from different chars

Sample		$v_2(sec^{-1})$	E_d(kcal/mole)
PVDC		2.2×10^{0}	16.2
PVDC*		4.2×10^{0}	17.6
PVDC**		2.2×10^{2}	20.1
Baddesley	(Undem)	2.1×10^{1}	20.4
Baddesley	(Dem)	1.5×10^{1}	19.4
Cynheidre	(Dem)	3.6×10^{1}	21.2
Bagworth	(Dem)	3.3×10^{0}	16.9
Longannet	(Dem)	6.1×10^{0}	18.0
Tilmanstone	(Dem)	1.8×10^{1}	19.9

PVDC* one of tenth of the normal sample size
PVDC** Heat-treated to 1973 K for 1 hr then gasified with CO_2 at 1023 K for 10 hr

Table 6.6 Kinetic parameters of CO desorption of γ-State C-O complex from different chars

Sample		$v_2(sec^{-1})$	E_d(kcal/mole)
PVDC		4.6×10^{6}	56.3
PVDC*		4.3×10^{6}	51.9
Baddesley	(Undem)	1.6×10^{7}	63.3
Baddesley	(Dem)	8.2×10^{7}	60.6
Cynheidre	(Dem)	2.4×10^{7}	63.8
Bagworth	(Dem)	2.8×10^{6}	53.0
Longannet	(Dem)	8.6×10^{6}	55.7
Tilmanstone	(Dem)	4.3×10^{5}	48.8

PVDC* Heat treated to 1973 K for 1 hr then gasified with CO_2 at 1023 K for 10 hr

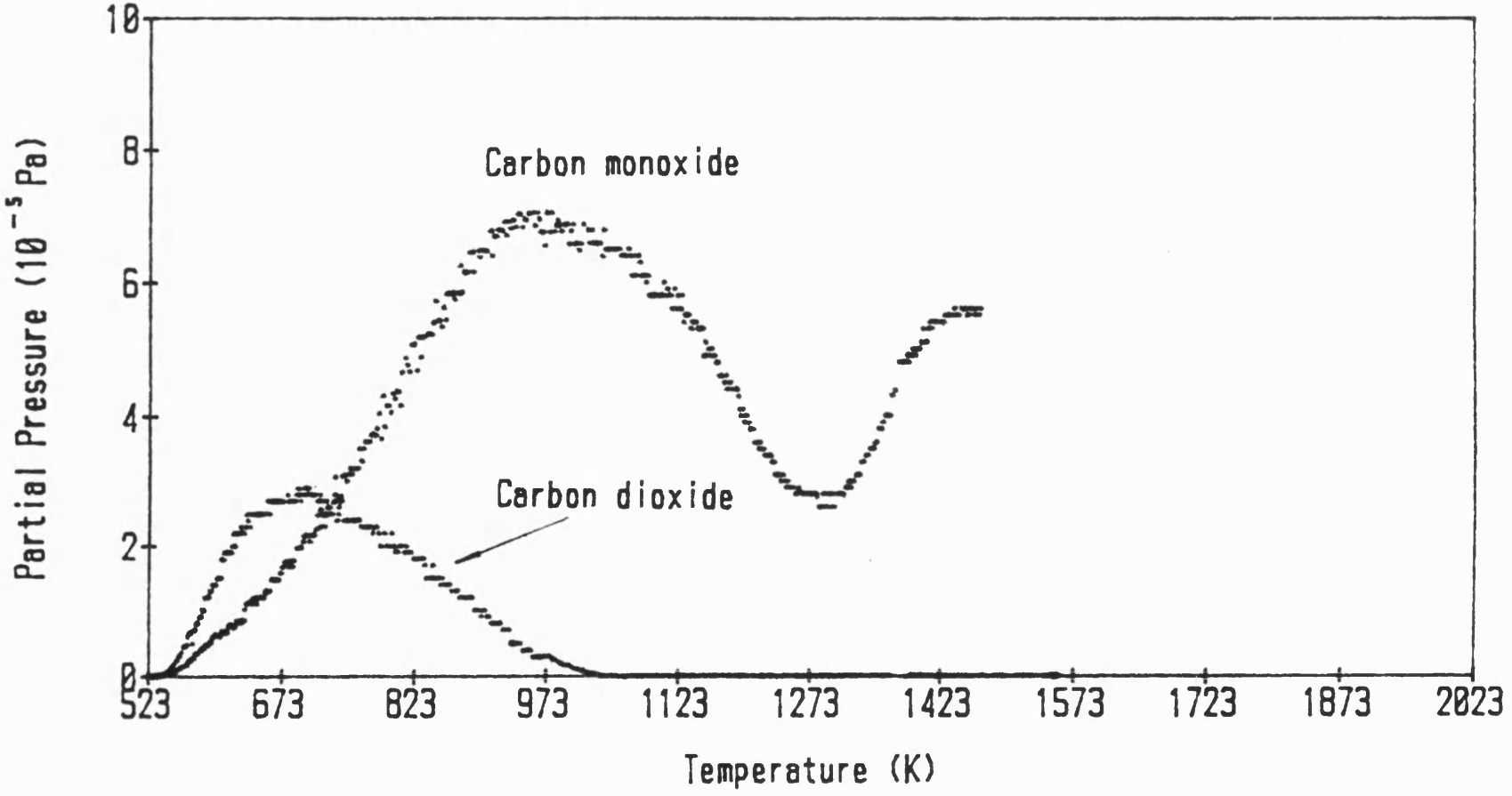

Figure 6.1 Classical TPD spectrum of PVDC char (1/10 of normal sample size) before gasification, to 1473 K.

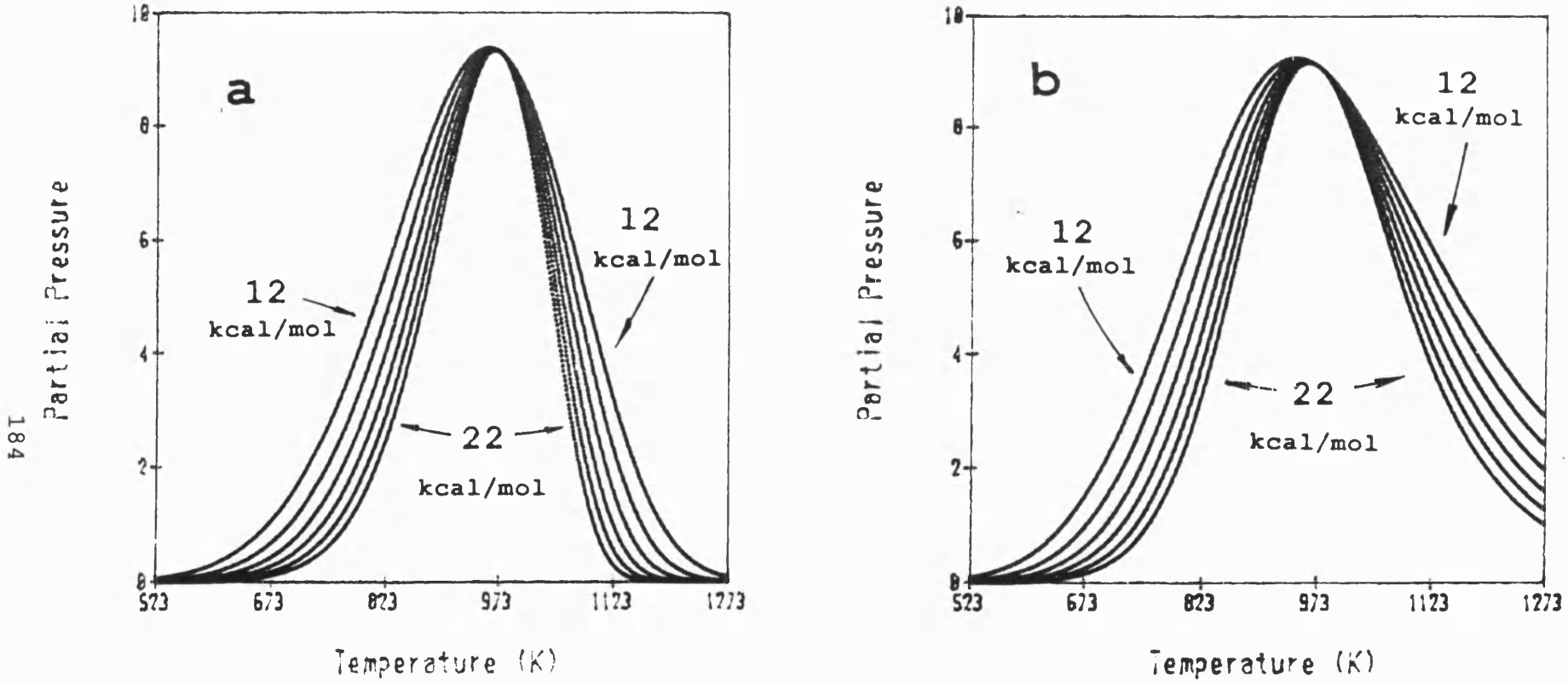

Figure 6.2 Theoretical desorption curves of pressure *vs* temperature of (a) first-order desorption and (b) second-order desorption, T_p = 973 K, E_d = 12-22 kcal/mol.

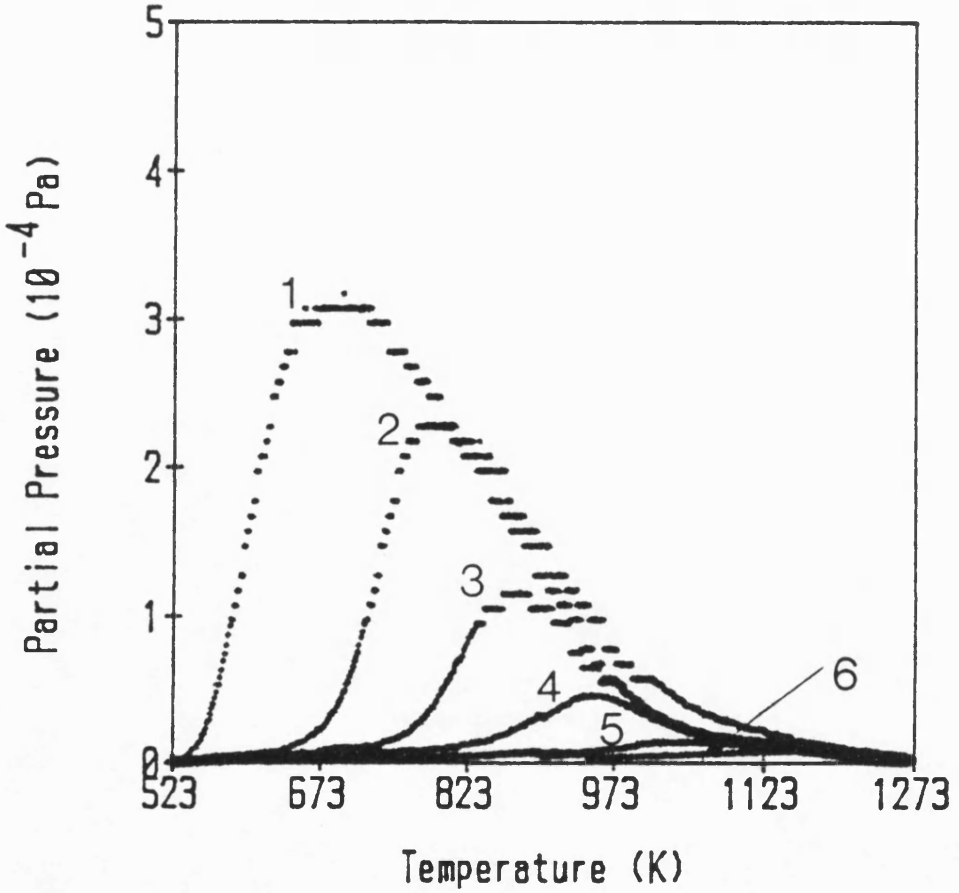

Figure 6.3 TPD spectra of CO_2 from PVDC char with different initial oxygen coverages. 1. saturated with O_2 at 523 K, 2. reheated to 623 K, 3. preheated to 723 K, 4. preheated to 923 K, 5. preheated to 1023 K, 6. preheated to 1123 K

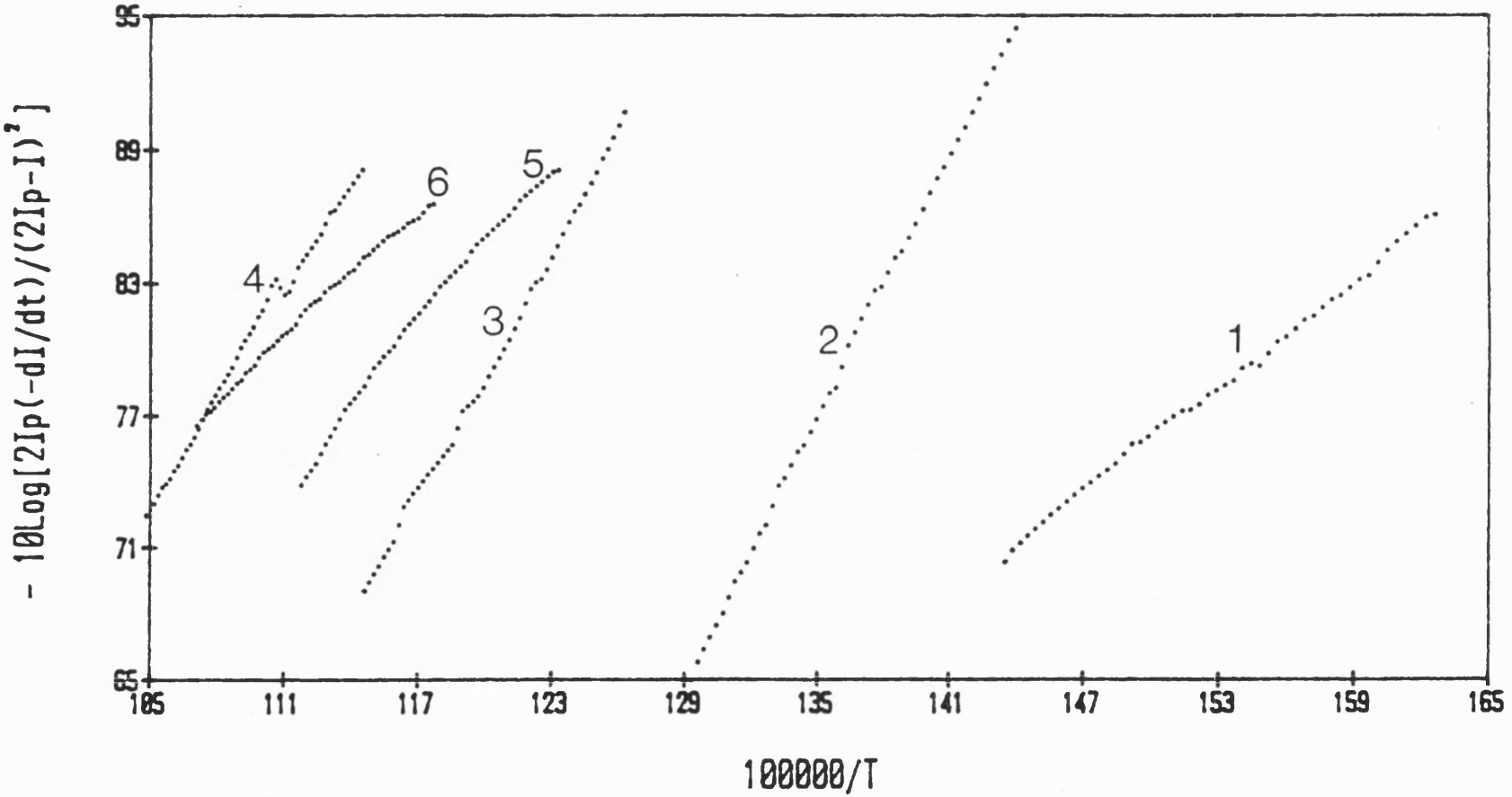

Figure 6.4 Semi-log plots of Equation (8.14) for CO_2 desorptions in Figure 6.3.

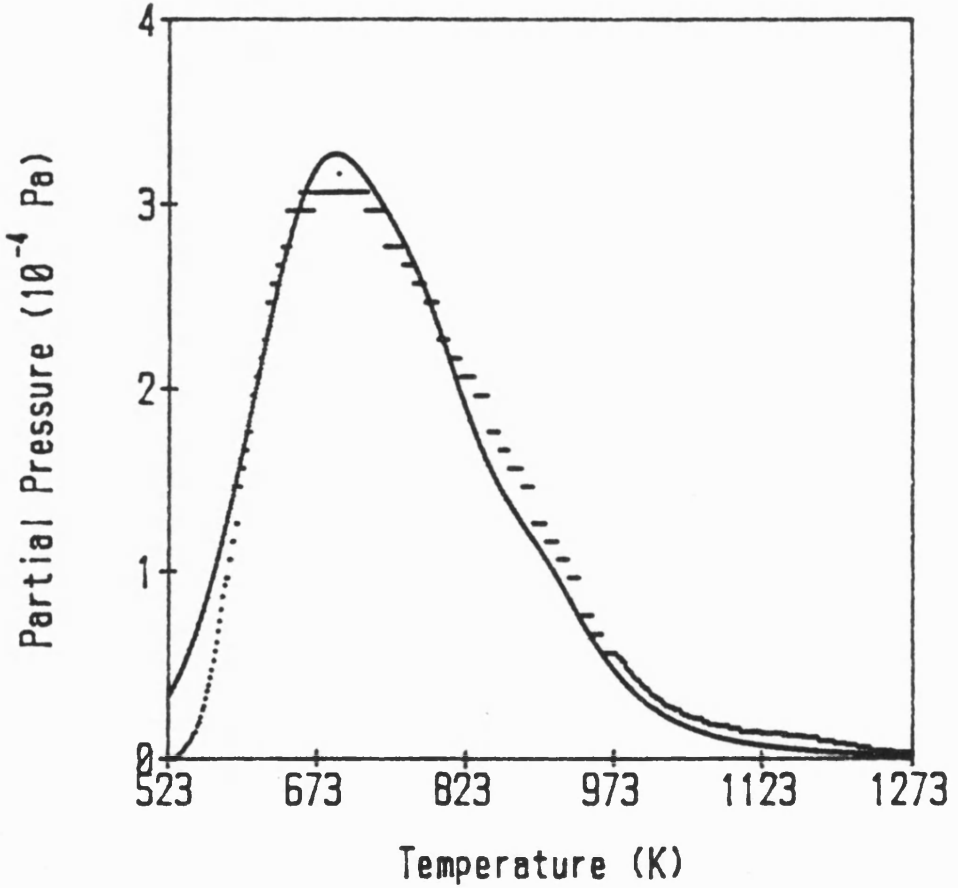

Figure 6.5 Theoretical curve of CO_2 pressure *vs* temperature of second-order desorption [$(T_p)_1$ = 693 K, $(T_p)_2$ = 793 K, $(T_p)_3$ = 923 K, $(E_d)_1$ = 14 kcal/mol, $(E_d)_2$ = 36 kcal/mol, $(E_d)_3$ = 45 kcal/mol]. and classical TPD curve of CO_2 before gasification (PVDC char, to 1273 K)

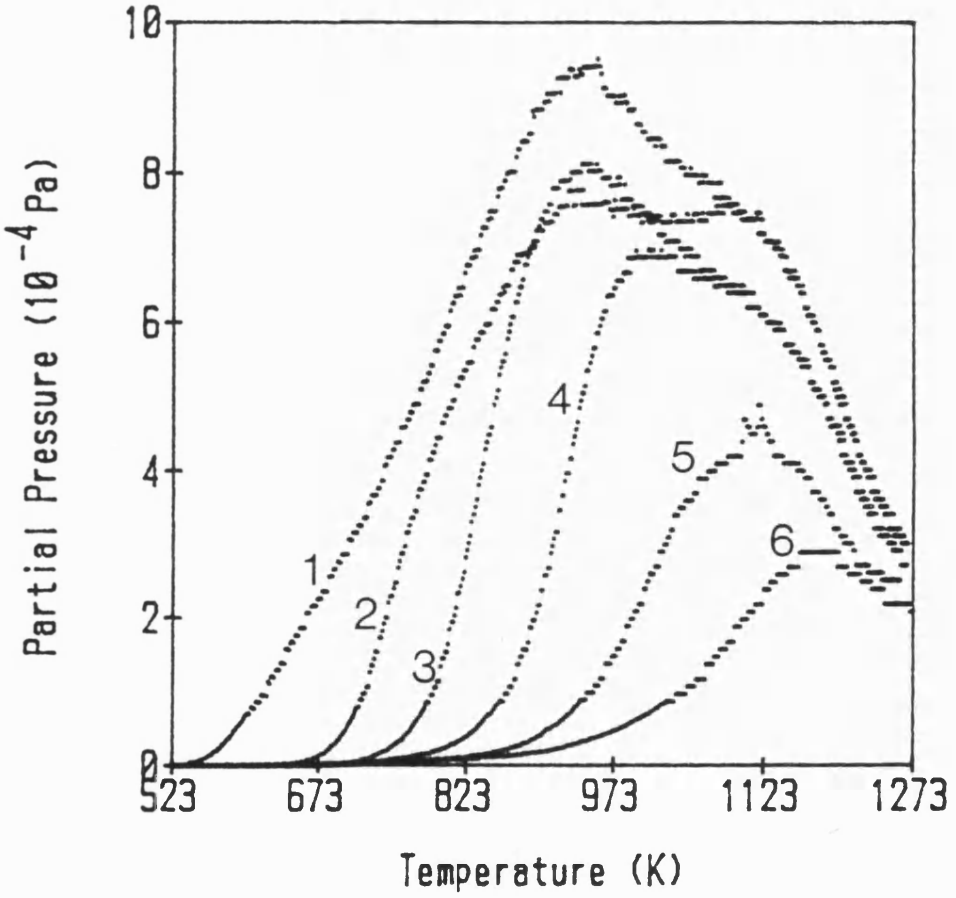

Figure 6.6 TPD spectra of CO from PVDC char with different initial oxygen coverages. 1. saturated with O_2 at 523 K, 2. preheated to 623 K, 3. preheated to 723 K, 4. preheated to 923 K, 5. preheated to 1023 K, 6. preheated to 1123 K

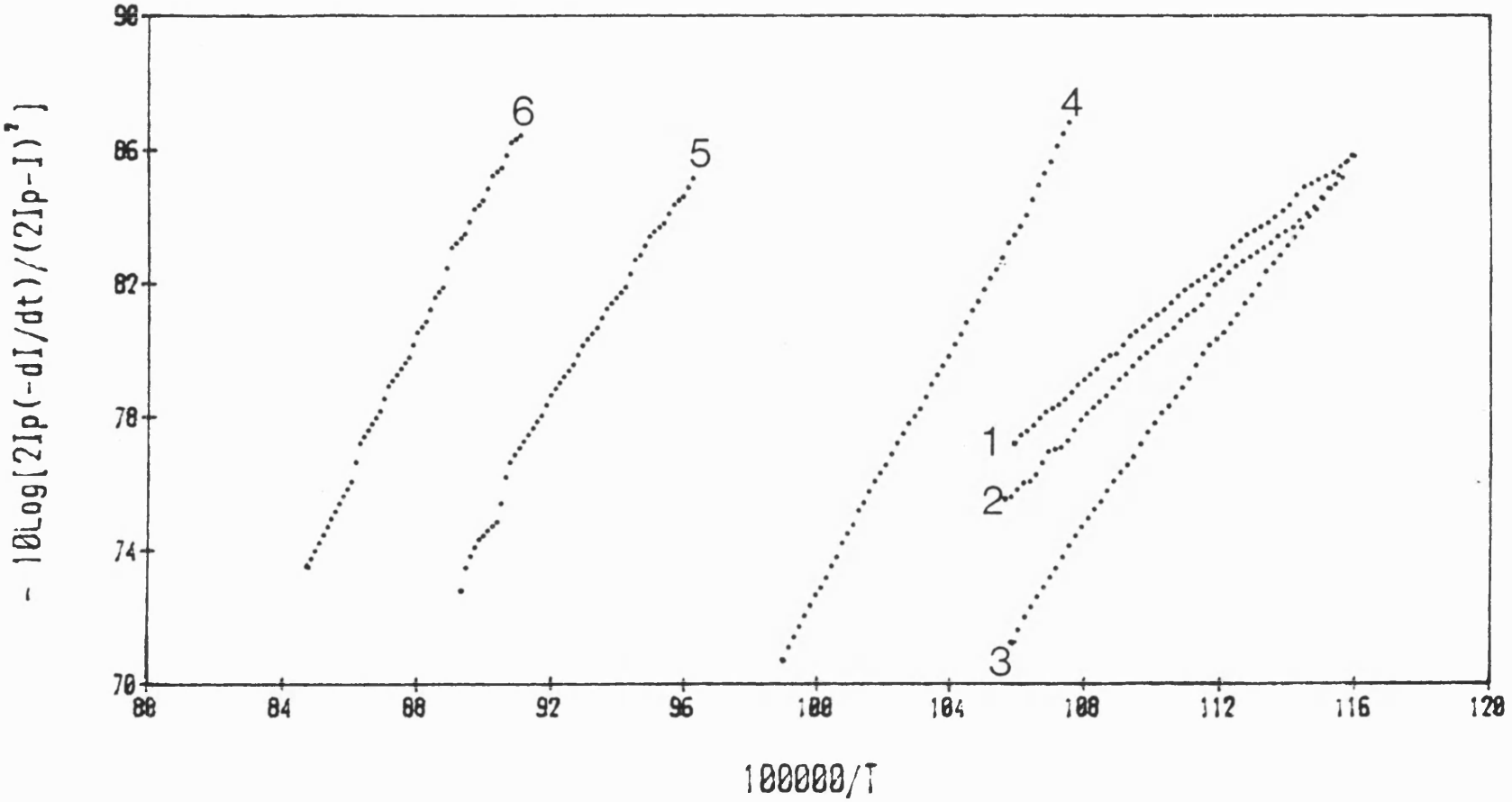

Figure 6.7 Semi-log plots of Equation (8.14) for CO desorption from α- and β-type of active sites on PVDC char surface in Figure 6.6.

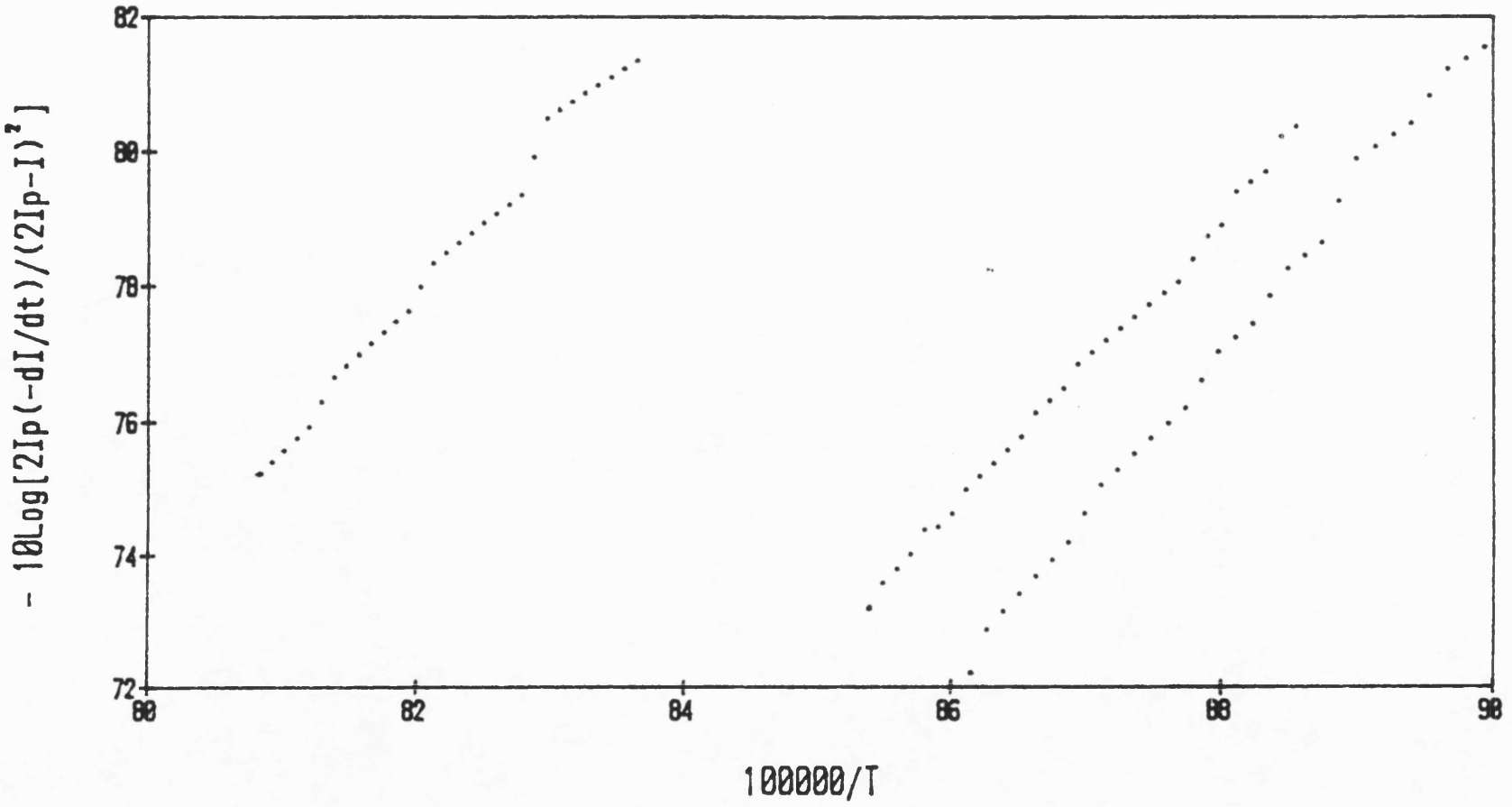

Figure 6.8 Semi-log plots of Equation (8.14) for CO desorption from γ-type of active sites on PVDC char surface.

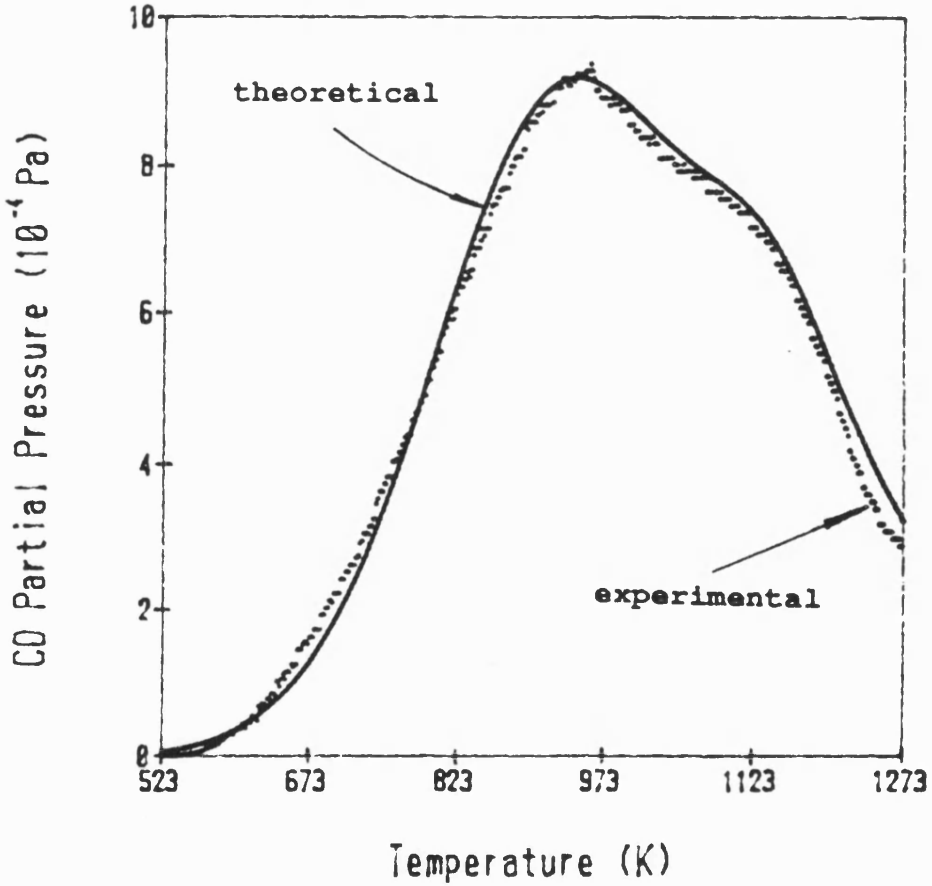

Figure 6.9 Theoretical curve of CO pressure *vs* temperature of second-order desorption [$(T_P)_\alpha$ = 973 K, $(T_P)_\beta$ = 1093 K, $(E_d)_\alpha$ = 14 kcal/mol, $(E_d)_\beta$ = 45 kcal/mol] and classical TPD curve of CO before gasification (PVDC char, to 1273 K).

Chapter 7

HYPOTHETICAL STRUCTURE OF C-O SURFACE COMPLEXES

As previously discussed in Chapter 6, analysis of TPD data provides information about the structural similarity between polycrystallite graphite and PVDC char and coal chars and information about desorption reaction and desorption activation energy, E_d, of such species involved, which is related to the strength of the bonds involved in the desorption process. By comparing these values with bond energies in similar organic compounds, assignments of the various desorption features to surface species can be tentatively made. It should be noticed, however, that it is difficult to get precise values of the bond energies on the graphite or char surface from E_d obtained from TPD. First, E_d is the sum of the activation energy for adsorption, E_a, and the surface bond energy, E_b:

$$E_d = E_a + E_b \qquad (7.1)$$

E_a is very low in the case of CO desorption on metal surfaces, for instance, [7.1], but is known to be of the order of 10 kcal/mol [7.2] or greater [7.3] for O_2 on graphite. Also, Sanderson has pointed out [7.4] that the reorganization energy of radicals after breaking the surface bond is an important contribution to the desorption energy,

and in graphite this energy is expected to be considerable, because of electron delocalization. Another complication to the determination of the bond strengths from TPD experiments is the high surface heterogeneity of carbonaceous materials, particularly for coal chars. For example, even the edges of the graphite particles contain various adsorption sites (zig-zag, arm-chair, etc.) [7.5] that lead to species of different stability, whose desorption will multiply or at least broaden the TPD features.

Despite the complexity of the surface structure and the large number of variables involved in the desorption activation energy, an assumption can be reasonably made that each surface species is likely to desorb in the same temperature range and that some qualitative trends can be established, which can help in the assignment of the TPD features to particular surface species. From this basis and a survey of the hypothetical structures of C-O surface complexes proposed by previous workers, a combined model of ether group and semiquinone group and a new mechanism for CO_2 gasification of carbonaceous substances proposed.

7.1 Structure of Graphite Crystallite

It is well-known that graphite is composed of extended sheet-like layers of atoms arranged in hexagonal networks

[7.6]. The stacking sequence of the layers was suggested as ABAB...by Hull [7.7] and latter determined by Hassel and Mark [7.8] and Bernal [7.9]. In the graphite crystal the layer planes are large and nearly perfect. Parallel layers in crystallites are ordered with respect to one another, so that the crystal structure is three-dimensional. Figure 7.1 shows a schematic graph of the perfect graphite lattice and the three-dimensional structure of graphite crystal. In practice, point defects and dislocation loops exist in graphite structure as reported by Thrower [7.10].

It is interesting to speculate briefly as to the different types of sites which would be expected at the edge of a graphite basal plane. Ideally, carbon-carbon distances of importance are 1.42, 2.46 and 2.84 A and the plane terminates probably with at least three configurations shown in Figure 7.2: zig-zag, arm-chair and one which is described in this thesis as wine-glass. Among them, the zig-zag configuration and arm-chair configuration have been discussed in detail [7.11] and it is known from theoretical calculations [7.11] that arm-chair sites are less reactive than zig-zag sites. Wine-glass sites were suggested by many authors [7.12] and it is probably the most reactive one and, therefore, will only occupy a small proportion of total surface area and active surface area.

From studies of the change in thermoelectric power of graphite upon the chemisorption of oxygen, it appears that basal plane carbon atoms have their σ-electrons and π-electrons tied up in chemical bonds with adjacent carbon atoms; edge carbon atoms have unpaired in-plane σ-electron [7.13, 7.14] and a conduction electron (π-electron) which form a carbon-oxygen bond with chemisorbed oxygen. A molecule of oxidizing agent (O_2, CO_2, H_2O, CO, *etc.*), therefore, could approach the edge of the basal plane with its bond essentially parallel to the c-axis of the graphite crystallites and form different surface groups according to the edge configuration of carbon and the oxidizing capability of the oxidant. If only considering those stable six-membered rings of C-O surface complexes, carbonyl group, semiquinone group, and ether group are possible candidates which can be formed in the adjacent layer planes. In these three surface groups, carbonyl group is very unlikely to be a suitable candidate because CO desorption from it should be of first-order and in contradiction with the second-order mechanism discussed in Chapter 6. Therefore, only ether group and semiquinone group are the possible candidates of the "extremely stable" C-O surface complexes described in Chapter 6.

Additionally, the structure of edge carbon atom in the basal plane is changeable after heat treatment at different

temperatures. Polley et al [7.15] observed that the surface area of Spheron 6 carbon black decreases with increasing heat treatment temperature. Beebe and Young [7.16] reported, from studies of adsorption heat, that the surface homogeneity of carbon black increases with increasing heat treatment temperature.

7.2 Structure of Polymer and Coal Chars

According to Franklin's division [7.17], polymer and coal chars belong to the category of hard carbons and their crystallographical structures were described [7.18] as "turbostratic" (unordered layers), *i.e.*, their structure is a random translation, about the a axis, and rotation, about the c axis of layer planes as illustrated in Figure 7.3 [7.19]. Noteworthy in this model is the presence of defects, vacancies and bends within the layer planes.

The very thorough x-ray investigation of Franklin on PVDC char [7.20] showed a high fraction (35%) of highly disordered carbon and she eventually visualized the structure as randomly oriented crystallites rigidly bound together by strong crosslinks [7.17]. Similar structures were observed in the coal chars by Hirsch [7.21] and Diamond [7.22, 7.23].

The crystalline structure of polymer and coal chars are turbostratic and their crystallite structure are of two dimensional nature and the three configurations of zig-zag, arm-chair and wine-glass described in Section 7.1 can also be distinguished in the basal plane of the model. However, the environmental situation of these sites is expected to be much more complicated and can have aliphatic carbon fragments protruding from it. This will present other carbon-carbon spacings to incoming oxidant molecules. The activated complex formed between oxidant and two surface carbon atoms would be expected to have different potential energy configurations, dependent upon the spacing between the carbon atoms. Thus, the activation energy for dissociative chemisorption of oxygen atom on carbon will vary with the carbon-carbon spacing to some extent and so broaden TPD peaks.

7.3 Ether Group Model

From the analysis of TPD spectra of carbon monoxide after water vapour gasification of PVC char at 773 K and above in an inert atmosphere and quenching at very high rate ($300K/s^{-1}$), Hermann and Huttinger [7.24] found that C-O surface complexes are extremely stable and the gasification medium has little influence on the nature and stability of these complexes. In contrast to carbon monoxide desorption

at very high temperatures, water vapour gasification of carbon results in carbon monoxide formation starting at a significantly lower temperature. They also observed that the concentration of active sites per unit of coke surface area is independent of the gasification treatment, if the existence of ether group is assumed. From this basis, they assumed that the extremely stable C-O surface groups are some ether groups (six-membered ring with a heterocyclic-bound oxygen atom) formed by the condensation of hydroxyl groups. They also proposed that the formation of the six-membered heterocyclic ring only occurs at zig-zag configuration of the edge of the basal plane of graphitic crystallites (see Figure 4(a)). Furthermore, they assumed that H_2O reacts with the stable C-O surface groups to form less stable desorbable C-O groups during gasification.

Their assumption that the stable carbon oxygen surface complexes are ether groups is supported in literature. According to Boehm *et al* [7.25] carbon-oxygen surface complexes existing as ethers exhibit the highest thermal stability. Garten and Weiss [7.26] concluded that the heterocyclic structure are formed by condensation of hydroxyl group, which was also reported by Ihnatowicz [7.27]. Halleux et al [7.28] showed that the "unreactive oxygen" of carbon reacts with sodium in liquid ammonia by formation of hydroxyl groups, which was explained by a

breakage of an ether bridge. Villars [7.29], who found that the "unreactive oxygen" of carbon does not react with Grignard reagents, concluded that the oxygen is bounded in ether structure.

If it is noticed that thermal dissociation of CO from this ether structure needs to break three bonds, one O-C σ-bond (~85 kcal/mol [7.30]) and two C-C σ/π-bonds (~80 kcal/mol [7.30]), it is obviously not difficult to understand the extreme stability of these groups. However, this model is in contradiction with the model of first-order desorption proposed by Hermann and Huttinger themselves [7.24] and is hard to reconcile with the second-order desorption model proposed in this research. Additionally, the ether group model seems too simple to explain the wide variety of C-O complexes on carbon surface as discussed in Chapter 4. Furthermore, the space between two edge carbon atoms (2.46 A) is too small to accommodate two hydroxyl groups as proposed by Hermann and Huttinger [7.24] (the bond length of O-H ~ 1.03 A [7.31]), if the strong repulsion between the two hydroxyl groups is considered. Therefore, the formation mechanism of the ether group must be different from their assumption.

7.4 Semiquinone Group Model

As mentioned in Chapter 4, Marchon *et al* [7.30, 7.32] measured the TPD spectra of polycrystalline graphite after exposing to O_2, CO_2, H_2O and CO respectively and distinguished five CO_2 desorption peaks and three CO desorption peaks. They also calculated the desorption activation energies of the surface species responsible for these peaks. By comparing the desorption activation energies with the bond energies in similar organic compounds, they assigned a semiquinone structure for the C-O surface complex responsible for the CO adsorption and desorption (see Figure 4(b)) and a lactone structure for the desorption of CO_2.

The high stability of semiquinone groups in the series of polycyclic aromatic compounds [7.33] gives strong support to the existence of semiquinones on the graphite surface. The thermal desorption of this species involves the breaking of two graphitic carbon-carbon bonds from the lattice (~80 kcal/mol) and explains the high desorption temperature. Some evidence for the existence of semiquinone groups on carbon surface has been observed [7.34, 7.35]. It has been assumed by many authors that CO_2 desorption results from the decomposition of lactone groups [7.36-7.40].

Marchon *et al* [7.30, 7.32] also reported that the TPD spectra of polycrystalline graphite after exposing to CO consists entirely of the desorption peaks of C-O complexes. They observed that no ^{12}CO is evolved in the case of ^{13}CO adsorption at high temperature, indicating that CO does not dissociate on the surface, but rather inserts into the graphitic lattice. One possibility is that ^{13}CO is physically adsorbed onto the carbon surface, but this is most unlikely since E_d is in the range of 65 - 85 kcal/mol which is much higher than expected for physically adsorbed species.

An alternative explanation is that the ^{13}CO molecule is inserted into an edge configuration on the carbon lattice either the configuration (a) or (b) in Figure 7.4. In the first case, which was not discussed by Marchon *et al* [7.30, 7.32], an ether group is formed and in the second case a semiquinone group. In the first case of desorption of the ^{13}CO molecule is reformed by breaking two bonds and in the second case by breaking three bonds.

The hypothetical structure of semiquinone group proposed by Marchon *et al* [7.30, 7.32] are in agreement with the present work, because CO desorption from a semiquinone group should be second-order as found in the analysis of TPD spectra in Chapter 6. Marchon *et al* [7.30, 7.32] did not

report the desorption peak of δ-state C-O complex and could not discuss its much higher stability than γ-state C-O complex. As discussed in Chapter 4, both of γ-state and δ-state C-O complexes participate in CO_2 gasification.

7.5 Ether and Semiquinone Groups Model

As discussed above, both the ether group model and the semiquinone group model do not offer a complete explanation for the mechanism of gasification. Furthermore, they cannot explain the regeneration of active surface sites during gasification of carbonaceous materials. Additionally, it is well-known that it is easier to break external carbon-carbon bonds (~80 kcal/mol) than internal graphitic ones (~115 kcal/mol), and at temperatures below 1500 K, a carbon-oxygen single bond can be thermally dissociated(~85 kcal/mol), but double bonds cannot (~175 kcal/mol) [7.30]. However, the burn-off and the porosity development of carbon during gasification indicate that these strong double bonds have to be dissociated in gasification process. Therefore, it is

logical to question how these bonds are broken and how such a high energy barrier is overcome.

In order to answer above questions, it is necessary to recall some observations from the measurement of TPD spectra of PVDC char quenched during CO_2 gasification at 1123 K:

(i) Only γ-type and δ-type of active surface sites participate gasification;

(2) γ-type and δ-type of active surface sites only cover about 5% of total surface area;

(3) The maximum desorption temperature of δ-state C-O complex is at around or above 1473 K;

(4) The desorption peaks of δ-state C-O complex are always larger than that of γ-state C-O complex.

(5) Only the desorption peak of δ-state C-O complex is dominant in the classical TPD spectrum of PVDC char heat treated at 1973 K before gasification.

The last two points indicate that δ-type active surface sites play a more important role in CO_2 gasification. If δ-type active sites are assigned an ether group structure because of its higher stability and γ-type active sites are assigned a semiquinone group structure, a new mechanism of CO_2 gasification can be proposed and a picture showing the successive development of active sites during gasification can be drawn in Figure 7.5.

It is assumed that gasification starts at the active surface sites occupied by an oxygen atom in ether group structures (or six-membered heterocyclic ring structures) rather than from empty active surface sites. It is believed that this kind active surface sites can be found in every kind of carbon after exposing it to an oxidizing agent. The proposed mechanism of gasification includes following four steps:

Step I. Breaking of the ether group. Because oxygen atoms are more electronegative than carbon atoms the conjugated π-electron is attracted to oxygen atom, the carbon atom connected to the oxygen atom becomes electropositive and easily attacked by the electronegative end of CO_2 (or O_2, H_2O, *etc.*) molecule. Under the influence of the electronic field of the oxygen atom of CO_2 molecule, the energy of the whole system decreases and the σ-bond between the oxygen atom and carbon atom in the ether group is more easily broken under gasification conditions than under the thermal desorption conditions;

Step II. Formation of semiquinone group. The dangling O atom formed in Step 1 is most unstable so that rearrangement to form a semiquinone group occurs. Semiquinone groups are less stable than ether groups;

Step III. Desorption of CO. CO desorption takes place from the semiquinone group. Under the influence of the

electronic field of O-atom in CO_2 molecule, the potential energy of the whole system is reduced and two C-C bonds between carbonyl and adjacent carbon atoms in the semiquinone group are more easily broken under gasification condition than under thermal desorption conditions. Expulsion of the CO molecule leads to the formation of an empty active surface site with wine-glass configuration;

Step IV. Regeneration of ether group. An oxygen atom from carbon dioxide molecule (or O_2, H_2O, CO *etc.*) occupies this "extremely" active site and forms a new ether group which is available for next cycle of gasification *via* Step I - IV. That is, a new active surface site regenerates.

In this mechanism the initial Step I involved rupture of an ether group, but it is postulated that semiquinone groups also exists on the surface. Thus it is possible to indicate the gasification cycle at Step III by rupture of a semiquinone group. Note also that the overall reaction is as expected:

$$CO_2 + CO = 2CO$$

This mechanism provides an easy explanation for the regeneration of active sites during the gasification process and it is also supported by the literatures in Section 7.3 and 7.4. It is assumed that the successive replacement of

edge carbon atoms in connection with an oxygen atom in an ether group by oxygen atoms leads to the successive development of porosity in the carbon and the successive development of TSA, ASA and RASA of the carbon during gasification. It also explains why CO_2 gasification can take place at lower temperature than that of thermal desorption.

The generally-accepted mechanism for CO_2 gasification of carbons is a single active site mechanism:

$$CO_2 + C_f \underset{k_{1b}}{\overset{k_{1f}}{\rightleftharpoons}} C(O) + CO \qquad (R.1)$$

$$C(O) \xrightarrow{k_3} C_f + CO \qquad (R.3)$$

Assuming steady state gasification:

$$\theta_o = \frac{k_{1f}[CO_2]}{k_3 + k_{1b}[CO] + k_{1f}[CO_2]} \qquad (7.1)$$

where θ_o is the fraction of active surface sites occupied by oxygen atoms, $[CO_2]$ and [CO] are partial pressures of CO_2 and CO respectively. Assuming (R.3) is the rate determining step (rds), the overall reation rate, R, can be described as:

$$R\ (s^{-1}) = k_3\theta_o = \frac{k[CO_2]}{1 + a[CO] + b[CO_2]} \qquad (7.2)$$

where $a = k_{1b}/k_3$, $b = k_{1f}/k_3$, $k = k_{1f}$.

There is much evidence that (R.1) is an equilibrium reaction and that (R.3) is the rds under a wide variety of conditions [7.41]. Therefore, the new mechanism proposed in this work must be consistent with this kinetic scheme. The reaction scheme in Figure 7.5 is a cyclic one and to compare it to the classical Langmuir-Hinshelwood scheme above, it is convenient to start at step IV which can be written as:

$$CO_2 + C_\delta \underset{k_{4b}}{\overset{k_{4f}}{\rightleftharpoons}} C_\delta(O) + CO \qquad (R.4)$$

where C_δ is identified as δ-type of active surface sites and $C_\delta(O)$ is identified as δ-state of C-O surface complexes. It can be seen that (R.4) is identical to (R.1) except that the active site C_f is identified as a δ-type of active site. Proceeding around the cyclic mechanism, Step I and II can be written as:

$$C_\delta(O) \xrightarrow{k_5} C_\gamma(O) \qquad (R.5)$$

where $C_\gamma(O)$ is identified as γ-state of C-O complexes. To complete the cycle, step III can be written as :

$$C_\gamma(O) \xrightarrow{k_6} C_\delta + CO \qquad (R.6)$$

(R.6) is identical to (R.3) except that the surface complex C(O) is identified as a γ-state of C-O surface complex.

Thus the new mechanism is similar to the classical one except that γ- and δ-states of C-O surface complexes and δ-

type of active surface site are utilised as identified by the TPD-MS studies in this work.

Applying steady state to τηε δ-state of C-O surface complex:

$$\frac{d\theta_\delta}{dt} = k_{4f}\theta_f[CO_2] - k_{4b}\theta_\delta[CO] - k_5\theta_\delta = 0 \qquad (7.3)$$

where θ_f is the fraction of unoccupied δ-type of active surface sites and θ_δ is the fraction of δ-state of C-O surface complexes. Applying steady state to the fraction of γ-state of C-O surface complexes, θ_γ, we have:

$$\frac{d\theta_\gamma}{dt} = k_5\theta_\delta - k_6\theta_\gamma = 0 \qquad (7.4)$$

$$\theta_\gamma = \frac{k_5}{k_6}\theta_\delta \qquad (7.5)$$

Because $\theta_f + \theta_\gamma + \theta_\delta = \theta_f + (1 + k_5/k_6)\theta_\delta = 1$ and $\theta_f = 1 - (1 + k_5/k_6)\theta_\delta$, from Equation (7.3) we have:

$$\theta_\delta = \frac{k_{4f}[CO_2]}{k_5 + k_{4b}[CO] + k_{4f}(1 + k_5/k_6)[CO_2]} \qquad (7.6)$$

If (R.5) is the rds, then $R = k_5\theta_\delta$. We have:

$$R = \frac{k_{4f}[CO_2]}{1 + a_1[CO] + b_1[CO_2]} \qquad (7.7)$$

where $a_1 = k_{4b}/k_5$, $b_1 = k_{4f}(1 + k_5/k_6)/k_5$. If (R.6) is the rds, then $R = k_6\theta_\gamma = k_5\theta_\delta$. We have:

$$R = \frac{k_{4f}[CO_2]}{1 + a_2[CO] + b_2[CO_2]} \qquad (7.8)$$

where $a_2 = k_{4b}/k_5$, $b_2 = k_{4f}(1 + k_5/k_6)/k_5$, *i.e.*, the same rate expression is obtained whether (R.5) or (R.6) is the rds. However, if (R.5) is the rds it is expected that $k_5 << k_6$, $k_5/k_6 << 1$ and $b_1 \approx k_{4f}/k_5$. With this approximation Equation (7.6) is very similar to Equation (7.2). Conversely if (R.6) is the rds it is expected that $k_5 >> k_6$, $k_5/k_6 >> 1$ and $b_1 \approx k_{4f}/k_6$. Thus the new mechanism is consistent with the classical Languir-Hinshelwood mechanism, except that there are slightly different interpretations of the rate constants.

References

[7.1] G. A. Somorjai, *"Chemistry in Two Dimension Surfaces"*, Cornell University Press, Ithaca, New York, (1981).

[7.2] R. C. Bansal, F. J. Vastola and P. L. Walker, Jr., J. *Colloid Interface Sci.*, **32**, 187(1969).

[7.3] S. R. Kelemen and H. Freund, *Carbon*, **23**, 619(1985).

[7.4] R. T. Sanderson, *"Chemical Bond in Organic Compounds"*, Sun and Sand, Scottsdale, AZ, (1976).

[7.5] R. N. Smith, D. A. Young and R. A. Smith, *Trans. Faraday Soc.*, **62**, 2280(1966).

[7.6] K. J. Masters, *PhD Thesis*, University of Bath, 1979.

[7.7] A. W. Hull, *Phys. Rev.*, **20**, 113(1922).

[7.8] O. Hassel and H. Mark, *Z. Phys.*, **25**, 317(1924).

[7.9] J. D. Bernel, *Proc. Roy. Soc. (Lond.)*, **A106**, 749(1924).

[7.10] P. A. Thrower, *Chem. and Phys. of Carbon*, **5**, 221(1969).

[7.11] S. E. Stein and R. L. Brown, *Carbon*, **23**, 105(1985).

[7.12] R. N. Smith, D. A. Young and R. A. Smith, *Trans. Faraday Soc.*, **62**, 2280(1966).

[7.13] R. H. Savage, *Ann. N. Y. Acad. Sci.*, **53**, 862(1954).

[7.14] F. Boulangier, X. Duval and M. Letort, "*Proceeding of the Third Carbon Conference*", Pergamon Press, New York, pp.257-264(1957).

[7.15] M. H. Polley, W. D. Schaeffer and W. R. Smith, *J. Phys. Chem.*, **57**, 1641 (1953).

[7.16] R. A. Beebe and D. M. Young, *J. Phys. Chem.*, **58**, 93(1954).

[7.17] R. E. Franklin, *Proc. Roy. Soc. (Lond.)*, **A209**, 196(1951).

[7.18] J. Biscoe and B. E. Warren, *J. Appl. Phys.*, **13**, 364(1942).

[7.19] J. C. Bokros, *Chem. Phys. of Carbon*, **5**, 10(1969).

[7.20] R. E. Franklin, ***Acta Cryst.***, **3**, 107(1950).

[7.21] P. B. Hirsch, *Proc. Roy. Soc. (Lond.)*, **A226**, 143(1954).

[7.22] R. Diamond, *Acta Crys.*, **11**, 129(1958).

[7.23] R. D. Diamond, *Phil. Trans. Roy. Soc.*, **A252**,

193(1960).

[7.24] G. Hermann and K. J. Huttinger, *Carbon*, **24**, 705(1986).

[7.25] H. P. Boehm and M. Voll, *Carbon*, **9**, 481(1971).

[7.26] V. A. Garten and D. E. Weiss, *Austr. J. Chem.*, **10**, 309(1957).

[7.27] M. Ihnatowicz, *Prace Glownego Inst. Gornictwa (Katowice)*, Kommun. 125(1952).

[7.28] A. Halleux, S. Delavarenne and H. Tschamler, *Fuel*, **40**, 74(1961).

[7.29] D. S. Villars, *J. Am. Chem. Soc.*, **70**, 3655(1948).

[7.30] B. Marchon, J. Carrazza, H. Heinemann and G. A. Somorjai, *J. Phys. Chem.*, **92**, 5744(1988).

[7.31] "*Handbook of Chemistry and Physics*", (69th ed.), CRC Press, Florida, (1988).

[7.32] B. Marchon, J. Carrazza, H. Heinemann and G. A. Somorjai, *Carbon*, **26**, 507(1988).

[7.33] E. Clar, "*Polycyclic Aromatic Hydrocarbons*", Academic, New york, (1964).

[7.34] M. S. Akhter, J. R. Keifer, A. R. Chughtai and A. R. Smith, *Carbon*, **23**, 289(1985).

[7.35] T. Tagahagi and I. Ishitani, *Carbon*, **23**, 619(1985).

[7.36] T. J. Fabish and D. E. Schleifer, *Carbon*, **22**, 19(1984).

[7.37] P. D. Koenig, R. G. Squires and N. M. Laurendeau, *Carbon*, **23**, 531(1985).

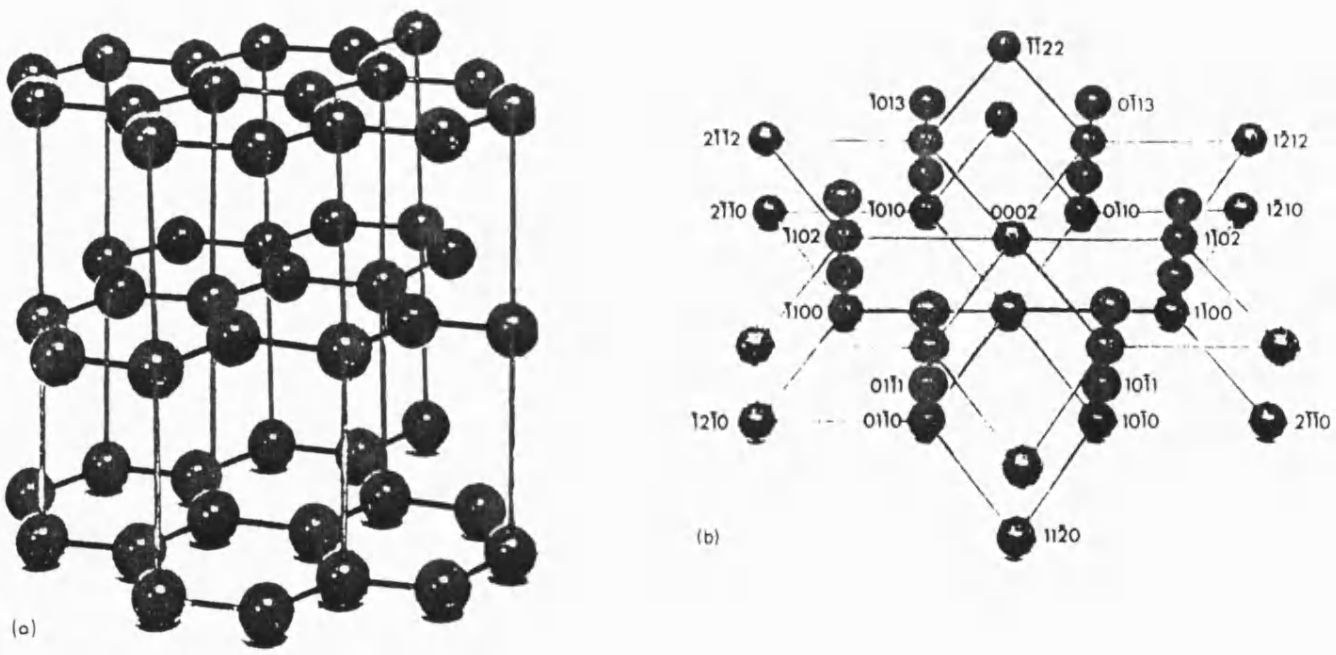

Figure 7.1 Schematic graph of (a) perfect graphite lattice and (b) three dimensional structure of graphite crystal

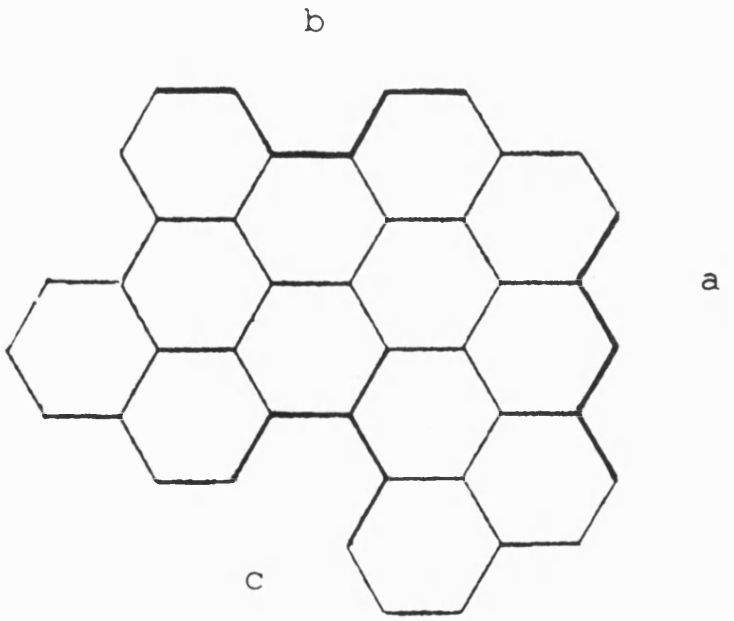

Figure 7.2 Three configurations of edge atoms on the basal plane of graphite: (a) zig-zag, (b) arm-chair and (c) wine-glass.

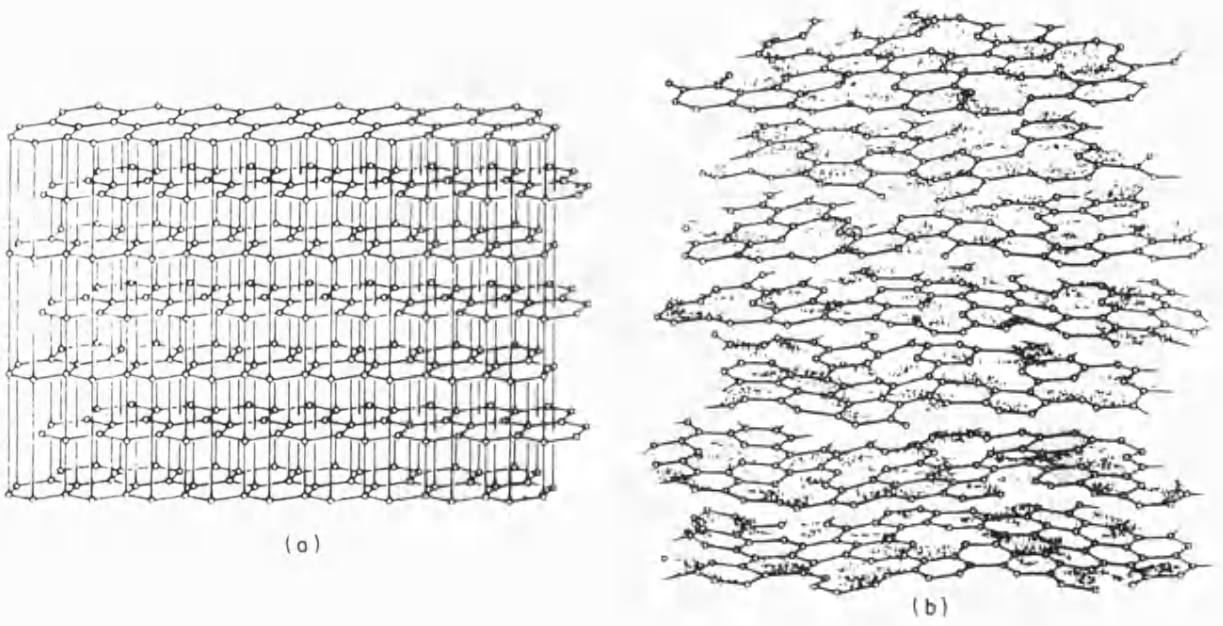

Figure 7.3 Schematic graph of (a) a three dimensional graphite lattice and (b) a turbostratic structure.

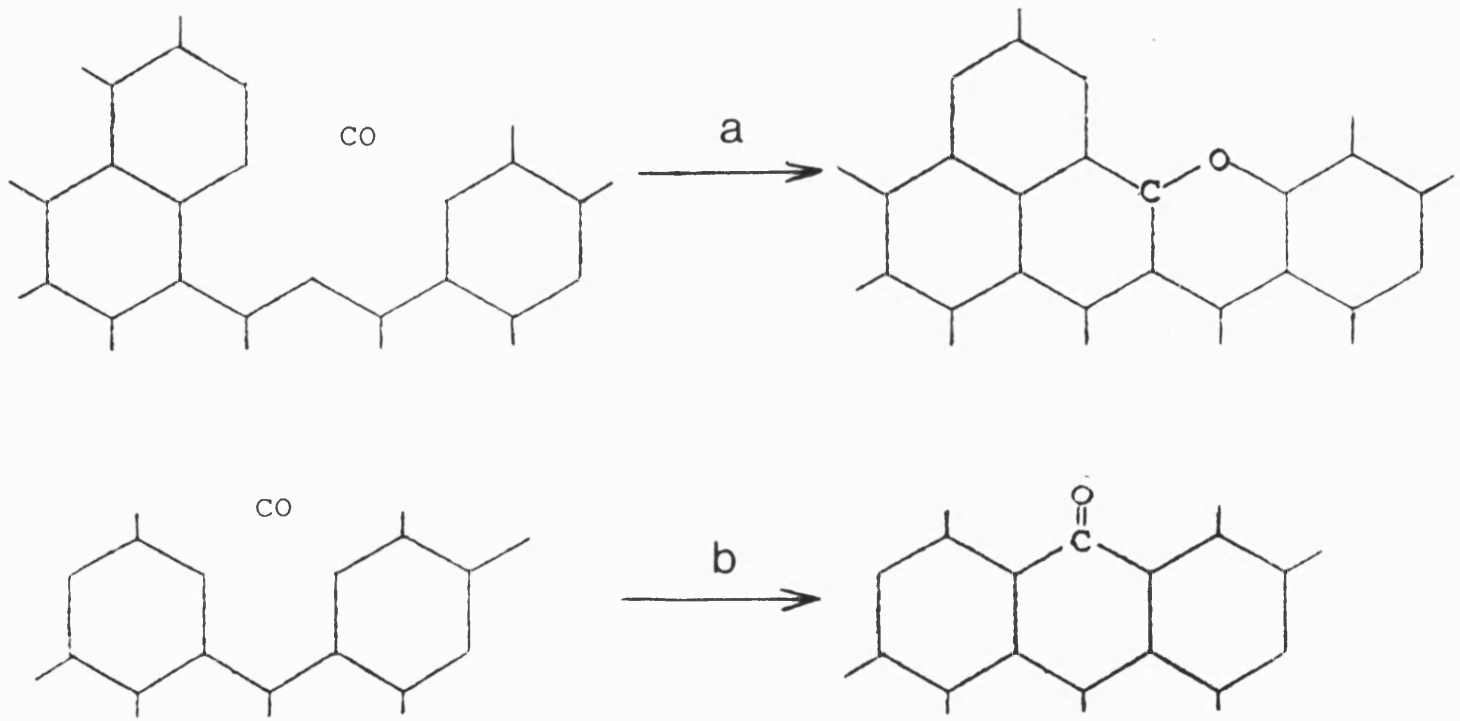

Figure 7.4 Formation of C-O surface complexes by CO adsorption (a) δ-state, (b) γ-state.

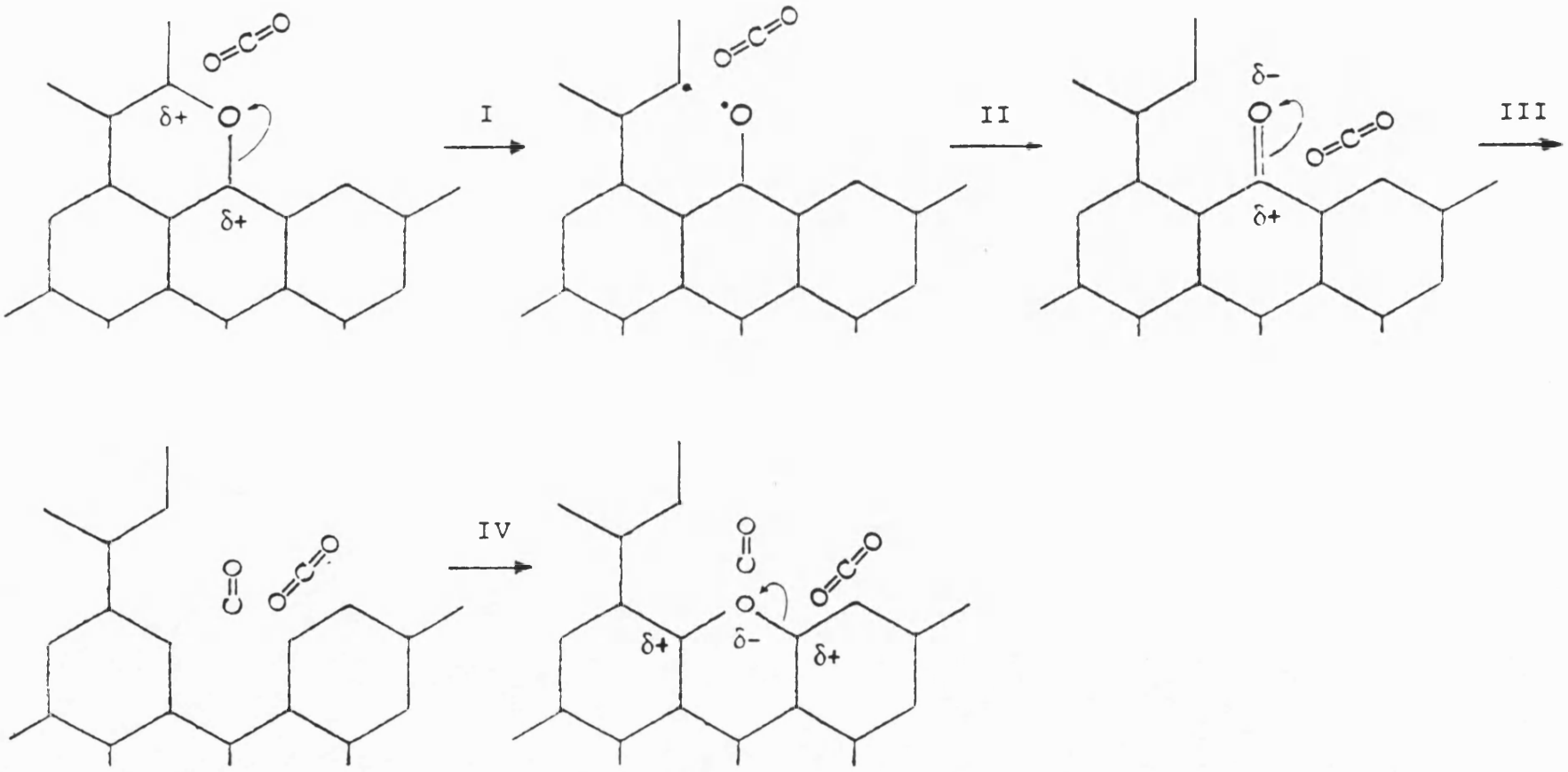

Figure 7.5 A combined model of ether and semiquinone groups for CO_2 gasification mechanism.

Chapter 8

SUMMARY AND SUGGESTIONS FOR FUTURE WORK

In this chapter the main conclusions of thesis are summarised and suggestions are made for future work

8.1 Summary

A method was devised for quantitative calibration of a TPD-MS system based upon the thermal decomposition of calcium carbonate and calcium oxalate. Calcium oxalate undergoes a two stage decomposition: the first stage produces CO and the second CO_2. Two secondary reactions in the decomposition of calcium oxalate under vacuum were observed: the disproportionation of CO produced in the first stage and the reduction of CO_2 produced in the second stage by reaction with fine carbon particles produced in the first stage. Therefore it is impossible to calibrate a dynamic TPD-MS system only with CaC_2O_4. The system must be calibrated with calcium carbonate first for CO_2 and then calibrated with CaC_2O_4 for both CO and CO_2. The extent of disproportionation of CO in the first stage of decomposition decreases following the increase of the sample size and varies from 52 - 54% the extent of the reduction of CO_2 in

the second stage increases progressively from 2.30 - 6.50% following the increase of sample size.

Classical TPD spectra were obtained from char surfaces which had been saturated with O_2 at 523 K. Each of the classical TPD spectra to 1273 K of PVDC char and a series of coal chars consists of a broad curve of CO_2 desorption and a CO desorption curve which consists of one peak at 973 K and one shoulder at 1083 K and, significantly, CO pressure at 1273 K which persists even after a long isothermal period. Another peak at around 1473 K occurs in the TPD spectra to 1473 K. Each of the TPD spectra after gasification and quenching of PVDC char and a series of coal chars shows two peaks, one is at 1223 K and another at around 1473 K. The four peak temperatures for different chars are very close to each other and are attributed to the desorptions of α-, β-, γ- and δ-states of C-O surface complexes. The first three peak temperatures, 973, 1083 and 1223 K are consistent with those found for polycrystallite graphite reported in literature. It provides some evidence of structural similarity of the surface of polycrystallite graphite and a wide range of chars. TPD spectra after gasification and quenching indicate that only γ- and δ-states of C-O surface complexes participate in CO_2 gasification. It is observed that mineral matter and potassium carbonate can promote the

relative abundance of these two types of active surface sites and, therefore, catalyse CO_2 gasification.

The area covered by γ- and δ-states of C-O surface complexes is named as reactive active surface area (RASA) to distinguish it from the total active surface area (TASA). RASA gives a better and more relevant linear correlation with the reactivity for CO_2 of a wide range of chars than does TASA before and after gasification.

By measuring TPD spectra of same sample with different initial surface coverages of surface oxides flash desorption theory was successfully applied in the kinetic study of TPD-MS spectra. It is revealed that the broad CO_2 desorption peak is the result of overlapping of three second-order desorption peaks and the desorption activation energies of them are 17, 36 and 41 kcal/mol respectively. The desorption of α-, β-, γ- and δ-states of C-O surface complexes are also of second-order desorption and the fixed activation energies of them are 17, 45, 55 and 82 kcal/mol respectively. The above second-order desorption mechanisms are also verified using a curve-fitting method. The second-order desorption energies for PVDC char and a series of coal chars are also very close to each other. It gives more evidence of structural similarity of the surface of a wide range of chars.

A model for the gasification process is proposed based upon the assumption that γ-state of C-O surface complexes has a hypothetical structure of semiquinone group and δ-state of C-O surface complexes has a structure of ether group. This model assumes that gasification takes place at ether group structure and can explain why carbon can be gasified at lower temperatures than those of thermal desorption temperatures of γ- and δ-states of C-O surface complexes, the regeneration of active surface sites and the porosity development during gasification.

8.2 Suggestion for Future Work

(1) CO_2 gasification reactivity of a char varies with :

i. temperature,

ii. the ratio of CO/CO_2,

iii. particle size,

iv. thermal history, *etc.*

Therefore, it is necessary to further elucidate the relationships of them.

(2) The experimental system can also be used in the study of water vapour gasification and it is expected that further evidence about the role of γ- and δ-states of C-O surface complexes in gasification can be obtained from it.

(3) Other experimental techniques, particularly infrared spectroscopy, have been used to study the functional groups on carbon surface. It is possible to obtain some information from the comparison of infrared spectra of carbon saturated with oxygen before gasification, carbon after CO_2 gasification and quenching, and carbon saturated with oxygen again after CO_2 gasification.

(4) This TPD-MS system can be used also in other research field, such as other adsorbent systems, thermal decomposition of organic and inorganic materials, *etc.*.

(5) This TPD-MS as a conventional analyser can also connect with normal gasification reactor or combustor by a molecular leak. However, further study about the calibration is needed in this case.

(6) The desorption mechanism of γ- and δ-states of surface carbon oxides needs further work with a high temperature furnace.

(7) The application of flash desorption theory needs further development to more complicated carbon surface conditions.

8.3 Conclusion

At the outset of this thesis its aims were summarized as following questions to be answered:

* How many types of active surface sites exist on the surface of carbons?

* On what type or types of active surface sites does gasification take place?

* What is the stoichiometry of C-O surface complexes, *i.e.*, what is the ratio of X/Y in the formula of C-O surface complex C_XO_Y?

* How do these different active surface sites develop during gasification?

* Is it correct to apply the results obtained from pure carbon to highly heterogeneous coal chars?

* Can the catalyst effect of some minerals, such as potassium carbonate be explained using active surface sites theory?

The work presented in this thesis has gone some way to answering these questions, although much more work remains to be done.